University of Alberta

Heat and Mass Transfer Effects in Monolith Reactors

By

Hemant More ©

A thesis submitted to the Faculty of Graduate Studies and Research
in partial fulfillment of the requirements for the degree of
Master of Science

in

Chemical Engineering

Department of Chemical and Materials Engineering
Edmonton, Alberta, Canada
Spring 2007

Library and Archives Canada

Published Heritage Branch

395 Wellington Street
Ottawa ON K1A 0N4
Canada

Bibliothèque et Archives Canada

Direction du Patrimoine de l'édition

395, rue Wellington
Ottawa ON K1A 0N4
Canada

Your file Votre référence
ISBN: 978-0-494-29999-9
Our file Notre référence
ISBN: 978-0-494-29999-9

NOTICE:
The author has granted a non-exclusive license allowing Library and Archives Canada to reproduce, publish, archive, preserve, conserve, communicate to the public by telecommunication or on the Internet, loan, distribute and sell theses worldwide, for commercial or non-commercial purposes, in microform, paper, electronic and/or any other formats.

The author retains copyright ownership and moral rights in this thesis. Neither the thesis nor substantial extracts from it may be printed or otherwise reproduced without the author's permission.

AVIS:
L'auteur a accordé une licence non exclusive permettant à la Bibliothèque et Archives Canada de reproduire, publier, archiver, sauvegarder, conserver, transmettre au public par télécommunication ou par l'Internet, prêter, distribuer et vendre des thèses partout dans le monde, à des fins commerciales ou autres, sur support microforme, papier, électronique et/ou autres formats.

L'auteur conserve la propriété du droit d'auteur et des droits moraux qui protège cette thèse. Ni la thèse ni des extraits substantiels de celle-ci ne doivent être imprimés ou autrement reproduits sans son autorisation.

In compliance with the Canadian Privacy Act some supporting forms may have been removed from this thesis.

While these forms may be included in the document page count, their removal does not represent any loss of content from the thesis.

Conformément à la loi canadienne sur la protection de la vie privée, quelques formulaires secondaires ont été enlevés de cette thèse.

Bien que ces formulaires aient inclus dans la pagination, il n'y aura aucun contenu manquant.

Canada

Abstract

This work presents an investigation of heat and mass transfer effects in catalytic monolith reactors used for automotive catalytic converters. It is shown that the Nusselt and Sherwood numbers in the entry region vary significantly depending on the reaction rate at the wall and the physical properties. Predictions from one and two dimensional models are compared. The effect of including the two dimensional momentum balance on predicted light-off behaviour is significant. The effect of catalytic washcoat geometry is tested to determine its effect on the light-off position and shape. It is seen that the shape of the washcoat has an influence on the shape of the light-off curve.

A study is presented on CO oxidation with very high fluid velocity in small reactors. It is shown that significant conversion may be achieved, which suggests that their use as pre-turbocharger catalyst is worth exploration.

Keywords: Monoliths, Heat Transfer, Light-off, Washcoat Geometry, Simulations, Three Dimensional, Pre-Turbo Catalysts, Turbulence

Acknowledgements

I am grateful to the many people who have contributed to the work described in this thesis. This is a difficult task, given the large number of people that have helped to design, implement, apply, criticize, sponsor and evangelize the work. I am going to try anyway, and if your name is not listed, rest assured that my gratitude is no less than for those listed below.

The first person I would like to thank is my supervisor, Dr. Robert E. Hayes. He has been the driving force behind this work. He has been an excellent mentor and great inspiration for me. I admire him for the enthusiasm and the drive he has towards quality work. I also admire him for the amount of patience he has shown in handling my numerous questions. And it goes without saying this work wouldn't have even started if it was not for Dr. Hayes's excellent guidance and support. Thank you Dr. Hayes

A special thanks to Dr. Martin Votsmeier of Umicore, Dr. Joseph Mmbaga, Dr. Ben Liu, Bob Barton and Paul Greidanus at University of Alberta for their help and support during my project. I would also like to thank my group members Anant, Rajab, Atreyee, Naeimeh and Stephen for their support.

I also want to acknowledge NSERC and Umicore for financial support and for giving me the opportunity to work on different projects. I would also like to thank the Center of Excellence in Integrated Nanotools for providing computational facilities.

Finally not the least, a very special thanks to my family, my parents, my brother, my sister, my in-laws without whom there is no meaning to all this. Their support, encouragement, faith and love cannot be substituted. A special thanks to Dolly for tolerating me and my unpredictable mood through the last year and still giving me that support. Thanks to my roommates Mridul, Japan and Ashish for the delicious food and all my friends, Mranal, Ritika, Aashima, Sankar, Varma, Hari, Rashmi, Swetha and Amrutha for showing that you can work and yet have fun as a graduate student.

TABLE OF CONTENTS

1. Introduction 1

2.0 Background and Literature Survey 3

2.1 The automotive catalytic converter 3

2.2 Heat and mass transfer in ducts 10

2.3 Boundary layer development 14

2.4 Correlations for heat transfer coefficients in circular ducts 22

2.4.1 Laminar flow correlations 22
2.4.2 Turbulent flow correlations 25
2.4.3 Transition flow 28

2.5 Concentration boundary layer and the mass transfer coefficient 29

2.6 Modelling monolithic reactor channels 30

2.7 Heat and mass transfer correlations for monolith channels 32

2.7 Review of modelling of monolith channels 36

2.9 Overview of the finite element method (FEM) 40

3. Two dimensional study of Nu and Sh numbers in monolith reactor for laminar flow. 43

3.1 Hydrodynamic entry length 44

3.2 Combined entry length without reaction 47

3.3 Combined entry length with first order reaction 55

3.3 Combined entry length with first order reaction in a washcoat 60

3.4 Comparison of one and two dimensional channel models 63

3.5 Concluding remarks 68

4. Comparison of model performance in predicting light-off 69

4.1 Two dimensional model of a single monolith channel 70

4.2 Three dimensional model of a single monolith channel 83

4.3 Concluding remarks 105

5. Heat and Mass Transfer in Turbulent Flow 106

5.1 The 1D-2D single channel model 107
5.2 Effect of gas velocity on conversion 110
5.3 Effect of channel diameter 113
5.4 Effect of internal diffusion 115
5.5 Prediction of Nu/Sh number for flow at high velocities 116
5.6 Concluding Remarks 121

6. Conclusions and Future Work 122

REFERENCES 125

LIST OF TABLES

Table 1: Thermal boundary conditions for developed and developing flow through singly connected ducts. 21

Table 2: Fully developed turbulent flow Nusselt numbers in a smooth circular duct for gases and liquids with Pr > 0.5. 27

LIST OF FIGURES

Figure 2.1: Magnified photograph of a cross section that was cut through the monolith. Note the uneven distribution of the washcoat. 6

Figure 2.2: Typical monolith channel shapes. 6

Figure 2.3: Mass transfer and reaction for a catalysis coated wall. 8

Figure 2.4: Convection heat transfer effects for a surface of arbitrary shape 11

Figure 2.5: Velocity boundary layer development over a flat plate. 14

Figure 2.6: Thermal boundary layer development over a flat plate. 15

Figure 2.7: Hydrodynamic entry length in a duct. 16

Figure 2.8: Simultaneous development of velocity and thermal boundary layers. 17

Figure 2.9: Separate development of boundary layers in a duct. 17

Figure 2.10: Flow and reaction in a single channel monolith 31

Figure 3.1: Velocity profile along the length of the reactor to examine the hydro-dynamically developing region without heat transfer. 45

Figure 3.2: Predicted development length comparison and comparison with relationship given by Durst and by Equation (3.1) and (3.2). 46

Figure 3.3: Local Nusselt number obtained from entry length solutions for laminar flow in a channel with constant wall temperature of 500 K. 51

Figure 3.4: Local Nusselt number obtained from entry length solutions for laminar flow in a channel with one property constant and other properties varying. 52

Figure 3.5: Local Nusselt number obtained from entry length solutions for laminar flow in a channel with one property varying and other properties constant. 53

Figure 3.6: Local Nusselt number obtained from entry length solutions for laminar flow in a channel with different wall temperature. 54

Figure 3.7: Local Nusselt number obtained from entry length solutions for laminar flow in a channel with constant wall flux. 55

Figure 3.8: Variation in Nu number along the axial direction for the case of reaction at the wall and comparison with constant wall flux and constant wall temperature cases at the same conditions. 59

Figure 3.9: Comparison of conversion for the case when there is a reaction in the washcoat and when there is a reaction at the wall for an inlet velocity of 1 m/s. 62

Figure 3.10: Comparison of conversion for the case of 1D – 2D model, reaction in the washcoat and reaction at the wall for an inlet velocity of 1 m/s. 65

Figure 3.11: Effect of varying the Nusselt number on conversion for a 1D- 2D model at an inlet velocity of 1 m/s. 66

Figure 3.12: Comparison of conversion for the case of 1D – 2D model, reaction in the washcoat and reaction at the wall for an inlet velocity of 36 m/s. 67

Figure 4.1: Solution domain for a 2D single monolith channel 70

Figure 4.2: Effect of length of reactor on the light-off curve for an inlet temperature ramp rate of 30 K/min at increasing reactor length for 2D model. The CO concentration is 5000 ppm. 77

Figure 4.3: Effect of length of reactor on the light-off curve for an inlet temperature ramp rate of 300 K/min for 2D model. The CO concentration is 5000 ppm. 78

Figure 4.4: Effect of neglecting momentum balance on the light-off curve for an inlet temperature ramp rate of 30 K/min at a GHSV of 80 000 h^{-1} for 2D model. The CO concentration is 5000 ppm. 79

Figure 4.5: Effect of neglecting momentum balance on the light-off curve for an inlet temperature ramp rate of 300 K/min at a GHSV of 80 000 h^{-1} for 2D model. The CO concentration is 5000 ppm. 80

Figure 4.6: Effect of diffusion on the light-off curve for an inlet temperature ramp rate of 30 K/min at a GHSV of 80 000 h^{-1}. The CO concentration is 5000 ppm. 81

Figure 4.7: Effect of momentum balance without diffusion limitation on the light-off curve for an inlet temperature ramp rate of 30 K/min at a GHSV of 80 000 h^{-1} for 2D geometry. The CO concentration is 5000 ppm. 82

Figure 4.8: Three dimensional model of a single channel monolith 84

Figure 4.9: Effect of washcoat shape on the light-off curve for an inlet temperature ramp rate of 30 K/min at a GHSV of 20 000 h^{-1}. The CO concentration is 5000 ppm 87

Figure 4.10: Effect of washcoat shape on the light-off curve for an inlet temperature ramp rate of 30 K/min at a GHSV of 80 000 h-1. The CO concentration is 5000 ppm. 88

Figure 4.11: Effect of length of reactor on the light-off curve for an inlet temperature ramp rate of 30 K/min at increasing reactor length for circle-in-square geometry. The CO concentration is 5000 ppm. 89

Figure 4.12: Effect of length of reactor on the light-off curve for an inlet temperature ramp rate of 30 K/min at increasing reactor length for square-in-square geometry. The CO concentration is 5000 ppm. 90

Figure 4.13: Effect of washcoat shape on the light-off curve for an inlet temperature ramp rate of 300 K/min at a GHSV of 80 000 h^{-1}. CO concentration is 5000 ppm. 91

Figure 4.14: Effect of length of reactor on the light-off curve for an inlet temperature ramp rate of 300 K/min for circle-in-square geometry. The CO concentration is 5000 ppm. 92

Figure 4.15: Effect of length of reactor on the light-off curve for an inlet temperature ramp rate of 300 K/min for square-in-square geometry. The CO concentration is 5000 ppm. 93

Figure 4.16: Effect of washcoat shape on the light-off curve for an inlet temperature ramp rate of 600 K/min at a GHSV of 80 000 h^{-1}. The CO concentration is 5000 ppm. 94

Figure 4.17: Effect of washcoat shape on the light-off curve for an inlet temperature ramp rate of 30 K/min at a GHSV of 80 000 h^{-1} with an imposed velocity profile at the inlet. The CO concentration is 5000 ppm. 95

Figure 4.18: Effect of washcoat shape on the light-off curve for an inlet temperature ramp rate of 30 K/min at a GHSV of 80 000 h^{-1} with a flat velocity profile at the inlet. The CO concentration is 5000 ppm. 96

Figure 4.19: Concentration profile for circle-in-square geometry along the length of reactor for an inlet temperature ramp rate of 30 K/min at a GHSV of 80 000 h^{-1} with an imposed velocity profile at the inlet. The CO concentration is 5000 ppm. 97

Figure 4.20: Concentration profile for circle-in-square geometry along the length of reactor for an inlet temperature ramp rate of 300 K/min at a GHSV of 80 000 h^{-1} with an imposed velocity profile at the inlet. The CO concentration is 5000 ppm. 98

Figure 4.21: Temperature profile for circle-in-square geometry along the length of reactor for an inlet temperature ramp rate of 30 K/min at a GHSV of 80 000 h^{-1} with an imposed velocity profile at the inlet. The CO concentration is 5000 ppm. 99

Figure 4.22: Temperature profile for circle-in-square geometry along the length of reactor for an inlet temperature ramp rate of 300 K/min at a GHSV of 80 000 h^{-1} with an imposed velocity profile at the inlet. The CO concentration is 5000 ppm. 100

Figure 4.23: Concentration profile for square-in-square geometry along the length of reactor for an inlet temperature ramp rate of 30 K/min at a GHSV of 80 000 h^{-1} with an imposed velocity profile at the inlet. The CO concentration is 5000 ppm. 101

Figure 4.24: Concentration profile for square-in-square geometry along the length of reactor for an inlet temperature ramp rate of 300 K/min at a GHSV of 80 000 h^{-1} with an imposed velocity profile at the inlet. The CO concentration is 5000 ppm. 102

Figure 4.25: Temperature profile for square-in-square geometry along the length of reactor for an inlet temperature ramp rate of 30 K/min at a GHSV of 80 000 h^{-1} with an imposed velocity profile at the inlet. The CO concentration is 5000 ppm. 103

Figure 4.26: Temperature profile for square-in-square geometry along the length of reactor for an inlet temperature ramp rate of 300 K/min at a GHSV of 80 000 h^{-1} with an imposed velocity profile at the inlet. The CO concentration is 5000 ppm. 104

Figure 5.1: Schematic representation of a 1D – 2D model 107

Figure 5.2: Variation of the fractional conversion with inlet channel velocity for three different Nusselt and Sherwood number values for inlet temperatures of 500 and 600 K. 112

Figure 5.3: Variation of the fractional conversion with inlet channel velocity for three different Nusselt and Sherwood number values for inlet temperature 600 K with channel diameter of 1.5 and 2 mm. 114

Figure 5.4: Variation of the fractional conversion with inlet channel velocity for fixed Nu and Sh with modified washcoat thickness and activity. The two curves for half thickness and original thickness coincide. 115

Figure 5.5: Local Sherwood number obtained from entry length solutions for turbulent flow in a channel with reaction at the surface of the catalyst. 119

Figure 5.6: Conversion obtained for turbulent flow in a channel with reaction at the surface of the catalyst 120

List of Nomenclature

A_S	Total Surface Area, m^2
a_A	Constant
C	Molar Density (Concentration), mol/m^3
C_0	Constant
C_1	Constant
C_A	Molar Density (Concentration) of Species, mol/m^3
C_{CO}	Molar Density (Concentration) of CO, mol/m^3
C_f	Total Molar Density (Concentration) of Fluid or Gas
C_i	Molar Density (Concentration) of Species i, mol/m^3
C_P	Constant Pressure Specific Heat of Fluid or Gas, J/Kg.K
C_V	Constant Volume Specific Heat of Fluid or Gas, J/Kg.K
C_μ	Constant
$C_{\varepsilon 1}$	Constant
$C_{\varepsilon 2}$	Constant
D	Diameter of channel or pipe, m
D	Diffusion Coefficient, m^2/s
Da	Damkholer Number
D_A	Diffusion Coefficient of A, m^2/s
D_{AB}	Diffusion Coefficient, m^2/s
D_{eff}	Effective Diffusion Coefficient, m^2/s
D_H	Hydraulic Diameter of Channel, m
d_p	Mean Pore Diameter, m

Gz	Graetz Number
ΔH	Enthalpy Change of Reaction, J/mol
h	Local convective heat transfer coefficient, $W/m^2.K$
$\overline{h}$	Average convective heat transfer coefficient, $W/m^2.K$
k	Thermal Conductivity of Fluid, W/m.K
k	Turbulent Energy, m^2/s^2
k_f	Thermal Conductivity of Fluid or Gas, W/m.K
K_{CO}	Adsorption Equilibrium Constant, m^3/mol
k_{CO}	Reaction Rate Constant, s^{-1}
k_{eff}	Effective Thermal Conductivity of Solid, W/ (m.K)
k_S	Thermal Conductivity of Washcoat, W/ (m.K)
k_m	Mass Transfer Coefficient, m/s
L	Length of Tube or Duct or Channel, m
L_C	Characteristic Length of Washcoat, m
Le	Lewis Number
L_{ent}	Hydrodynamic Entrance length, m
$L_{ent,\,C}$	Entrance Length for Concentration Boundary Layer, m
$L_{ent,\,T}$	Thermal Entrance Length, m
L_R	Arbitrary Scaling Factor
M	Molecular Mass of Species
M_A	Molecular Mass of Molecule A
Nu	Nusselt Number
Nu_H	Nusselt Number for Constant Wall Flux Condition

Nu_T	Nusselt Number for Constant Wall Temperature Condition
P	Total Pressure, Pa
p	Pressure, Pa
Pe	Peclet Number
Pr	Prandtl Number
q	Total Heat Transfer Rate, W
q''	Convective Heat Flux, W/m^2
q_s''	Constant Surface Heat Flux, W/m^2
R	Gas Constant, J/mol K
R	Radius of Duct or Channel, m
r	Radial Coordinate in Cylindrical Coordinate System, m
R_A	Reaction Based on Surface Area, mol/ (m^2.s)
R_{CO}	Reaction Rate of CO based on Washcoat Volume, mol/(m^3.s)
Re	Reynolds Number
Sc	Schmidt Number
Sh	Sherwood Number
T	Temperature, K
T_b	Bulk Temperature, K
T_f	Temperature of Fluid or Gas, K
T_s	Surface Temperature, K
T_w	Wall Temperature, K
T_{WC}	Temperature of Washcoat, K
$\langle T \rangle$	Mixing Cup Temperature, K

T_∞	Temperature of Fluid, K
u_τ	Wall Friction Velocity $\left(u_\tau = \sqrt{\frac{\tau_w}{\rho}}\right)$, m/s
u_∞	Free Stream Velocity, m/s
V	Velocity of Fluid or Gas, m/s
v	Velocity of Fluid or Gas, m/s
v_z	Velocity in Axial Direction, m/s
v_r	Velocity in Radial Direction, m/s
v_m	Inlet Velocity, m/s
Y_A	Mole Fraction of Component A
$Y_{A,WC}$	Mole Fraction of Component A in Washcoat
Y_{Af}	Mole Fraction of Fluid or Gas
$\langle Y_A \rangle$	Mixing Cup Concentration
Y_{CO}	Mole Fraction of CO
Y_{O2}	Mole Fraction of O_2
x	Coordinate in the Cartesian System, m
x_c	Critical Length, m
y	Coordinate in the Cartesian System, m
y^*	Dimensionless Distance
z	Axial Coordinate in Cylindrical Coordinate System, m
z'	Length Scale
∇	Gradient

Greek Letters

ρ	Density of Fluid or Gas, m/s
ρ_S	Density of Solid (Washcoat or Substrate), kg/m^3
ε	Dissipation Rate of Turbulent Energy, m^2/s^3
ε	Washcoat Porosity
τ	Tortuosity Factor
σ_k	Constant
σ_ε	Constant
δ	Velocity Boundary Layer Thickness, m
δ_c	Concentration Boundary Layer Thickness, m
δ_T	Thermal Boundary Layer Thickness, m
θ_T	Dimensionless Temperature
η	Dynamic Viscosity of Fluid or Gas, m^2/s
τ_w	Wall Shear Stress, N/m^2
μ	Kinematic Viscosity of Fluid or Gas, Pa-s
ν_T	Turbulent Viscosity of Fluid or Gas

Subscripts

A	Relating to Species A
b	Bulk Value
f	Fluid Properties
i	one of a series of n

o	Inlet Condition
s	Solid Properties (Washcoat or Substrate)
w	Properties at Wall
∞	Free Stream Properties

List of Abbreviations

1D	One Dimensional
2D	Two Dimensional
3D	Three Dimensional
GHSV	Gas Hourly Space Velocity
LHHW	Langmuir-Hinshelwood-Hougen-Watson
ppm	Parts Per Million (1 in 10^6)

1. Introduction

Over the past thirty years, government regulations have limited the amount of harmful emissions that can be emitted to the atmosphere from automotive exhaust gases. These regulations have, in turn, dictated the use of catalytic converters in the exhaust pipe. The catalytic converter typically consists of a monolith honeycomb substrate, the channels of which are coated with a catalytic washcoat. The desire to use computer aided design has created a need to build reliable mathematical models to predict their behaviour. A catalytic converter model is potentially complex, and involves a number of issues including heat and mass transfer both in the gas phase and within the catalytic monolith.

The main objective of the thesis is to study, using computer models, the single channel monolith reactor in one, two and three dimensions. The main focus is on the heat and mass transfer effects. The first part of the study involved a critical examination of the Nusselt and Sherwood numbers present in two dimensional channels with reaction at the walls. Although there are a lot of literature studies on this area, there remains a lack of consensus. The second major area of study was influence of the washcoat geometry on the light-off behavior using two and three dimensional modelling. Because of the manufacturing methods, the washcoat is often non-uniform in thickness. It is shown that the washcoat shape influences the light-off behavior. The extent of the effect depends on the operating conditions. The light-off, or cold start, performance of catalytic converters is considered crucial, because most of the emissions are released during this period. Furthermore, there is a strong interest in being able to model correctly the performance of catalytic converters during the standard driving cycle tests that are routinely performed by catalyst manufacturers.

Also, in recent years a variety of factors, including toxic emissions limits, fuel economy, greenhouse gas emissions, cost and overall efficiency; have coincided to bolster the use of turbocharged Diesel engines in the automotive sector. Compared with gasoline engines, Diesel engines have some emission control problems, including lean operation, soot formation and low exhaust gas temperature. Different types of catalytic converters

have been proposed, including close coupled catalysts in addition to standard under floor converters. A proposal that has been made to install a small catalyst before the turbocharger to remove some of the CO from the exhaust gas prior to the main catalyst. A preliminary study to determine the feasibility of this idea was also undertaken.

The breakdown of the rest of this thesis is given in the following.

Chapter 2 gives a general overview on the evolvement of catalytic converters and various aspects involved in the modelling of the catalytic converter. Also present in this chapter is a general introduction to heat transfer in circular ducts. Important literature is discussed in this chapter. Also a summary of the past work done in the study of heat and mass transfer in monoliths using one, two and three dimensional modeling is given.

In Chapter 3, the hydrodynamic length and combined entry length problems are examined and discussed. Results are presented for heat transfer in channels for laminar flow for the case of constant wall temperature, constant wall flux and when there is a reaction at the wall. Also, presented are the results obtained by adding a washcoat of finite thickness with internal diffusion limitation. A comparison between one and two dimensional channel models is presented.

Chapter 4 summarizes the work on two and three dimensional models model of single channel monolith reactor. Here are presented the effect of shape of washcoat and effect of model precision on light-off characteristics.

In Chapter 5, the effect of high velocities and effect of channel diameter at high velocities on conversion is presented. These results are obtained using a one dimensional model in the gas and a two dimensional model for the washcoat.

Finally in chapter 6, some general conclusions about the above mentioned subjects are drawn, and suggestions for future work are given.

2.0 Background and Literature Survey

This chapter provides an introduction to the automotive catalytic converter, and some of the issues faced when modelling them. Heat and mass transfer play an important role in these reactors; therefore, a survey of the literature on heat and mass transfer correlations in duct flow is also given.

2.1 The automotive catalytic converter

Government regulations require that automobile manufactures control the amount of pollutants such as carbon monoxide (CO), hydrocarbons (HC) and oxides of nitrogen (NO_X) that are present in the exhaust of vehicles powered by internal combustion engines. Prior to 1966, exhaust emissions were uncontrolled, but, starting with California in 1966, and followed by the U.S. Federal Government in 1968, strict controls on automotive exhaust emissions began to be implemented. The initial regulations placed limits on the amounts of HC and CO that could be emitted into the atmosphere. Following the introduction of the Clean Air Act of 1970 in the U.S.A., a further decrease in emissions of CO, HC and NO_X was mandated. Early reductions in emissions could be achieved by modifications to engines, however, as the emission limits were reduced, it became evident that some treatment of exhaust gases was necessary to meet the government regulations and at the same time preserve fuel economy.

The post treatment of the exhaust gases in the early years of regulations was primarily focused on oxidation of CO and HC. Oxidation reactions can be either homogeneous (thermal oxidation) or catalytic. Some early units did use thermal oxidation reactors, however, catalytic oxidation has many advantages, provided that a suitable reactor can be designed. Catalytic oxidation of CO and HC is more effective at low temperatures, e.g. as low as 250 °C, whereas thermal oxidation requires higher temperatures. Furthermore, removal of NO_X cannot be achieved in a thermal reactor. As a result, the catalytic converter has been widely adopted as the most technically and economically viable

system in auto-exhaust purification service, and is essentially the only one currently in use (Hayes and Kolaczkowski, 1997).

There are two types of automotive catalyst used today; the three-way catalyst (TWC) and the oxidation catalyst (DOC). The oxidation catalyst is used to oxidize CO and HC to CO_2 and water, and the converter is called as oxidation converter. NO present in the exhaust stream may also be further oxidized to NO_2, especially at higher temperatures. The catalyst usually contains platinum or palladium as the primary active ingredient. The following overall oxidation reactions take place:

$$C_xH_y + \left(x+\frac{y}{2}\right)O_2 \rightarrow xCO_2 + \frac{y}{2}H_2O \qquad (2.1)$$

$$2CO + O_2 \rightarrow 2CO_2 \qquad (2.2)$$

$$2NO + O_2 \rightarrow 2NO_2 \qquad (2.3)$$

Oxidation converters are used mainly for lean burn engines, such as the Diesel engine, where there is a large excess of oxygen present in the exhaust (about 6 % by volume). This converter cannot control NO_X, although some NO_2 production can be beneficial in oxidizing carbon in a downstream particulate filter, if installed. These latter units are designed to trap particulate matter (soot) from Diesel engines and allow their oxidation.

Lean burn engines offer many advantages compared to stoichiometric operation, including lower NO_X production and better fuel economy. However, although NO_X production is relatively low, the concentration is usually not low enough to meet government imposed limits. Therefore, for gasoline engines, the three way catalytic converter was developed. In this system, the engine operates with a stoichiometric air to fuel ratio. The oxidation of CO and HC is achieved by reaction of both the remaining oxygen in the exhaust, as well as the oxygen from the NO_X. The removal of the oxygen from the NO_X is a reduction reaction, which is achieved with the aid of an additional

catalyst, which is usually rhodium. The overall reactions which take place in a TWC can be represented as:

$$C_xH_y + \left(x+\frac{y}{2}\right)O_2 \rightarrow xCO_2 + \frac{y}{2}H_2O \quad (2.4)$$

$$2CO + O_2 \rightarrow 2CO_2 \quad (2.5)$$

$$2NO + 2CO \rightarrow 2CO_2 + N_2 \quad (2.6)$$

Note that these are global reactions only; the actual reaction mechanisms are much more complex and still not entirely clear.

Regardless of the choice of the catalyst, it is necessary to support it on a porous support, which is then introduced into the reactor. The role of the porous support is to disperse the active catalyst over a wide surface area to increase activity. A very classical reactor type used in the process industries is the fixed bed reactor, which contains a bed of porous particles which contain the catalyst. Some early catalytic converters used a small packed bed of catalyst pellets, however, a number of problems, such as catalyst attrition, high pressure drop and bed movement resulted in their early abandonment. At present, the monolith honeycomb reactor is used. The monolith reactor consists of thousands of small diameter channels (ducts) through which the reacting gas flows. The walls of the channels are coated with a layer of catalytically active material; this layer is called the washcoat. This design gives a low pressure drop, is structurally stable, and gives a high surface area to volume ratio, provided that small diameter channels are used. The monolith structure can be made from either metallic alloy or ceramic.

Monolith channels come in variety of shapes, such as circular, square, triangular, hexagonal or sinusoidal (Bhattacharya et al., 2004). They can be made to have a specific size, wall thickness, cell density, and hence a known free cross-sectional flow area. A typical monolith channel is as shown in Figure 2.1 (Hayes and Kolaczkowski, 1997), while some different shapes of monoliths channels are shown in Figure 2.2.

Figure 2.1: Magnified photograph of a cross section that was cut through the monolith. Note the uneven distribution of the washcoat.

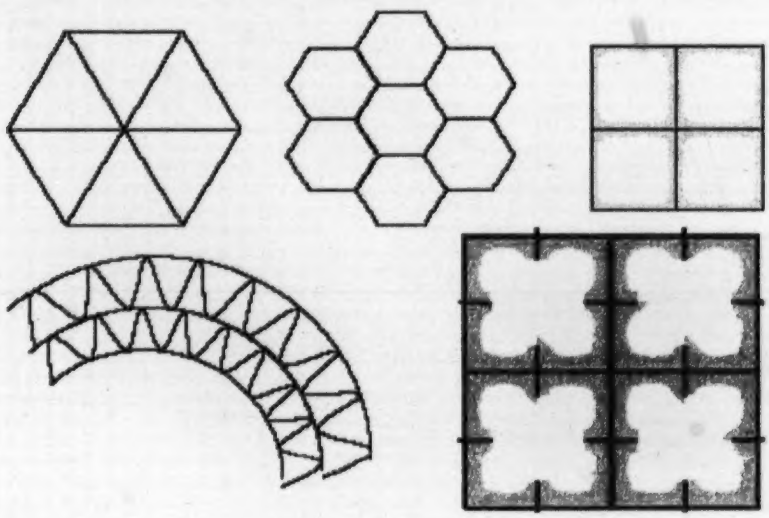

Figure 2.2: Typical monolith channel shapes.

There is a wide selection of high thermal resistance ceramic materials available that can be used as a support material. According to Alexander and Umehara (1995), cordierite has been used to form ceramic monoliths since their inception in 1975. Metal alloys such as fecralloy steel, are also used as support materials. The selection of support depends on the temperature range of operation and catalyst system selected. S-shaped metal supports are widely used nowadays. The surface of the monolith is coated with a layer of high surface area material known as the washcoat. The catalyst is dispersed in the washcoat. Typically a thin washcoat is desired, and a thickness of around 10 μm is a good design target. However, because of the method of manufacture, washcoat thickness usually varies around the perimeter of the channel and can vary from 10 μm up to 150 μm or more. The most widely used washcoat material is gamma alumina ($\gamma - Al_2O_3$), which has a high internal surface area. The choice of washcoat material, small additions of a component to the washcoat and calcining/pretreatment conditions can have a significant influence on the characteristics of the catalyst.

The monolith reactor has been widely used in other catalytic combustion applications, including stationary systems (for example, turbines) (Hayes & Kolaczkowski, 1994) environmental, power and chemical processing applications (Hayes & Kolaczkowski, 1997; Prasad et al., 1984; Donsi et al., 2002) and oxidation of volatile organic compounds (VOC). They have also been used for other reactions, notably liquid-phase hydrogenations (Cybulski and Moulijn, 1994). There widespread use have created a need to build reliable mathematical models to predict the behavior of reacting system such as temperature and concentration, both locally and globally, which in turn influences the design requirements and materials choice.

Typically the monolith reactors used in automotive applications have a channel hydraulic diameter of around 1 mm. Indeed, possibly the most common monolith support is the ceramic one produced by Corning which contains 400 cells (channels) per square inch (CPSI). The channels in this support are about 1 mm in size, which is reduced slightly by the application of the catalytic washcoat. Notwithstanding the relatively high velocity of the exhaust gas in the channels (of the order of 1 to 10 m/s), the small channel size means

that the flow is laminar for most typical automotive applications. The Reynolds number is typically in the range 10-1000.

The performance of the reactor is heavily influenced by heat and mass transfer effects, and to a lesser extent by the hydrodynamics. Figure 2.3 illustrates the mechanism of mass transfer and reaction for a catalyst coated wall (Hayes and Kolaczkowski, 1997).As the reactants move along in the fluid phase, they are transported to the catalyst external surface by molecular diffusion. Once they reach the catalyst external surface, they then diffuse into the porous washcoat where the react. They then diffuse back to the external surface, and thence to the bulk fluid. Heat transfer occurs in an analogous manner; by conduction in the fluid phase and in the washcoat. There are thus two potential sources of mass transfer limitation. The rate of diffusion to the external surface is called external mass transfer limitation. The diffusion limitation in the washcoat is called internal mass transfer limitation.

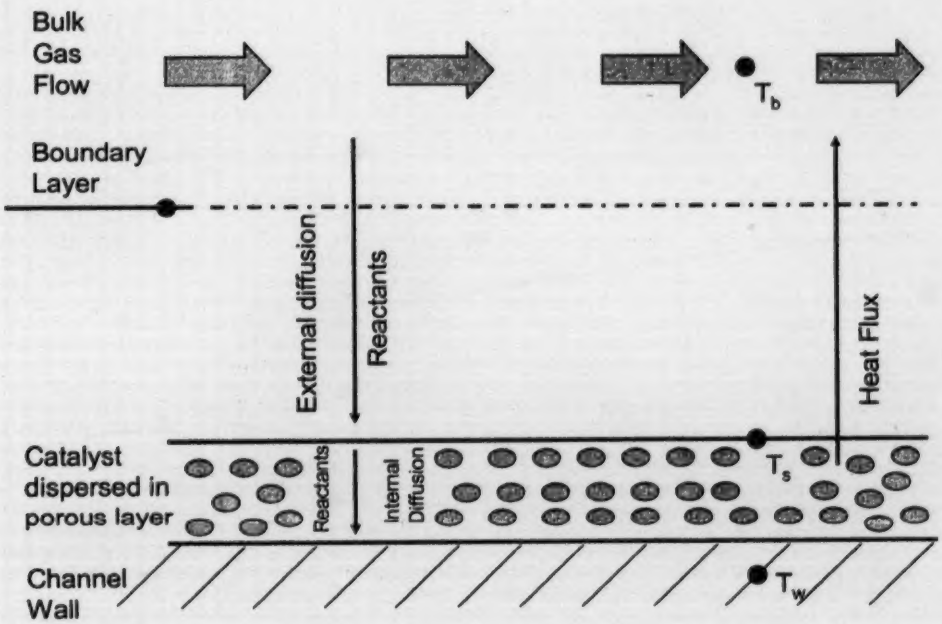

Figure 2.3: Mass transfer and reaction for a catalysis coated wall.

The magnitude of the radial temperature and concentration gradients depends on the relative rates of heat and mass transfer and chemical reaction. The rate of reaction is controlled by the intrinsic kinetics. If the intrinsic rate of reaction is slower than the mass transfer steps, then the rate determining step is the reaction, and the reactor is said to be in the kinetically controlled regime. If the intrinsic rate of diffusion is lower than the intrinsic rate of reaction, then mass transfer will affect the rate. For large external mass transfer resistance, the external surface concentration may be significantly lower than the average bulk concentration. In the extreme case, the catalyst concentration at the surface may go zero and the rate is controlled solely by the rate of external mass transfer.

For bounded flows such as that exist in ducts, the entire system behaves like a well developed boundary layer. At the reactor inlet, the reaction may be kinetically controlled if the temperature is low. As the temperature in the reactor increases, a point may be reached where the rate of reaction may increase very rapidly owing to the Arrhenius temperature dependence of rate constants. This point where the reaction becomes very fast is sometimes referred to as the light-off point, or the ignition point, and the assumption is often made that after light-off, the concentration at wall approaches zero and the reaction is then mass transfer controlled. This assumption has been shown not necessarily to be true (Hayes and Kolaczkowski, 1994). In the automotive literature, the term light-off is also commonly used to refer to the inlet temperature where the conversion in the reactor reaches 50 %. The inlet gas temperature is then called the light-off temperature.

Because the monolith channels are small, it is very difficult to measure experimentally the process variables within the channels. As a result, use has been made of computer simulation as a tool in understanding the phenomena occurring inside of monolith channels. Computer simulation has been used as and particularly in understanding heat and mass transfer effects.

2.2 Heat and mass transfer in ducts

As noted in the previous section, heat and mass transfer play very important roles in catalytic monoliths. The external heat and mass transfer are frequently quantified using heat and mass transfer coefficients, which are in turn usually expressed in terms of the dimensionless Nusselt and Sherwood numbers. Many studies of heat and mass transfer in ducts have been reported, leading to many correlations. However, there is still a degree of uncertainty regarding the correct values to use in the reacting flow case. Before reviewing the methodologies employed in the modelling of monolith reactors, we therefore return to the basics and review heat and mass transfer in circular ducts and summarize some of the literature correlations proposed for different conditions.

Heat is defined as the transfer of thermal energy from one point to another that occurs as a result of temperature difference. Whenever there is a temperature difference, heat transfer must occur. There are three primary modes of heat transfer, namely, conduction, convection and radiation. Conduction refers to the heat transfer that occurs in a stationary medium, convection refers to the heat transfer that occurs between a moving fluid and a surface (or within a moving fluid), and radiation refers to the heat transfer that occurs via electromagnetic radiation.

In this work we are interested in convective heat transfer between the moving fluid and the channel surface. As a result of fluid flow over a heated surface, hydrodynamic and thermal boundary layers develop. The transport of thermal energy across this boundary layer is often expressed using a convective heat transfer coefficient, discussed shortly.

Convective heat transfer is usually classified as either natural or forced, according to the nature of the flow. Forced convection occurs when the flow is caused by external means, such as by a pump or a fan. Natural convection occurs when the flow is driven by density difference between the fluid particles, caused by temperature variations in fluid. No matter how the convective heat transfer occurs, the rate equation for transfer across a fluid/solid interface is of the form (Incorpera and DeWitt, 2002):

$$q" = h(T_S - T_\infty) \tag{2.7}$$

Where $q"$ is the convective heat flux (W/m^2) and is proportional to the difference between the surface temperature (T_S) and fluid temperature (T_∞). Equation (2.7) is commonly referred to as Newton's law of cooling. The proportionality constant, h, is called the convection heat transfer coefficient.

Figure 2.4 illustrates convective heat transfer from a body of arbitrary shape. The flow conditions may vary from point to point on the surface, therefore, $q"$ and h can also vary along the surface. This fact gives rise to the concept of local and average heat transfer coefficients. The total heat transfer rate, q, can be obtained by integrating the local flux over the entire surface.

$$q = \int_{A_S} q" \, dA_S \tag{2.8}$$

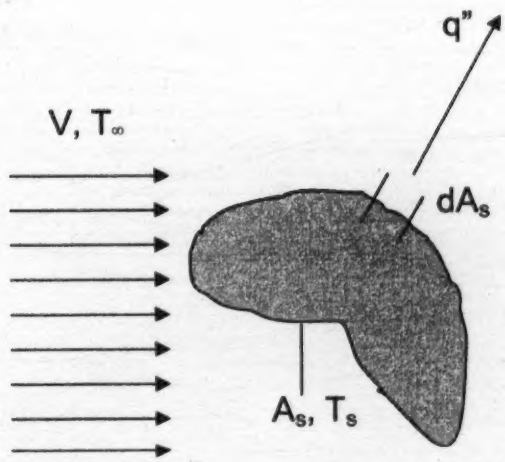

Figure 2.4: Convection heat transfer effects for a surface of arbitrary shape

Substituting the flux from Equation (2.7); and assuming a constant surface temperature gives:

$$q = (T_S - T_\infty) \int_{A_S} h\, dA_S \tag{2.9}$$

Defining an average convective heat transfer coefficient for the entire surface, $\bar{h}$, the total heat transfer rate is expressed as:

$$q = \bar{h}\, A_S (T_S - T_\infty) \tag{2.10}$$

By equating Equation (2.9) and Equation (2.10), it follows that the local and the average convective heat transfer coefficients are related as follows:

$$\bar{h} = \frac{1}{A_S} \int_{A_S} h\, dA_S \tag{2.11}$$

It is important to understand the difference between local and average heat transfer coefficients. Indeed, most correlations for Nusselt number, and most engineering calculations, use the *average* heat transfer coefficient. However, as will be shown shortly we are usually interested in the local value. The heat transfer coefficient is a defined value, that is, it assumes a value such that the rate of heat transfer is predicted accurately with the selected driving force (Hayes and Kolaczkowski, 1997). First, the driving force is selected and then the heat transfer coefficient is defined so that the rate of heat transfer across the boundary layer is accurately predicted. We recall here that the fluid velocity at the surface is zero, and thus the heat transfer there is governed by conduction. Specifying the conduction at the surface using Fourier's law, and equating it to the convection heat transfer defined by Newton's law, gives:

$$h(T_S - T_\infty) = -k_f \left(\frac{\partial T}{\partial y} \right)_{y=0} \tag{2.12}$$

Equation (2.12) can be written in dimensionless form by defining a dimensionless coordinate ($y^* = y / L$) and dimensionless temperature:

$$\theta_T = \frac{T_S - T}{T_S - T_\infty} \tag{2.13}$$

Substituting these definitions into Equation (2.12) and rearranging gives:

$$\left[\frac{\partial \theta_T}{\partial y^*}\right]_{y^*=0} = \frac{Lh}{k_f} = \mathrm{Nu} \tag{2.14}$$

Equation (2.14) relates the dimensionless temperature gradient at the surface to the physical properties of the system, and is represented by a dimensionless quantity known as the Nusselt number, Nu. The Nusselt number is used to characterize heat transfer to and from a moving fluid. The Nusselt number depends on the Reynolds number:

$$\mathrm{Re} = \frac{DV\rho}{\mu} \tag{2.15}$$

and the Prandtl number

$$\mathrm{Pr} = \frac{C_p \mu}{k_f} \tag{2.16}$$

Nu is often determined experimentally, because it is not usually possible to calculate or measure the temperature gradient at the surface especially in turbulent flow.

2.3 Boundary layer development

The heat transfer coefficient depends on the conditions in the boundary layer (which are influenced by the surface geometry), the nature of fluid motion and fluid properties (thermodynamic or transport). One of the most important properties of the boundary layer is the flow pattern, that is, whether the boundary layer is laminar or turbulent. Flow is laminar when the velocities are free of any macroscopic fluctuations, i.e. fluid motion is highly ordered. In a laminar boundary layer it is possible to identify streamlines along which particles move. Turbulent flow is characterized by velocity fluctuations and turbulent boundary layer flow is highly irregular. Because of these fluctuations, heat transfer coefficients tend to be higher for turbulent flow. Typical boundary layer development over a flat plate is shown in Figure 2.5 for illustration purposes. As the fluid encounters the leading edge of the plate, the fluid velocities goes to zero at the surface. The shear force propagates into the fluid causing an ever increasing boundary layer. After some critical distance is passed, the boundary layer undergoes a rapid transition from laminar to turbulent flow. The boundary layer is normally considered to include the fluid with a velocity less than 99 % of the free stream velocity.

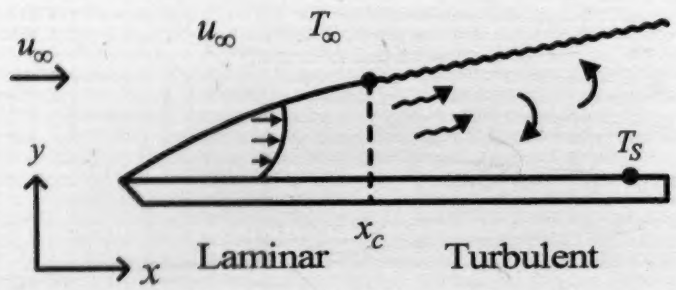

Figure 2.5: Velocity boundary layer development over a flat plate.

If (for example) the surface temperature of the plate is higher then the fluid temperature, then energy is passed from the plate surface to the fluid, causing a thermal boundary layer to develop. This boundary layer will also increase in thickness with distance from the leading edge. The thermal boundary layer will in general not be same thickness as the velocity boundary layer. The diagram of a thermal boundary layer is shown in Figure 2.6.

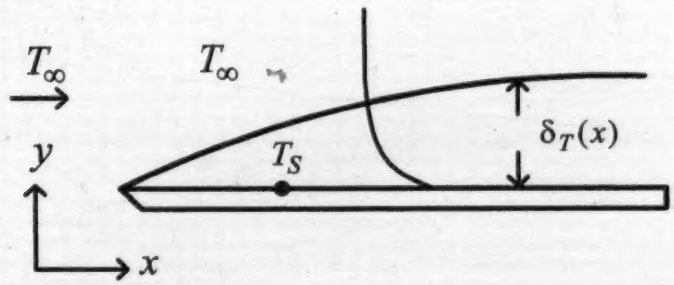

Figure 2.6: Thermal boundary layer development over a flat plate.

The boundary layer is normally considered to end when the dimensionless temperature reaches 98 to 99 % of the free stream temperature, that is, when:

$$\theta_T = \frac{T_S - T}{T_S - T_\infty} = 0.99 \tag{2.17}$$

The thermal boundary layer thickness, δ_T, and the velocity boundary layer thickness, δ, are related by the Prandtl number of the fluid:

$$\frac{\delta}{\delta_T} \approx \mathrm{Pr}^{0.33} \tag{2.18}$$

For a gas, the Prandtl number is less than one, therefore the thermal boundary layer is thicker than the velocity boundary layer, that is, the thermal boundary layer develops more rapidly than the hydrodynamic boundary layer. The Reynolds number is a

dimensionless parameter that is used to characterize a flow pattern. For flow over a flat plate, the transition to turbulence occurs at a Reynolds number (with reference to distance from the leading edge) of about 200,000 to 500,000.

For boundary layer development in the entrance of a circular duct additional factors must be considered. Because the domain is bounded by the walls, the fluid outside the boundary layer is affected by the growth of the boundary layer. The velocity of the fluid in the boundary layer is lower than the free stream velocity of the fluid, so, by the law of conservation of mass, the free stream velocity of fluid must increase as the boundary layer thickness increases. At the point where the boundary layer thickness equals the radius of the duct, no further growth is possible and the flow is considered to be fully developed. The length of duct that passes before the flow becomes fully developed is called the hydrodynamic entry length. This process is illustrated in Figure 2.7.

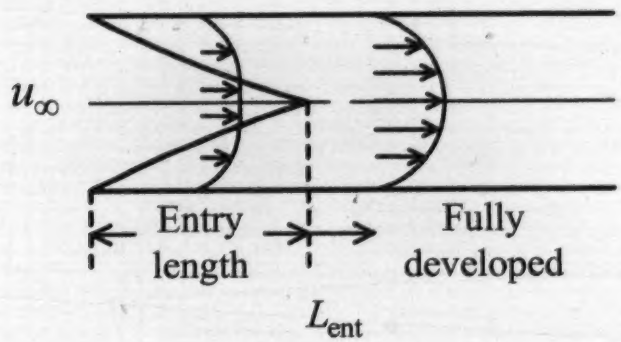

Figure 2.7: Hydrodynamic entry length in a duct.

The entry length depends on the tube diameter, D, and the Reynolds number Re (based on diameter). A common expression for the hydrodynamic entrance length (L_{ent}) is (Hayes and Kolaczkowski, 1997):

$$\frac{L_{ent}}{D} = 0.035\,\mathrm{Re} \tag{2.19}$$

Further discussion on the entry length and additional correlations are given in Chapter 3.

If the surface temperature of the duct is different from the fluid temperature, heat transfer occurs and a thermal boundary layer, and corresponding thermal entry length, will also develop. Note that two conditions are possible. Both the hydrodynamic and thermal boundary layers may start to develop from the duct entrance. This case is referred to as simultaneously developing flow, or a combined entry length flow. Figure 2.8 shows this case for Pr >1.

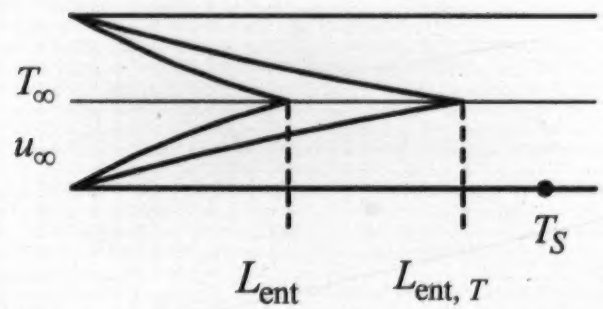

Figure 2.8: Simultaneous development of velocity and thermal boundary layers.

Alternatively, the flow may be fully developed before heating or cooling starts, in which case only a thermal boundary layer is present. This situation is shown in Figure 2.9.

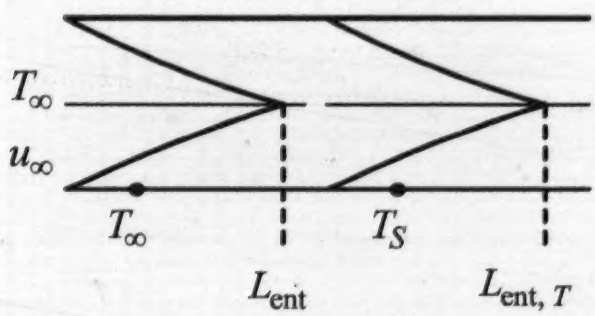

Figure 2.9: Separate development of boundary layers in a duct.

If the boundary condition of the surface of the tube is fixed by imposing either a uniform temperature or a uniform flux, a thermally developed condition is eventually reached. This is equivalent to saying that the dimensionless fluid temperature distribution is constant. This condition is represented as:

$$\frac{d\theta_T}{dz} = 0 \tag{2.20}$$

In other words, the dimensionless temperature profile is constant:

$$\theta_T = \frac{T_S - T}{T_S - \langle T \rangle} = \text{constant} \tag{2.21}$$

For laminar flow, a common expression for the thermal entrance length is (Hayes and Kolaczkowski, 1997):

$$\frac{L_{ent,T}}{D} = 0.035\,\mathrm{Re}\,\mathrm{Pr} \tag{2.22}$$

The thermal and the velocity entrance lengths are thus different. For gases, the thermal entrance length is the smaller of the two, because the Prandtl number is less than one.

For fully developed flow inside of a duct, there is no well defined fluid temperature outside of the boundary layer, and therefore no obvious surroundings temperature for defining the driving force. The temperature used is therefore the mixing cup temperature of the fluid in the channel. The mixing cup temperature is defined as:

$$\langle T \rangle = \frac{\int_0^R v_z(r)\rho C_V T(r) r\,dr}{\int_0^R v_z(r)\rho C_V r\,dr} \tag{2.23}$$

For laminar flow, the thermal boundary conditions at the inside wall of the duct plays an important role in determining the average heat transfer flux. The same conditions apply for the case of turbulent flows, but are useful mainly for laminar flows. Shah and London (1978) attempted to systemize the thermal boundary conditions. Numerous thermal boundary conditions can be specified for a duct of uniform cross sectional area. The two classical conditions are the constant wall temperature and the constant wall flux conditions. Shah and London (1978) classified the boundary conditions in three groups:

1. A specified axial wall temperature distribution T_S
2. A specified axial wall heat flux distribution q'
3. A specified combination of axial wall temperature and axial heat flux distribution

To specify these boundary conditions, the following nomenclature was used by Shah and London. The first character (T or H) represents axially constant wall temperature or axially constant heat flux. The second character (1, 2 or 3) represents the above boundary conditions in peripheral direction. For example, H1 represents a constant axial flux with a constant peripheral surface temperature. Shah and London (1978) summarized the thermal boundary conditions for developed and developing flows through singly connected ducts and is given in Table 1. The following nomenclature is used in Table 1:

a'	Duct wall thickness
D_h	Hydraulic diameter of the actual duct
K_p	Peripheral wall heat conduction parameter, $k_W a'/kD_h$
k	Thermal conductivity of fluid
k_W	Thermal conductivity of wall material
m	Exponent in equation, dimensionless
n	Outer normal coordinate at a point on the duct wall inside periphery Γ
n^*	Coordinate n/D_h measured along the outer normal direction at the duct wall inside periphery, dimensionless
q'	Wall heat transfer rate per unit length of duct
q''_p	Peripheral local wall heat flux
R_W	Wall thermal resistance, $k/U_W D_h$
s	Tangential coordinate at a point on the duct wall inside periphery Γ
s^*	Tangential coordinate, s/D_h
t	Temperature of the fluid to a specified arbitrary datum
t_a	Ambient fluid temperature
t_m	Bulk average fluid temperature
t_W	Wall or fluid temperature at the inside duct periphery Γ
t_{Wo}	Wall temperature at the outside duct periphery Γ
$t_{W,m}$	Perimeter average wall temperature
x	Axial (flow direction) coordinate in Cartesian or cylindrical coordinate systems
y, z	Cartesian coordinates across the flow cross section
Γ	Inside periphery of duct wall
γ	Radiative wall heat flux boundary condition parameter

Subscripts

e	Initial value at the entrance of the duct or where heat transfer starts
x	Arbitrary section along the duct length, a local value rather than mean value
W	Wall or fluid at wall

Table 1

Thermal boundary conditions for developed and developing flow through singly connected ducts[†]

Designation	Description	Equations	Applications
T	Constant wall temperature peripherally as well as axially	$t\|_\Gamma = t_W$ = constant, independent of (x, y, z)	Condensers, evaporators, automotive radiators (at high flows)
T3	Constant axial wall temperature with finite normal wall thermal resistance	$t_{Wo}(x,y,z) = t_{Wo}(y,z)$, independent of x $\left\|\frac{\partial t}{\partial n^*}\right\|_\Gamma = \frac{1}{R_W}\left(t_{Wo} - t\|_\Gamma\right)$	Same as those of T with finite wall thermal resistance
T4	Nonlinear radiant-flux boundary condition	$T_a(x,y,z) = T_a(y,z)$, independent of x $\left\|\frac{\partial T^*}{\partial n^*}\right\|_\Gamma = -\gamma\left[T^*\|_\Gamma^4 - T_a^{*4}\right]$	Radiators in space power systems, high temperature liquid-metal facilities, high temperature gas flow systems
H1	Constant axial wall heat flux with constant peripheral wall temperature	q'(x) = constant, independent of x $t\|_\Gamma = t_W$ = constant, independent of (y, z)	Same as those of H4 for highly conductive materials
H2	Constant axial wall heat flux with uniform peripheral wall heat flux	q'(x) = constant, independent of x $k\left\|\frac{\partial t}{\partial n}\right\|_\Gamma$ = constant, independent of (y, z)	Same as those of H4 for very low conductive material with the duct having uniform wall thickness
H3	Constant axial wall heat flux with finite normal wall thermal resistance	q'(x) = constant, independent of x $\left\|\frac{\partial t}{\partial n^*}\right\|_\Gamma = \frac{1}{R_W}\left(t_{Wo} - t\|_\Gamma\right)$	Same as those of H4 with finite normal wall thermal resistance and negligible peripheral wall heat conduction
H4	Constant axial wall heat flux with finite peripheral wall heat conduction	q'(x) = constant, independent of x $\frac{q_p'' D_h}{k} - \left\|\frac{\partial t}{\partial n^*}\right\|_\Gamma + K_p\left\|\frac{\partial^2 t}{\partial s^{*2}}\right\|_\Gamma = ($	Electric resistance heating, nuclear heating, gas turbine regenerator, counterflow heat exchanger
H5	Exponential axial wall heat flux	$q_x' = q_e' e^{mx^*}$ $t\|_\Gamma = t_W$ = constant, independent of (y, z)	Parallel and counterflow heat exchangers with appropriate values of m
Δt	Constant axial wall to fluid bulk temperature difference	$\Delta t(x) = t_{W,m} - t_m$ = constant, independent of x $t\|_\Gamma = t_W$ = constant, independent of (y, z)	Gas turbine regenerator

[†] The Δt boundary condition is primarily applied to thermally developing flow. For fully developed flow, it is the same as H1 boundary condition.

So far the discussion has been limited to incompressible fluid. In combustion applications, the fluid is a gas which expands considerably with temperature, so that the density is not constant. It is therefore incorrect to speak of a fully developed profile in the classical sense, because as long as there is heating, the velocity increases. Also when a reaction occurs at the wall, the boundary condition is neither constant wall temperature nor constant wall flux. Hence, we should be careful while choosing the value of h for use in combustion applications. The above problem can of course be eliminated by solving the proper transport equations for both laminar and turbulent flow, but this can be computationally expensive.

2.4 Correlations for heat transfer coefficients in circular ducts

As discussed earlier, the heat transfer coefficient is conveniently expressed in terms of a non-dimensional parameter known as Nusselt number. The Nusselt number typically depends on the Reynolds and Prandtl numbers. Because of the importance of duct flow in chemical engineering, many attempts have been made to correlate these parameters. In the following, some common expressions are presented for flow in ducts, with an emphasis on developing flow.

2.4.1 Laminar flow correlations

The circular tube thermal entrance problem, known as the Graetz problem, was first investigated by Graetz in 1883 and later quite independently by Nusselt in 1910. The subject of laminar flow in ducts has been studied extensively, and various results are available in literature for a variety of duct cross sections and surface conditions. These results have been compiled in a monograph by Shah and London (1978).

Fully developed velocity and temperature profiles

For a fully developed laminar flow in a circular duct, for incompressible fluids, with constant physical properties the Nusselt number is a function only of the type of boundary condition. For a constant wall temperature boundary condition, the fully

developed Nusselt number is equal to a constant 3.656, while for a constant wall flux boundary condition it is equal to a constant 4.364 (Shah and London, 1978). These results are valid when axial heat conduction and viscous heating effects are neglected.

Effect of axial heat conduction

Axial conduction can be important for the constant wall temperature case, but it does not affect the value of Nusselt number for the constant wall flux case. The Peclet number (Pe = Re Pr) determines whether or not axial conduction is significant or not. Michelsen and Villadsen (1974) employed the method of orthogonal collocation and determined Nusselt number for various Peclet numbers. Then correlations are:

$$Nu = 4.1807\left(1 - 0.0439Pe + ...\right) \qquad \text{For Pe} < 1.5 \tag{2.24}$$

$$Nu = 3.6568\left(1 + \frac{1.227}{Pe^2} + ...\right) \qquad \text{For Pe} > 5 \tag{2.25}$$

Effect of viscous dissipation

The following result for constant heat rate is proposed by Tyagi (1966):

$$Nu = 4.364\frac{1}{1 + 4.364Br} \tag{2.26}$$

Br is the Brinkman number,

$$Br = \frac{\mu V^2}{\left(g_c J q_W'' D\right)} \tag{2.27}$$

Finite wall thermal resistance, T3

Hickman analyzed the thermal entry length problem by a Laplace transform technique and presented a formula for the asymptotic Nusselt number (Shah and London, 1978):

$$Nu = \frac{1 + \left(48/11\right)R_W}{\left(59/220\right) + R_W} \tag{2.28}$$

Radiant flux boundary condition, T4

Kadaner et al. presented the following approximate formula for Nusselt number (Shah and London, 1978):

$$Nu = \frac{8.728 + 3.66\gamma T_a^3}{2 + \gamma T_a^3} \tag{2.29}$$

Specified wall heat flux distribution and H

H1-H4 boundary conditions yield the same heat transfer results for developed velocity and temperature profiles for the symmetrically heated duct. Tyagi presented the following formula for Nusselt number (Shah and London, 1978):

$$Nu = \frac{48}{11}\left(\frac{1}{1 + (3/44)S^* + (48/11)Br'}\right) \tag{2.30}$$

Effect of internal energy sources

If thermal energy is generated within the fluid due to its internal energy, that heat is transferred at the surface and there will be an effect on Nusselt number. Tao (1961) developed the following expression for Nusselt number:

$$\mathrm{Nu} = 4.364\frac{1}{1 + 0.068Q} \tag{2.31}$$

Thermal entry length with fully developed velocity profile

Graetz and Nusselt (Shah and London, 1978) considered an incompressible fluid flowing through a circular tube, with temperature independent physical properties, having a fully developed velocity profile and a developing temperature profile. The tube was maintained at a constant and uniform temperature. The resulting energy equation with the initial and boundary conditions is known as the Graetz problem, and in this case the value of Nu is well known i.e. the Nusselt numbers are, in principle, infinite at x = 0 and decay to their asymptotic (fully developed) values with increasing x.

For the constant wall temperature condition, Kays presents a correlation for average Nusselt number attributed to Hausen, which is of the form (Incorpera and DeWitt, 2002):

$$Nu = 3.66 + \frac{0.0668(D/L)\mathrm{Re}_D \mathrm{Pr}}{1 + 0.04[(D/L)\mathrm{Re}_D \mathrm{Pr}]^{2/3}} \tag{2.32}$$

For Constant wall flux, Shah (1975) presents a correlation for average Nusselt number, which is of the form:

$$Nu_0 = \begin{cases} 1.953\left(\mathrm{RePr}\frac{D}{L}\right)^{1/3}; & \left(\mathrm{RePr}\frac{D}{L}\right) \geq 33.3 \\ 4.364 + 0.0722\,\mathrm{RePr}\frac{D}{L}; & \left(\mathrm{RePr}\frac{D}{L}\right) < 33.3 \end{cases} \tag{2.33}$$

Combined Entry length

For combined entry length, a correlation for average Nusselt number is given by Sieder and Tate (Incorpera and DeWitt, 2002):

$$Nu = 1.86\left(\frac{\mathrm{Re}_D \mathrm{Pr}}{L/D}\right)^{1/3}\left(\frac{\mu}{\mu_s}\right)^{0.14} \tag{2.34}$$

$$\begin{bmatrix} T_S = \text{constant} \\ 0.48 < \mathrm{Pr} < 16{,}700 \\ 0.0044 < \left(\frac{\mu}{\mu_s}\right) < 9.75 \end{bmatrix}$$

2.4.2 Turbulent flow correlations

In turbulent duct flow, the hydrodynamic entrance and thermal entrance lengths are reportedly much shorter than the corresponding lengths in laminar flow. Therefore, results on fully developed turbulent fluid flow and heat transfer are frequently used

without reference to entrance regions except for low Prandtl number liquid metals, since entrance effects are more pronounced for such fluids even in turbulent duct flows.

The thermal boundary conditions specified in Table 1 for laminar flows, are also valid for turbulent flows. However, these boundary conditions are not analyzed for fluids with $Pr \geq 0.5$, because, at high Pr, the thermal resistance is primarily very close to the wall which results in a flat temperature profile over most of the cross section regardless of the thermal boundary conditions. This is not true with low-Pr fluids; the thermal resistance is distributed over the entire cross section which results in temperature profiles similar to laminar flows and is therefore influenced by thermal boundary conditions.

Turbulent flow Nusselt numbers are strongly affected by the variations in fluid properties over the flow cross section induced by large temperature differences. Therefore, these results are valid only for small temperature differences. The functional dependence of Nusselt number upon Re and Pr numbers change considerably for different ranges of Prandtl number. For the case of the combined entry length problem, it is necessary to have a nozzle or bellmouth entrance to approximate this boundary condition.

If the nozzle and tube walls are smooth and the free stream turbulence level is low, a laminar boundary layer will initially form even though the Re number is greater than 2300. In this case, a transition to turbulence will take place farther down the tube. Because of the initial laminar layer, the Nusselt number may not be significantly higher than the fully developed turbulent-flow value. However, if a boundary layer trip is provided at an appropriate point near the tube entrance, a turbulent boundary layer can be obtained virtually from the beginning of the tube, and then the Nu number will be higher in both the entry region and the purely thermal entry region. The boundary layer is apparently always turbulent if the Re number is sufficiently high to result in a turbulent flow far downstream. Some of the most frequently used correlations for turbulent flow are as given in Table 2 (Kakac et al., 1987):

Table 2: Fully Developed Turbulent Flow Nusselt Numbers in a Smooth Circular Duct for Gases and Liquids with Pr > 0.5.

Investigators	Correlations	Remarks
Reynolds	$Nu = (f/2)\,\mathrm{Re}\,\mathrm{Pr}$	Based on single layer model. sometimes referred to as the "Reynolds Analogy" and is theoretically valid for Pr = 1
Nusselt	$Nu = 0.024\,\mathrm{Re}^{0.786}\,\mathrm{Pr}^{0.45}$	Originated by Nusselt, modified by a number of investigators. For Pr < 1 and $10^3 \le \mathrm{Re} \le 10^6$
Prandtl, Taylor	$Nu = \dfrac{(f/2)\,\mathrm{Re}\,\mathrm{Pr}}{1+5(f/2)^{1/2}(\mathrm{Pr}-1)}$	Based on two layer model. Derived independently by Prandtl in 1910 and by Taylor in 1916. For $\mathrm{Pr} \le 10$ and $5\times10^3 \le \mathrm{Re} \le 5\times10^6$
Dittus & Boelter	$Nu = \begin{cases} 0.024\,\mathrm{Re}^{0.8}\,\mathrm{Pr}^{0.4} & \text{for heating} \\ 0.024\,\mathrm{Re}^{0.8}\,\mathrm{Pr}^{0.3} & \text{for cooling} \end{cases}$	Developed for $0.7 \le \mathrm{Pr} \le 120$ and $2500 \le \mathrm{Re} \le 1.24\times10^5$.
Colburn	$Nu = (f/2)\,\mathrm{Re}\,\mathrm{Pr}^{1/3}$ $Nu = 0.023\,\mathrm{Re}^{0.8}\,\mathrm{Pr}^{1/3}$	For $0.5 \le \mathrm{Pr} \le 3$ and $10^4 \le \mathrm{Re} \le 10^5$
Petukhov, Kirillov and Popov	$Nu = \dfrac{(f/2)\,\mathrm{Re}\,\mathrm{Pr}}{C+12.7(f/2)^{1/2}(\mathrm{Pr}^{2/3}-1)}$ where $C = 1.07 + \dfrac{900}{\mathrm{Re}} - \left[\dfrac{0.63}{1+10\,\mathrm{Pr}}\right]$ $Nu = \dfrac{(f/2)\,\mathrm{Re}\,\mathrm{Pr}}{1.07+12.7(f/2)^{1/2}(\mathrm{Pr}^{2/3}-1)}$	The first Petukhov et al. correlation agrees with the most reliable experimental data on heat and mass transfer. It is valid for $0.5<\mathrm{Pr}<10^6$ and $4000 \le \mathrm{Re} \le 5\times10^6$. The second is simplified version of the first.
Gnielinski	$Nu = \dfrac{(f/2)(\mathrm{Re}-1000)\,\mathrm{Pr}}{1+12.7(f/2)^{1/2}(\mathrm{Pr}^{2/3}-1)}$	For $0.5 \le \mathrm{Pr} \le 2000$ and $2300 \le \mathrm{Re} \le 5\times10^6$

2.4.3 Transition flow

Heat transfer results are uncertain in transition flow because of a large number of parameters required to characterize how and when transition occurs. The following correlation developed by Churchill for $0 < \mathrm{Pr} < \infty$ and $2100 \le \mathrm{Re} \le 10^6$, spanning laminar, transition and turbulent flow regimes, is recommended for calculating transition flow Nusselt numbers (Kakac et al., 1987):

$$Nu^{10} = Nu_l^{10} + \left\{ \frac{\exp[(2200 - \mathrm{Re})/365]}{Nu_l^2} + \frac{1}{Nu_t^2} \right\}^{-5} \tag{2.35}$$

Where

$$Nu_l = \begin{cases} 3.657 & \text{for T boundary condition} \\ 4.364 & \text{for H boundary condition} \end{cases} \tag{2.36}$$

$$Nu_t = Nu_o + \frac{0.079(f/2)^{1/2}\,\mathrm{Re}\,\mathrm{Pr}}{(1+\mathrm{Pr}^{4/5})^{5/6}} \tag{2.37}$$

$$Nu_o = \begin{cases} 4.8 & \text{for T boundary condition} \\ 6.3 & \text{for H boundary condition} \end{cases} \tag{2.38}$$

Gnielinski correlation is also valid for transition flow and is given by (Kakac et al., 1987):

$$Nu = \frac{(f/2)(\mathrm{Re}-1000)\,\mathrm{Pr}}{1+12.7(f/2)^{1/2}(\mathrm{Pr}^{2/3}-1)} \tag{2.39}$$

2.5 Concentration boundary layer and the mass transfer coefficient

A concentration boundary layer is developed in a similar manner to the thermal boundary layer if the concentration at the surface of the plate is different from the concentration in the bulk fluid. If the thickness of the boundary layer is δ_C, then the ratio of velocity boundary layer thickness to the concentration boundary layer thickness is:

$$\frac{\delta}{\delta_C} = \mathrm{Sc}^{0.33} \tag{2.40}$$

Where, Sc is the Schmidt number, defined as:

$$\mathrm{Sc} = \frac{\mu}{\rho D_{\mathrm{AB}}} \tag{2.41}$$

The relationship between the thermal and concentration boundary layer thickness depends on the ratio of the Schmidt and Prandtl numbers. Combining Equations (2.18) and (2.40) gives the following relationship:

$$\frac{\delta_T}{\delta_C} = \left(\frac{\mathrm{Sc}}{\mathrm{Pr}}\right)^{0.33} = \left(\frac{\alpha}{D_{\mathrm{AB}}}\right)^{0.33} = \mathrm{Le}^{0.33} \tag{2.42}$$

The ratio of the Schmidt number to the Prandtl number is known as the Lewis number. For many gases it has a value of around one.

In a manner analogous to the heat transfer coefficient, we can define a mass transfer coefficient for predicting the rate of mass transfer. The dimensionless concentration gradient at the wall defines the Sherwood number, as follows:

$$\mathrm{Sh} = \frac{k_m L}{D_{\mathrm{AB}}} \tag{2.43}$$

where, k_m is the mass transfer coefficient, L is the length and D_{AB} is the molecular diffusion coefficient. It is analogous to the Nusselt number. The entrance length for the concentration boundary layer is approximately equal to:

$$\frac{L_{ent,C}}{D} = 0.035\,\mathrm{ReSc} \tag{2.44}$$

When the Lewis number equals, the thermal and the concentration lengths are equal.

The heat and mass balance equations are mathematically identical in form and frequently have identical boundary conditions. The Colburn heat and mass transfer analogy states that for a convection problem that has the same geometry, flow pattern and boundary conditions for heat and mass transfer, then the solution of the mass transfer problem can be obtained by taking the solution of the heat transfer problem and substituting the Sherwood number for the Nusselt number and the Schmidt number for the Prandtl number and vice versa. In catalytic combustion applications, the boundary conditions are often not the same for both heat and mass transfer, but in many cases the analogy is employed regardless.

2.6 Modelling monolithic reactor channels

Mathematical modelling of monolith reactor channels has been used over the past thirty years or so to assist the design and development of automotive catalytic converters. Models of varying complexity have been reported, ranging from one dimensional models without washcoat effects to two dimensional models that include diffusion in the washcoat, and effects such as solid phase conduction, radiation, homogeneous ignition and interactions between the monolith channels. Three dimensional models are rare, largely because of the computational cost in their solution. A complete mathematical model of monolithic reactor will involve solving a three dimensional model with momentum, energy and mass balance equations solved simultaneously. An overview of

the processes occurring in the monolith channel is illustrated in Figure 2.10 (Sinha et al., 1961).

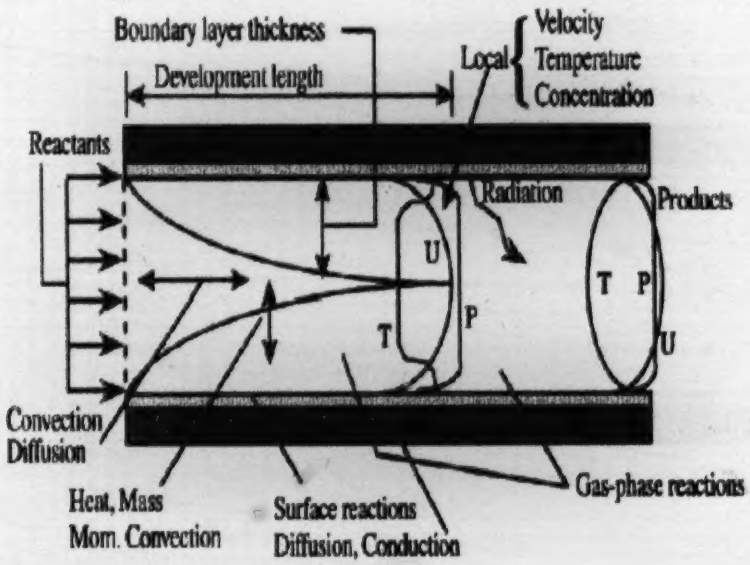

Figure 2.10: Flow and reaction in a single channel monolith

When it comes to modelling the monolith channel, a one dimensional model is often used. The one dimensional model ignores the radial variations in temperature, velocity and concentration and couples the fluid to the wall using heat and mass transfer coefficients. It is therefore not surprising that there have been several papers devoted to the determination of values of Nu and Sh in monolith reactors. As noted earlier in the chapter, the boundary conditions for reacting flows are neither constant wall temperature nor constant wall flux, and should therefore the Nu and Sh should lie somewhere between the values for these two limiting cases. In the following sections, several proposed correlations for the Nu and Sh in reacting channels are reviewed. This is then followed by a discussion of some of the literature on monolith modelling in general.

2.7 Heat and mass transfer correlations for monolith channels

Probably the earliest suggestion for the use of correlations in monolith reactors was proposed by Hawthorn (1974). His proposed correlations for Nu and Sh numbers were simply based on the earlier work of Kays and London (1964) on laminar flow in ducts using constant wall temperature boundary conditions, as follows:

$$Nu = 3.66\left\{1 + 0.095\,\frac{D_T}{L}\,Pe_H\right\}^{0.45} \tag{2.45}$$

$$Sh = 3.66\left\{1 + 0.095\,\frac{D_T}{L}\,Pe_M\right\}^{0.45} \tag{2.46}$$

One point to note is that these equations predict average values for the entire reactor length, and may lead to error if used to predict local values. However, these correlations will also clearly not predict the correct Nu and Sh because the reacting boundary condition is not correctly accounted for. Note that the Colburn heat and mass transfer analogy is used to compute Sh.

In many of the early 1D models, the correlation obtained by Hawthorn (1974) was used. However, many studies both theoretical (Hayes and Kolaczkowski, 1994; Groppi, Tronoconi, Belloli and Forzatti, 1995; Hayes, Kolaczkowski, Thomas and Titiloye, 1996; Wanker, Raupenstauch and Staudinger, 2000; Gupta and Balakotaiah, 2001) and experimental (Vortuba, Sinkule, Hlavaceck and Skrivanek, 1975; Ullah, Waldrum, Bennett and Truex, 1992; Holmgren and Andersson, 1998) have shown that in the presence of a fast superficial reaction, the Hawthorn correlation was not valid. Hayes and Kolaczkowski, 1994; Groppi et al., 1995; Gupta and Balakotaiah, 2001 suggested that the transfer coefficients and thus Nusselt and Sherwood numbers are strongly sensitive to the presence of a reaction at the wall. The thermal energy released by the combustion reaction affects the radial velocity, temperature and concentration profiles, and hence the Nu and Sh number values. Many correlations intended to take these effects into account have been proposed by different researchers. Groppi et al. (1995) proposed a correlation for Nusselt number via an interpolation formula between the constant flux and constant

temperature Nusselt number (discussed shortly). The effect of reaction was included via the Damkohler number. Hayes and Kolaczkowski (1999) demonstrated that Nusselt number depends on inlet gas temperature and reactant inlet mole fraction and the above correlation is not able to correctly describe the observed trends. Hayes and Kolaczkowski, 1999; Wanker et al., 2000, all claimed that heat and mass transfer coefficients have to be calculated by considering the simultaneous development of thermal, concentration and hydrodynamic boundary layer.

With the increase in computational power, the solution of the thermal entry problem with full Navier-Stokes equations and variable properties have become easier. Van Male et al., 2004 investigated the heat and mass transfer in square micro-channels. Pagliarini (1989 and 1991) solved the full Navier-Stokes equations to study the effect of Peclet number on heat transfer with the assumption of constant fluid properties. The author claimed that the heat transfer efficiency depends strongly on the Peclet number, as the diffusion of momentum and heat in axial direction cannot be neglected even at Peclet number larger than the conventional limit of 50. Even the low Pe range is of interest for many catalytic combustion applications.

Many of the currently used correlations for monoliths are based on an interpolation between the values for constant wall temperature and constant wall flux conditions. Grigull and Tratz, 1995 proposed correlations for non-reacting fluids for constant wall temperature and constant wall flux conditions as follows:

$$Nu_T = 3.655 + 6.874\left(\frac{Gz}{1000}\right)^{0.488}\exp\left(-\frac{57.2}{Gz}\right) \tag{2.47}$$

$$Nu_H = 4.364 + 8.68\left(\frac{Gz}{1000}\right)^{0.506}\exp\left(-\frac{41.0}{Gz}\right) \tag{2.48}$$

Tronoconi and Forzatti (1992) proposed the following correlation for the simultaneous boundary layer development for Pr = 0.7 with constant wall temperature.

$$Nu_T = 3.657 + 8.827\left(\frac{Gz}{1000}\right)^{0.545} \exp\left(-\frac{48.2}{Gz}\right) \tag{2.49}$$

Hayes (1996) proposed the following correlation for the simultaneous boundary layer development with constant wall flux for Pr = 0.7.

$$Nu_H = 4.364 + 13.18\left(\frac{Gz}{1000}\right)^{0.524} \exp\left(-\frac{60.2}{Gz}\right) \tag{2.50}$$

Groppi et al. (1995) proposed that Nu in a system with chemical reaction at the wall could be computed using interpolation formula given by Brauer and Fettig (1966). This formula interpolates between Nu_T and Nu_H and is given as follows:

$$\frac{Nu - Nu_H}{Nu_T - Nu_H} = \frac{Da\ Nu}{(Da + Nu)\ Nu_T} \tag{2.51}$$

Where, Da is the Damkholer number, which for a first order reaction is given by:

$$Da = \frac{\eta k_S D_T}{4 D_a} \tag{2.52}$$

Equation (2.51) may be rearranged to express Nu explicitly as:

$$2Nu = Nu_H - Da\frac{Nu_H}{Nu_T} + \sqrt{\left(Nu_H - Da\frac{Nu_H}{Nu_T}\right)^2 + 4DaNu_H} \tag{2.53}$$

Most of the work previously reported is devoted to circular channels. For square channels, Groppi et al., (1995) proposed correlations for Nu in the thermally developing region with hydrodynamically developed flow. For constant wall temperature and constant wall flux conditions the two correlations are, respectively:

$$Nu_T = 2.977 + 6.854\left(\frac{Gz}{1000}\right)^{0.5174} \exp\left(-\frac{42.49}{Gz}\right) \tag{2.54}$$

$$Nu_H = 3.095 + 8.933\left(\frac{Gz}{1000}\right)^{0.5386} \exp\left(-\frac{6.7275}{Gz}\right) \tag{2.55}$$

Groppi and Tronoconi (1997) proposed correlations for triangular channels. For constant wall temperature and constant wall flux they are:

$$Nu_T = 2.495 + 6.507\left(\frac{Gz}{1000}\right)^{0.434} \exp\left(-\frac{44.02}{Gz}\right) \tag{2.56}$$

$$Nu_H = 1.890 + 6.066\left(\frac{Gz}{1000}\right)^{0.439} \exp\left(-\frac{30.71}{Gz}\right) \tag{2.57}$$

There are also experimental investigations in the literature. Vortruba et al. (1975) proposed a correlation for Sherwood number based on experimental data from chemical vaporization experiment:

$$Sh = 0.705\left(\mathrm{Re}\frac{d}{L}\right)^{0.43} Sc^{0.56} \tag{2.58}$$

This correlation predicts relatively low values for the Sherwood number, and it is not usually used at present. Uberoi and Pereira (1996) also proposed an empirical model for the gas-solid mass transfer in monolith channels:

$$Sh = 2.696\left(1 + 0.139\,\mathrm{Re}\,Sc\frac{d}{L}\right)^{0.81} \tag{2.59}$$

Finally, an expression proposed by Holmgren and Andersson (1998) is:

$$Sh = 3.53\exp\left(0.0298\,\mathrm{Re}\,Sc\frac{d}{L}\right) \tag{2.60}$$

In spite of all of the previous investigations, there remains a lack of consensus as to the best values of heat and mass transfer coefficients to use when performing one dimensional modelling of monolith reactors.

2.7 Review of modelling of monolith channels

This section presents a brief overview of some of the more relevant literature works on the modelling of monolith channels, especially as related to heat and mass transfer effects. There are many studies describing experimental, modelling and simulation results in monoliths. Different models of monolithic reactors have been developed at different levels of complexity. The most accurate is the three dimensional model in which the equation of motion is considered, but it is computationally expensive to solve. Two dimensional models, both steady state and transient, have also been developed. In most of the cases, the momentum balance equations are not solved, and a parabolic or a flat velocity profile is used. In some papers, the momentum balance equation coupled with mass and energy balance equations have been solved. However, computational time increases with the complexity of the model. Solution of a 2D model coupled with Navier-Stokes equation used to take many hours, so oversimplified 1D model were often used. However, with present day computational power, a 2D model takes much less time than before. 1D model may lead to incorrect results if thermal and mass fluxes between bulk gas phase and surface are not correctly evaluated. Therefore, proper estimation of local fluxes and inter-phase transfer coefficient is needed.

Wei (1975) reviewed the early literature on shallow packed-bed type converters and monoliths. Articles by Cybulski and Moulijn (1994), Lox and Engler (1997), Groppi, Tronoconi, and Forzatti (1999) and books by Becker and Pereira (1993) and Hayes and Kolaczkowski (1997) summarize the recent progress in the field (As cited in Ramanathan et.al, 2006).

Heck, Wei, and Katzer (1976) and Young and Finlayson (1976) presented early modelling and simulations of monolithic reactor using one dimensional two phase models

and two dimensional models with radial gradients. Experimental and theoretical results on the simultaneous development of velocity and concentration profiles in the entrance region of an isothermal monolithic converter were presented by Boersma, Tielen, and Van Der Bann in the year 1978. Hegedus (1975), Hegedus, Oh, and Baron (1977) and Oh, Baron, Cavendish and Hegedus (1978) presented experimental results for CO and H_2 oxidation in monoliths under isothermal and adiabatic conditions.

Young and Finlayson (1976) presented transient simulations for CO oxidation using two dimensional models with radial gradients (they neglected the conduction in solid) as well as one dimensional two phase models. Heck et al. (1976) reported that a simple 1D model was adequate for predicting monolith behaviour. Lee and Aris (1977) developed a 2D two phase model which included radiation effects. Otto and LeGray (1980) validated their model with experimental results and presented model predictions regarding the efficiency of converter for different designs. Oh et al. (1982) through a one-dimensional adiabatic channel model studied the response of a monolithic catalytic converter to step changes in feed temperature.

These as well as many other authors claimed that the local heat and mass transfer reaches a peak at ignition points. In 2001, Gupta and Balakotaiah claimed that the peak in the transfer coefficients was false and arises due to the Gibbs phenomenon associated with the approximation of discontinuous functions by polynomials or other continuous functions i.e. the true transfer coefficients take a discontinuous downward jump from the slow reaction (constant flux) asymptote to the fast reaction (constant wall temperature) asymptote at the ignition point. This latter behaviour was shown by Leung et al. (1996)

Oh and Cavendish (1982) used a one dimensional two phase model with constant Nusselt and Sherwood numbers to simulate the transient behaviour of the automobile catalytic converter with global kinetic models for all of the main reactions. Zygourakis (1993) considered position dependent transfer coefficients with radially non-uniform flow distributions to simulate the transient behaviour. Tronoconi and Forzatti (1992) and Groppi, Tronoconi, Belloli and Forzatti (1995) compared 1D and 2D model predictions

using position dependent transfer coefficients in the mass transfer controlled region for 1D model. They concluded that a 1D model can adequately describe the ignited branches with position dependent transfer coefficients.

Most of the studies of the monolithic reactor used dimensionless form of the transport, energy and mass balance equations. Most were also confined to specific cases (reactor kinetics) and limited ranges of parameter values (Ramanathan et al., 2003). Eigenberger (1972) and Oh and Cavendish (1982) presented transient simulations which illustrated the light-off behavior and propagation of temperature fronts in monoliths and packed beds respectively. Please, Hagan and Schwendeman (1994), Leighton and Chang (1995) and Keith, Chang and Leighton (2001) analyzed the propagation of the ignition front in the monolith using a 1D two phase model with constant transfer coefficients. However, they neglected the washcoat diffusion which is known to have a significant influence on the light-off behaviour of the converter in some cases.

Papoutsakis and Ramkrishna (1980), Silvia et al. (2001) focused on the analytical solution of the Graetz problem using the classical wall boundary conditions (T and H), by solving the energy equation including axial conduction for given velocity profiles in the circular channel. As cited in Donsi et al., 2005, other researchers assumed fully developed parabolic velocity profile in the channel, solving the energy equation with axial gas diffusion but with constant fluid properties, not only for circular ducts (Nguyen, 1991; Bihr, 1995; Nguyen, 2001; Kilic, 2004) but also for annular ducts (Weigand et al., 1997), rhombic ducts (Lee and Lee, 2002) and irregular ducts (Uzun and Ünsal, 1997).

Al-Ali and Selim, 1992 (for circular channels) and Spiga and Morini, 1996; Tunc and Bayazitoglu, 2002 (for rectangular channels) solved the momentum equation for determination of velocity profile and substituted that into the energy equation to get a solution. Shome and Jensen (1992) used a very fine grid at the tube inlet and revisited the available solutions for simultaneously developing laminar flow and heat transfer in ducts. The coupled momentum and energy balance equations were solved with the assumption of constant fluid properties and negligible gas axial conductivity.

Although the wall concentration is lower than the average radial concentration, Hayes and Kolaczkowski (1994) demonstrated that true mass transfer control may be difficult to achieve in a 1-2 mm diameter channel at moderate temperatures, although they suggested that it is easier to achieve in larger diameter channels. They defined a catalytic reaction number whose value determined whether or not a reaction was in the mass transfer or kinetic control regime. The controversy over controlling mechanism has led to some confusion concerning the values of Nusselt and Sherwood numbers.

Ramanathan et al. (2004) and Hayes et al. (2004) suggested that the ignition of catalytic monoliths is also influenced by geometry effect, which must be taken into account when modelling catalytic monolithic reactors. Hayes and Kolaczkowski (1994); Leung et al. (1996), Mukadi and Hayes (2002), Hayes et al. (2004) clearly showed that diffusion limitation is significant under many operating conditions. There are two important types of potential mass transfer limitations in these reactors. The first is diffusion limitation in the washcoat owing to fast reaction and second is the transverse diffusion of reactants from bulk gas phase to the surface of the washcoat. Many early researchers neglected the washcoat diffusion, which lead to errors in the prediction of the reactor performance. Dalla Betta et al., (1992); Leung et al., (1996); Hayes et al., (2001) suggested the use of "diffusion barriers" to control the reaction rate.

Most of the models developed are based on laminar flow. In reality, a certain degree of turbulence may be there, which will enhance the heat and mass transfer rates. The flow is, for most applications, naturally turbulent when entering the monolith and a turbulent to laminar transition takes place over some distance in the channel. Turbulence can also be generated by the monolith walls at the entrance and also by the surface roughness of the channel walls. Not much work has been done on turbulence in monolithic reactors, since the techniques available to turbulence intensities are difficult to use in small channels.

Direct numerical simulations (DNS) have been used to resolve all the scales of turbulence but they are very time consuming and have so far only been solved for simple flows. Some indirect measurements of the inlet effects of turbulence and developing boundary

layers are available. Borsema et al. (1978) and Wendeland (1980) claimed that inlet effects increases the conversion significantly.

2.9 Overview of the finite element method (FEM)

In this work, the partial differential equations used to describe the momentum, energy and mole conservation equations were solved using the finite element method (FEM). A brief overview of the FEM is given in this section.

The finite element method approximates a PDE problem with a problem that has a finite number of unknown parameters. The advantages of FEM are the ease of handling complex geometries, straightforward implementation of non-uniform meshes and the simple incorporation of flux boundary conditions. The FEM solution of a problem involves the following steps (Hayes and Kolaczkowski, 1997):

a) discretizing the domain
b) expressing the differential equation in weak form
c) discretizing the weak form
d) integrating the discrete weak form
e) assembling the discrete integrated weak form into a global system of simultaneous equations to give the solution

In FEM, the domain is divided into sections called elements. The elements must account for the entire solution domain and no two elements may overlap. For a 1D domain, elements are line segment of domain. For a 2D domain, elements are rectangles, triangles or quadrilaterals. For a 3D domain, elements are tetrahedrons or hexahedrons. Associated with an each element are a set of nodes. Each end point corresponds to nodes in a line element and the apexes of the triangles or quadrilaterals are nodes. The finite element solution of the problem gives values of the dependent variables at the node points,

interpolation techniques are then used between node points in order to obtain a solution throughout the entire domain.

Galerkin method is generally used to solve the partial differential equations using FEM. It is simple to implement and can be used even when other methods such as Rayleigh-Ritz cannot be used. In the Galerkin method, the independent variable is approximated by a finite series in which the general 'shape' of the solution is assumed to be known. It is based on the method of weighted residuals. The approximation is of the form:

$$\phi(x,y) = \sum_{i=1}^{n} \gamma_i \phi_i(x,y) \tag{2.61}$$

Where, n is the number of nodes in the element, i denote nodes, ϕ_1, ϕ_2 ..... ϕ_n and γ_1, γ_2.....γ_m are constants. Using conduction in one dimension as an example, the governing equation is:

$$\frac{\partial}{\partial x}\left(k\frac{\partial T}{\partial x}\right) = 0 \tag{2.62}$$

Depending on the boundary conditions, a solution for Equation (2.62) exists. Substitution of a temperature field $T_a(x)$ which is not the solution results in the residual:

$$\frac{\partial}{\partial x}\left(k\frac{\partial T_a}{\partial x}\right) = R_E\left(T_a, x\right) \tag{2.63}$$

We cannot find the exact solution of the problem using numerical methods and therefore the goal is to find a value of T_a which minimizes the residual, R_E. Ideally R_E should be zero, but this cannot be achieved. The principle of MWR is now applied to the residual i.e. the residual is multiplied by a weighting function, W(x), then find the values for T_a which minimizes the integral of the weighted residual, I_D:

$$I_D = \int_0^L W(x) R_E\left(T_a, x\right) dx \tag{2.64}$$

To obtain a good solution, a higher order approximation of W(x) is required for a global minimization. This is not desirable from mathematical point of view and the minimization is therefore carried out piecewise on each element of the domain, giving one equation for each element. In the Galerkin method, the weighting functions are the interpolation functions used in the finite elements.

The approximate solution must also have second derivatives since the differential equation to be solved usually contains second derivative terms. This condition is restrictive because of the piecewise nature of approximation. The principle of integration by parts is used to relax this condition and it transfers half of the differentiation to the interpolation function. In one dimension it is given by:

$$\int_0^L W(x)\frac{\partial}{\partial x}\left(k\frac{\partial T}{\partial x}\right)dx = W(x)k\frac{\partial T}{\partial x}\Big|_0^L - \int_0^L \frac{\partial W(x)}{\partial x}\left(k\frac{\partial T}{\partial x}\right)dx \qquad (2.65)$$

The integrated form, represented by Equation (2.65), is known as the weak form of the original equation as it contains only first derivatives. When the weak equation is written in discrete form, the boundary condition term vanishes for all interior elements. It is usually necessary to use a numerical method to integrate the elementary integral equations. The most commonly used method is Gaussian quadrature. If we consider a 1D function which is to be integrated over the domain [-1, 1] as follows:

$$I = \int_{-1}^{1} f(\xi)d\xi \qquad (2.66)$$

Then, Gaussian quadrature states that the value of the integral is equal to the sum of the product of weighting functions and the value of the function $f(\xi)$ is given as follows:

$$I = \int_{-1}^{1} f(\xi)d\xi = \omega_1 f(\xi_1) + \omega_2 f(\xi_2) + \ldots + \omega_i f(\xi_i) + \ldots \qquad (2.67)$$

3. Two dimensional study of Nu and Sh numbers in monolith reactor for laminar flow

In Chapter 2 some of the many correlations proposed for heat and mass transfer coefficients in circular ducts for laminar flow were discussed, both in the entry length and for the fully developed flow cases. Further, some of the attempts at deriving correlations for reacting flows were presented. Indeed, it might be tempting to assume that this problem is now so classical that there is nothing more to discover in this area. However, it should be pointed out that much of the classical and currently accepted results were originally developed using a number of simplifying assumptions, including incompressible flow (constant density fluid) and constant physical properties. Variable properties, such as viscosity and density, are expected to influence the velocity profile shape. Further, for a gas, there will be flow acceleration as long as the fluid is heated, which is certainly the case when an exothermic chemical reaction occurs.

Entry length calculations have mostly been made using simplified forms of the Navier-Stokes equations, owing to a historical lack of computational power for the complete solution. In spite of recent advances in computer power and software sophistication, much of the historical work has not been revisited. For the reacting case, the wall boundary condition is neither constant temperature nor constant flux, so the classical equations do not apply in any case. Although there have been attempts in the past to account for this, there is still some disagreement in the literature as to the best equations to use. One can eliminate all of the uncertainty involved with making any approximations by solving the proper transport equations, but this can lead to costly solutions, in spite of the recent increase in computer power.

The purpose of this chapter is to explore the Nu and Sh number behaviour for a compressible fluid for the case of constant wall temperature, constant wall flux and when there is a reaction at the wall, to enable a critical examination of earlier work.

3.1 Hydrodynamic entry length

As seen in Chapter 2, the fluid undergoes a flow development after it enters a circular tube. This entry length problem for developing flow is very classical, and has been the subject of much investigation. The hydrodynamic entry length can be expressed in terms of the entry length to pipe diameter ratio, which depends on the Reynolds number, and is usually given as:

$$\frac{L_{ent}}{D} = C_1 \mathrm{Re} \tag{3.1}$$

The constant C_1 has been reported by different researchers to have a value in the range of 0.03 to 0.08. A review of the literature on entry length is given in a recent paper by Durst et al. (2005). They point out that Equation (3.1) ignores the influence of the diffusion of momentum, which could be expected to be significant at very low Reynolds number. A relationship to account for the diffusion effect was proposed by Atkinson et al., 1969 (ref. 22 in Durst):

$$\frac{L_{ent}}{D} = C_0 + C_1 \mathrm{Re} \tag{3.2}$$

Recently, Durst et al. (2005) investigated developing laminar pipe flow. They reported that even Equation (3.2) does not correctly predict the development length for Reynolds number less than 100. As a first step in the present investigation, the hydrodynamic development length in a circular pipe was studied, based on the full solution of the equation of motion. Steady laminar flow is governed by the Navier Stokes equation:

$$\rho(v\bullet\nabla)v = \nabla\bullet\left[-pI + \eta\left(\nabla v + (\nabla v)^T\right) - \left(\frac{2\eta}{3} - \kappa\right)(\nabla\bullet v)I\right] \tag{3.3}$$

The equation of continuity (conservation of mass) at steady state is:

$$\nabla\bullet(\rho v) = 0 \tag{3.4}$$

This equation was solved in a 1 mm diameter tube, length 10 cm, using the finite element method. The boundary conditions used were flat velocity profile at the inlet, zero slip condition at the wall, symmetry condition at the axis and zero normal shear stress at the outlet. The range of Reynolds number used was 0.5 to 1550. The solution to the model was obtained using the finite element method package COMSOL multiphysics. Triangular elements were used with a fine mesh near the wall to capture the sharp gradients there. The total simulation time for one simulation was around 20 minutes.

Figure 3.1 shows the axial centreline velocity as a function of distance. As is well known, the centreline velocity increases to twice the average velocity as the boundary layer develops. The point where the centreline velocity reached 98 % of the final value was used as a criterion for fully developed flow (Durst et al., 2005)

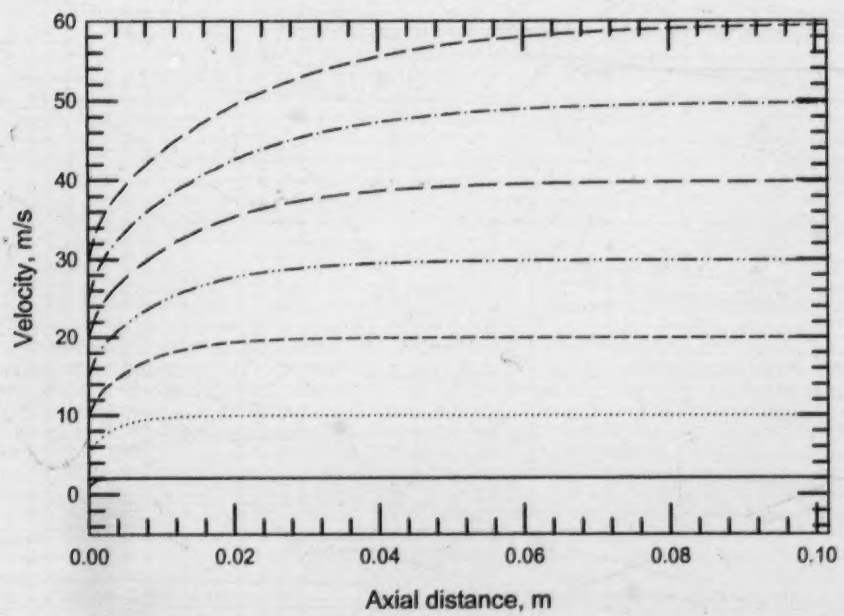

Figure 3.1: Velocity profile along the length of the reactor to examine the hydro-dynamically developing region without heat transfer.

The behaviour of the entry length as a function of Re is shown graphically in Figure 3.2. For comparison purposes, the results predicted from Equation (3.1) using C_1=0.035 and from Equation (3.2) using C_0=0.619 and C_1=0.0567 are also shown (Durst et al., 2005). It is seen that neither solution matches our results. Indeed, our results indicate that the developing flow solution is bounded by two asymptotic solutions corresponding to the low and high Reynolds regions respectively. At high Re there is a linear dependence of the entry length on Re, whilst at low Re it is constant. The two solutions can be combined using the asymptote matching technique of Usagi and Churchill (1972) to give a solution of the form:

$$\frac{L_{ent}}{D} = \left[(0.54)^{1.62} + (0.05\,\mathrm{Re})^{1.62}\right]^{\frac{1}{1.62}} \tag{3.5}$$

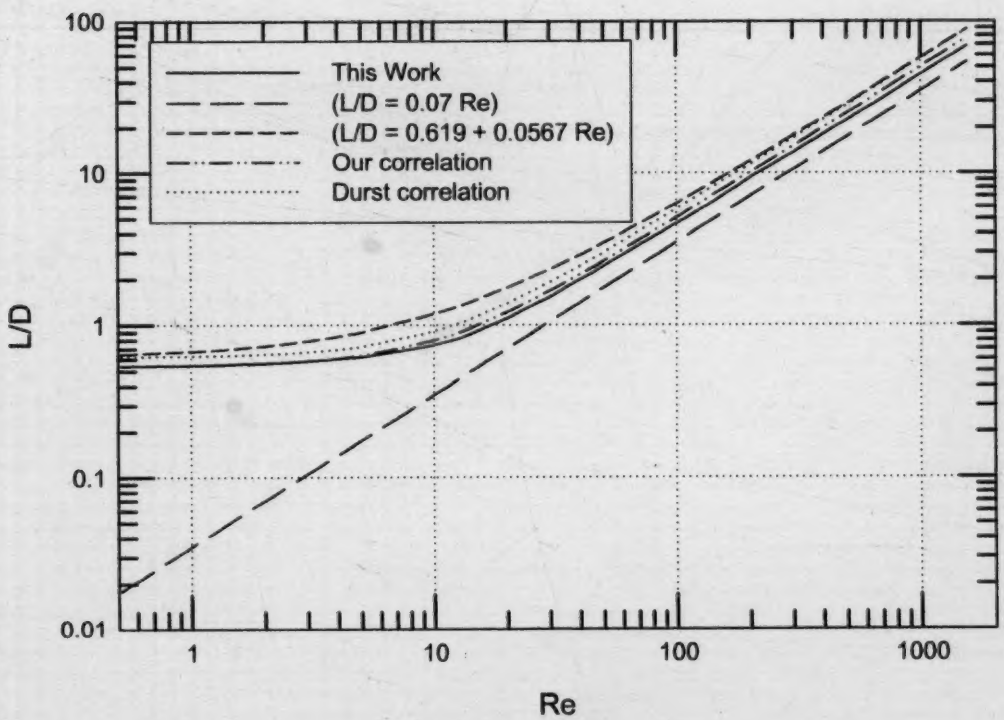

Figure 3.2: Predicted development length comparison and comparison with relationship given by Durst and by Equation (3.1) and (3.2).

Equation (3.5) predicts the numerical data within a maximum error of 11 %. Durst et al. (2005) also computed these constant and found them to be $C_0 = 0.619$ and $C_1 = 0.0567$ and the correlation given by Durst is given as follows:

$$\frac{L_{ent}}{D} = \left[(0.619)^{1.6} + (0.0567\,\mathrm{Re})^{1.6} \right]^{\frac{1}{1.6}} \tag{3.6}$$

The correlations given in Equation (3.5) and Equation (3.6) are compared with the modeling results and are also shown in Figure (3.2). This asymptotic solution at low Re suggests that accurate modelling of the low Re solution is necessary to capture accurately the developing length. However, it should be pointed out that for Re less than 10, the hydrodynamic entry region will be less than one channel diameter. In this case, for monolith reactors of typical length of greater than at least 25 diameters, one could probably safely ignore the entry region and assume fully developed flow everywhere.

3.2 Combined entry length without reaction

In Chapter 2, some of the correlations proposed for simultaneous development of velocity and thermal boundary layers were presented. Most of these correlations are based on various assumptions, such as linearization of momentum equation, solution of energy equation decoupled from the momentum equation, hence neglecting the thermal expansion effect on flow, or constant fluid properties (As cited in Donsi et al., 2005).

Despite the recent increase in computational power and improvement in accuracy of numerical solvers, there has not been a great deal of advance reported since the classical review of Shah and London (1978). Reading the literature, it also appears that the classical combined entry length problem has not been revisited for variable density fluids.

In this stage of the investigation, steady state simulations were performed to examine the hydrodynamically developing region and thermal entry region with heat transfer for laminar flow in tube for the two classical boundary conditions at the wall; constant wall

temperature and constant wall flux. The Navier Stokes equations given by Equations (3.3) and (3.4) were coupled with the conduction-convection equation. The gas was assumed to be ideal, and the density was assumed to be given by the ideal gas law. The boundary conditions for the momentum balance equations were the same as used previously. The energy balance for the gas is given by:

$$\nabla\cdot\left(k_f \nabla T\right) - \left(\rho C_p\right)_f v\cdot\nabla T = 0 \tag{3.7}$$

The boundary conditions are:

$$T = T_o \text{ at } z = 0 \text{ and } r \neq R \tag{3.8}$$

$$\frac{\partial T}{\partial z} = 0 \text{ at } z = L \text{ and } r \neq R \tag{3.9}$$

$$\frac{\partial T}{\partial r} = 0 \text{ at } r = 0 \text{ for all } z \tag{3.10}$$

The wall conditions were either constant wall temperature:

$$T = T_W \text{ at } r = R \text{ for all } z \tag{3.11}$$

or constant wall flux:

$$q_s'' = \text{constant at } r = R \text{ for all } z \tag{3.12}$$

The Nusselt number value was calculated from the computed radial temperature profiles as follows:

$$Nu = \frac{D}{\left(T_W - \langle T\rangle\right)} \left.\frac{\partial T}{\partial r}\right|_{r=R} \tag{3.13}$$

The mixing cup temperature $\langle T\rangle$ is given by:

$$\langle T \rangle = \frac{\int_0^R v_z(r)\rho C_V T(r) r\, dr}{\int_0^R v_z(r)\rho C_V r\, dr} \tag{3.14}$$

The operating condition used was a four inch tube with an inlet velocity of 10 m/s which corresponds to a Reynolds number of 515, referenced at T = 350 K and P = 1 atm. The wall temperature was fixed at 500 K for constant wall temperature condition. The thermal conductivity of the gas in units of W/ (m·K) was taken as that of air, expressed as a linear function of temperature using values from (Incropera and DeWitt, 2002).

$$k_f = 1.679\times10^{-2} + 5.073\times10^{-5}T \tag{3.15}$$

The heat capacity was expressed as a fourth order polynomial in temperature (Hayes and Kolaczkowski, 1997).

$$C_P = 28.09 + 0.1965\times10^{-2}T + 0.4799\times10^{-5}T^2 - 1.965\times10^{-9}T^3 \tag{3.16}$$

The density was calculated from the ideal gas law.

$$\rho = \frac{PM}{RT} \tag{3.17}$$

The fluid viscosity was expressed as a second order polynomial in temperature (Hayes and Kolaczkowski, 1997).

$$\mu = 7\times10^{-11}T^2 + 6\times10^{-8}T - 1\times10^{-5} \tag{3.18}$$

In the first instance, the fluid was assumed to have constant properties, as in the classical analysis. This simulation was performed to test the software and to verify the classical result. The simulator was then run for the case of variable properties. The results from both cases are shown in Figure 3.3. For the case of the constant density fluid, the classical result was obtained, however, for the case of the ideal gas, the Nusselt number shows a drop below the final asymptotic value of 3.66 is reached. This result seen for the ideal gas has not been reported before in the literature, as far as we know.

To test which property had the most effect on the Nusselt number, a series of simulations were performed in which (a) one property was held constant and the rest allowed to vary with temperature and (b) all properties except one were held constant. Figure 3.4 and 3.5 shows the result from these simulations. It is seen that density, thermal conductivity and viscosity variations all have a significant effect on the Nusselt number in the entry region.

Since it was observed that properties varying with temperature have an effect on the Nu value, simulations were next performed with different wall temperature to see whether increasing or decreasing the wall temperature had an effect on the Nu value or not. The results from these simulations are shown in Figure 3.6. It was observed that changing the wall temperature has a significant effect on the Nu value. It is perhaps not surprising that the entry region Nu will change when the temperature difference changes. When the temperature difference between the wall and bulk changes the heating rate will also change. As a result the acceleration of fluid will be affected, as will the values of the physical properties.

However, an important consequence of this type of behaviour in the entry region is that it is not possible to obtain a single simple correlation for the Nu number as a function of reciprocal Gz number, for this region as discussed in Chapter 2. Thus, the interpolation formula of Brauer and Fettig (1966) cannot be used with perfect accuracy.

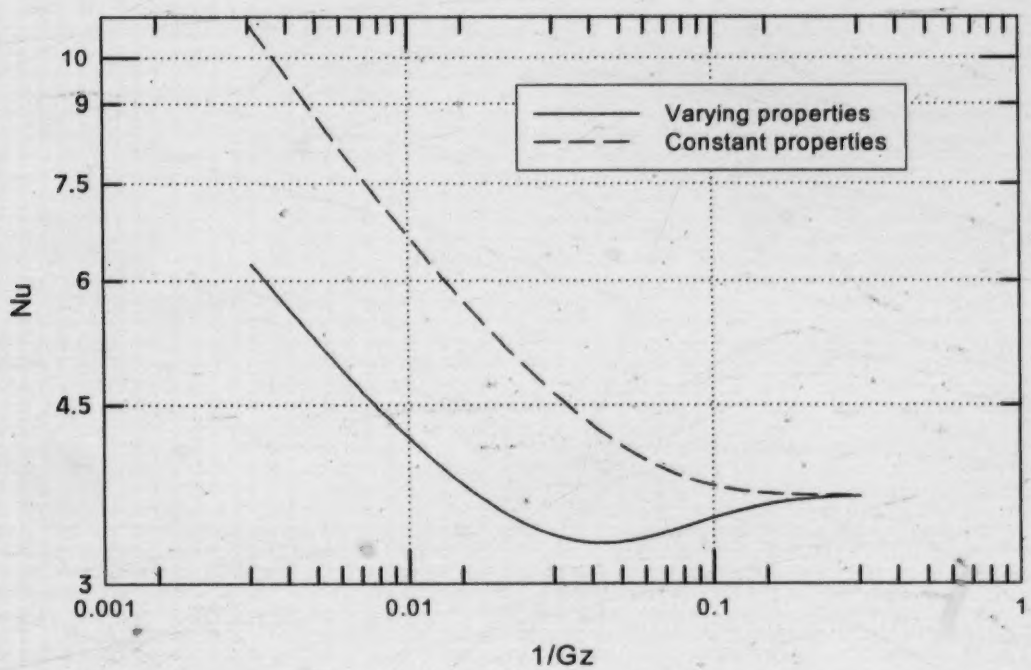

Figure 3.3: Local Nusselt number obtained from entry length solutions for laminar flow in a channel with constant wall temperature of 500 K.

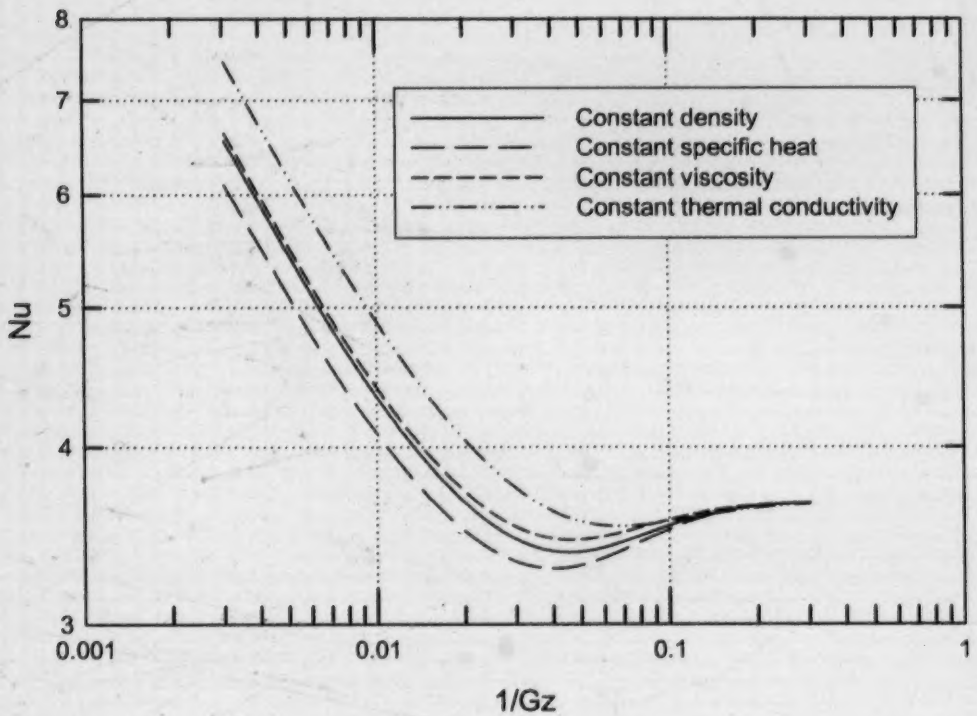

Figure 3.4: Local Nusselt number obtained from entry length solutions for laminar flow in a channel with one property constant and other properties varying.

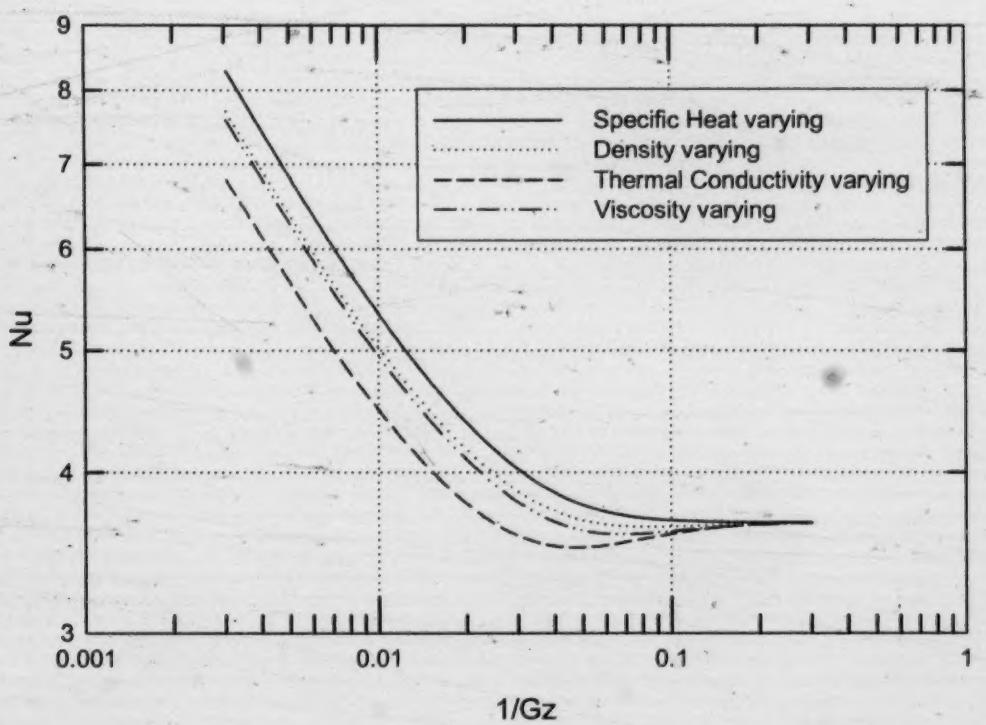

Figure 3.5: Local Nusselt number obtained from entry length solutions for laminar flow in a channel with one property varying and other properties constant.

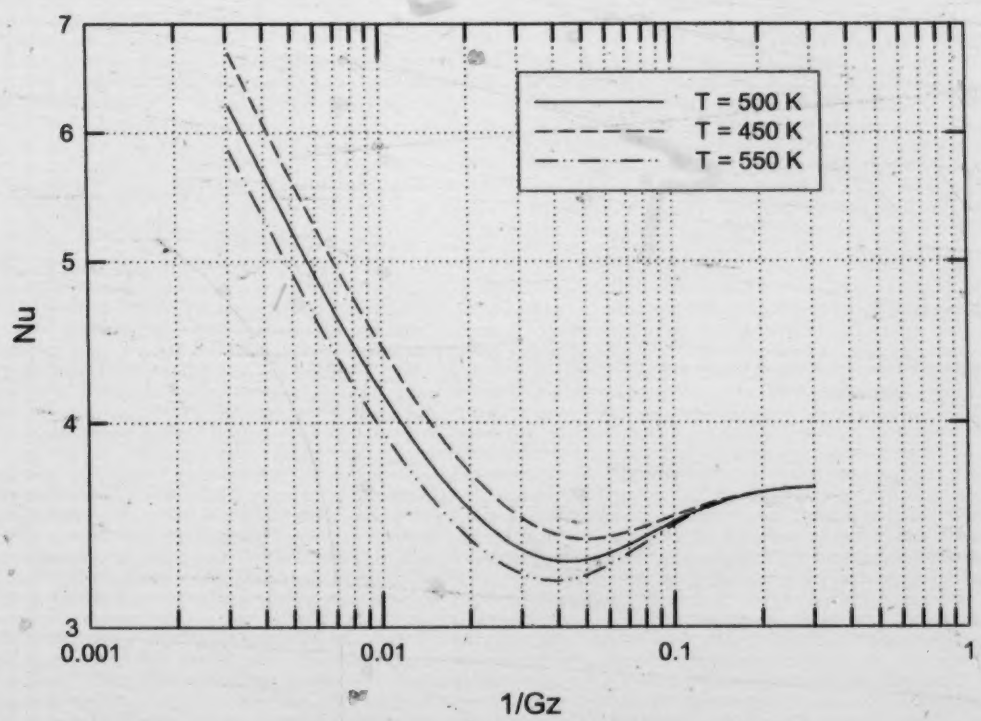

Figure 3.6: Local Nusselt number obtained from entry length solutions for laminar flow in a channel with different wall temperature.

The entry region calculations were repeated for constant wall flux boundary conditions. The operating condition used was a 1 mm diameter tube, length 10 cm, with an inlet velocity of 7 m/s which corresponds to a Reynolds number of 361, referenced at T = 350 K and P = 1 atm. The wall flux was fixed at 500 W/m^2.

The results obtained from this simulation are shown in Figure 3.7. It can be seen that the Nusselt number reaches a constant value of 4.34 for a fully developed incompressible fluid, which agrees with the literature. For the case with varying properties, the asymptotic Nusselt number is slightly lower than the value of 4.34, but the results are very close. There also seems to be much less difference between the constant and variable properties cases.

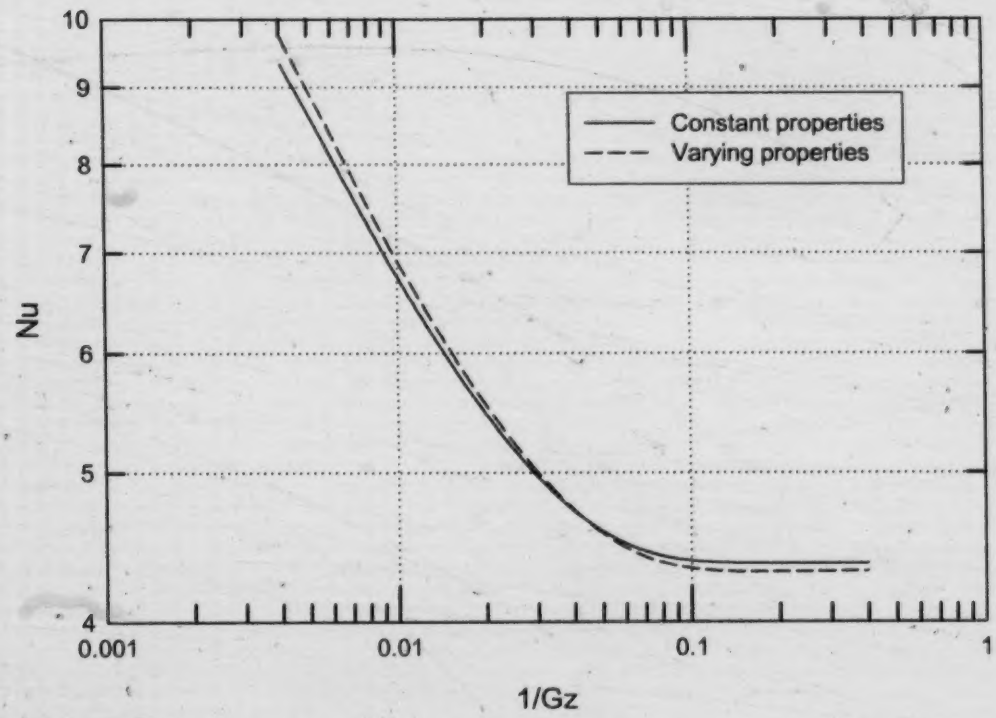

Figure 3.7: Local Nusselt number obtained from entry length solutions for laminar flow in a channel with constant wall flux.

3.3 Combined entry length with first order reaction

Now we consider a case where we introduce a first order reaction at the surface of the tube. In Chapter 2 some of the literature studies on the case of wall reaction were reported. There is no general agreement about the behaviour of the Nusselt and Sherwood numbers in this case. In view of the results obtained with non-reacting fluids of variable properties, it was decided to re-visit this case as well.

For these simulations, the momentum, mass and energy balance equations were solved simultaneously. The momentum equation and associated boundary conditions were the

same as given previously. The energy balance is given by Equation (3.7). The boundary conditions used were also the same as before, except at the wall, where the condition is:

$$k\frac{\partial T}{\partial r} = (-\Delta H)(-R_A) \text{ at r = R for all z} \tag{3.19}$$

The mole balance for the gas phase written in terms of the mole fraction is:

$$\nabla\cdot(D_A\, C\nabla Y_A) - v\cdot C\nabla Y_A = 0 \tag{3.20}$$

The boundary conditions used were:

$$Y_A = Y_{Ao} \text{ at } z = 0 \text{ and } r \neq R \tag{3.21}$$

$$\frac{\partial Y_A}{\partial r} = 0 \text{ at } r = 0 \text{ for all } z \tag{3.22}$$

$$-D_A\frac{\partial Y_A}{\partial r} = (-R_A) \text{ at } r = \text{R for all } z \tag{3.23}$$

$$\frac{\partial Y_A}{\partial z} = 0 \text{ at } z = L \text{ and } r \neq R \tag{3.24}$$

The molecular diffusion coefficient, D_A, may be calculated from the Fuller equation (Fuller et al., 1966).

$$D_A = a_A\left(\frac{T^{1.75}}{P}\right) \tag{3.25}$$

The temperature has units of Kelvin and pressure has units of Pa, to give D_A in m^2/s. The value of constant a_A depends on the species.

The Nusselt number is calculated in the same manner as described earlier. The Sherwood number was calculated from the radial concentration profiles as follows:

$$\mathrm{Sh} = \frac{D}{\left(\langle Y_A \rangle - Y_{AW}\right)} \left.\frac{\partial Y}{\partial r}\right|_{r=R} \tag{3.26}$$

$\langle Y_A \rangle$ is the mixing cup concentration and is given by:

$$\langle Y_A \rangle = \frac{\int_0^R v_z(r) Y_A(r) r dr}{\int_0^R v_z(r) r dr} \tag{3.27}$$

The first order reaction was arbitrarily based on literature values for the oxidation of propane, which is often taken as a model reaction is catalytic combustion studies. The rate equation used was (Benedetto et al., 2005):

$$\left(-R_A\right) = 1\times10^6 \exp\left(\frac{-10900}{T}\right) Y_A \qquad \frac{\mathrm{mol}}{\mathrm{m}^2 s} \tag{3.28}$$

The operating conditions used were a four inch tube with an inlet velocity of 36 m/s which corresponds to a Reynolds number of 334, referenced at T = 650 K and P = 1.05 atm. The inlet propane mole fraction was 0.015.

Benedetto et al. (2005) studied the effect of superficial reaction on mass and energy fluxes between gas and solid phase in the presence of entrance effects. They demonstrated that in the presence of reaction, Nu could be significantly enhanced by the perturbation induced by the surface reaction on temperature, concentration and flow field at the point of ignition. Simulations were performed with the reaction at the wall and attempts were made to verify their results.

To verify the result by Benedetto et al., (2005) Nusselt number was plotted against the inverse of Graetz number. They illustrate that there is jump in the Nusselt number at the light-off location. Figure 3.8 shows the result from our simulation and no such jump in Nusselt number is seen at the point of light-off. The reason for the discrepancy between our result and the result reported by Benedetto may be because of slightly different conditions used in the simulations.

It is observed in our results that the Nu curve follows closely the constant wall flux condition. However, as noted from the results presented earlier, and also from the literature, we expect this behaviour to vary considerably with operating conditions. However, we conclude that a general simple correlation that exactly reproduces the entry length Nu and Sh is probably not possible. Instead of seeking such a prize, we examine the agreement that can be achieved by using approximations. Prior to this, however, we consider a case with a reactive catalytic washcoat.

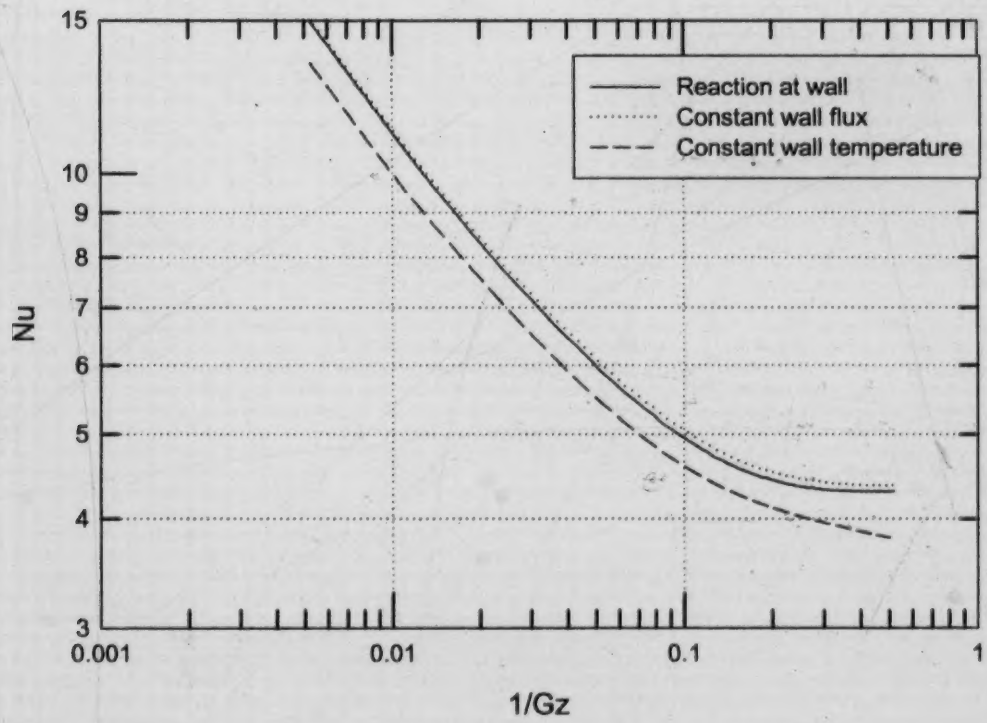

Figure 3.8: Variation in Nu number along the axial direction for the case of reaction at the wall and comparison with constant wall flux and constant wall temperature cases at the same conditions.

3.3 Combined entry length with first order reaction in a washcoat

We now consider the case with a catalytic washcoat of finite thickness. Thus, instead of having all of the reaction occurring at the surface of the catalyst, we add a finite layer of washcoat. Within the washcoat, the reactants diffuse and react on the active catalyst sites with an associated release or absorption of heat (Hayes and Kolaczkowski, 1997). This two-dimensional model of the channel is the same as described previously. The washcoat consisted of an annular ring around the perimeter of the channel.

For axi-symmetric steady state flow in a circular tube the radial and axial components of the equations of motion are given by Equation (3.3) and (3.4). The mole balance equation for the gas is given by Equation (3.20). The boundary conditions used were:

$$Y_A = Y_{Ao} \text{ at } z = 0 \text{ and } r \neq R \tag{3.29}$$

$$\frac{\partial Y_A}{\partial r} = 0 \text{ at } r = 0 \text{ for all } z \tag{3.30}$$

$$\frac{\partial Y_A}{\partial z} = 0 \text{ at } z = L \text{ and } r \neq R \tag{3.31}$$

The energy balance for the gas is given by Equation (3.7). The boundary conditions used were:

$$T = T_o \text{ at } z = 0 \text{ and } r \neq R \tag{3.32}$$

$$\frac{\partial T}{\partial z} = 0 \text{ at } z = L \text{ and } r \neq R \tag{3.33}$$

$$\frac{\partial T}{\partial r} = 0 \text{ at } r = 0 \text{ for all } z \tag{3.34}$$

The porous washcoat is modelled as a continuum in which the active species diffuse and react. Assuming an effective diffusion coefficient based on the total volume of the washcoat, we can write the mole balance equation for species A in the catalytic washcoat in terms of the mole fraction as:

$$\left(D_{\text{eff}}\right)_A \nabla\left(C \nabla Y_A\right) - \left(-R_A\right) = 0 \tag{3.35}$$

The effective diffusion coefficient, D_{eff}, is assumed not to depend on concentration. It is based on the entire cross sectional area of the washcoat, both solid and void space, and includes terms for the washcoat porosity and tortuosity. If we assume that Knudsen diffusion dominates in the catalyst pores, the effective diffusion coefficient can be written as (Hayes and Kolaczkowski, 1997):

$$\left(D_{\text{eff}}\right)_A = \frac{\varepsilon}{\tau} 97 d_p \left(\frac{T}{M_A}\right)^{0.5} \tag{3.36}$$

In this study we used the properties of air in the mole and energy balances. The properties such as thermal conductivity, specific heat and density were calculated as described before. The energy balance for the washcoat for a single reaction is:

$$\nabla \cdot \left(k_{\text{eff}} \nabla T\right) + \left(-\Delta H_R\right)\left(-R_A\right) = 0 \tag{3.37}$$

k_{eff} is the effective thermal conductivity and its value is taken equal to 1.5 W/ (m.K). The washcoat density was taken as 1300 kg/m^3 (Hayes and Kolaczkowski, 1997).

The same kinetic model was used as described in Equation (3.28), but it was modified to account for the fact that the reaction occurs throughout the washcoat volume rather than only at the surface. Thus we divide Equation (3.28) by the characteristic length defined as volume/surface area, of the washcoat. The rate equation is given as follows:

$$(-R_A) = \frac{1\times10^6 \exp\left(\frac{-10900}{T}\right) Y_A}{L_C} \quad \frac{\text{mol}}{\text{m}^3 s} \tag{3.38}$$

Simulations were performed with the same conditions as for reaction at the wall case, except that an inlet velocity of 1 m/s was used. The fractional conversion along the axis in the gas phase is shown in Figure 3.9 below. The result from the simulation is compared with the result obtained for the reaction at the wall case and we can see that there is a difference in the conversion when the reaction takes place in the washcoat which implies that washcoat diffusion may be important.

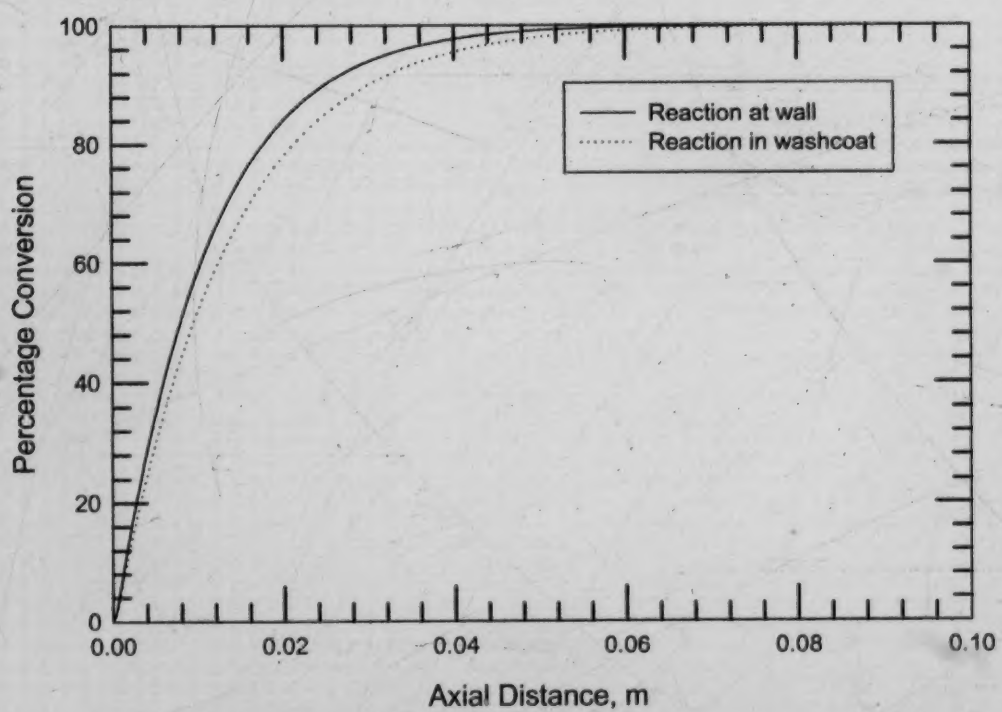

Figure 3.9: Comparison of conversion for the case when there is a reaction in the washcoat and when there is a reaction at the wall for an inlet velocity of 1 m/s.

3.4 Comparison of one and two dimensional channel models

Ultimately, the reason for desiring an accurate representation of the Nu and Sh in the channel is so that a one dimensional model may be used for the gas phase. Computationally, such a model is much faster than the 2D model, which might be important in applications such as parameter optimization, where a very large number of simulations must be performed. In this section a comparison is made over some range of operating conditions between a model in which the flow is modelled correctly and in which it is approximated.

We define a new model which is called the 1D-2D model. The first dimension refers to the number of space dimensions in the channel, and the second to the number in the washcoat. The full 2D model with washcoat diffusion is thus referred to as the 2D-2D model. The 2D channel model with all reaction at the wall is thus called a 2D-1D model in this system. For the 1D-2D model, the mole and energy balance equations in the washcoat are the same as for the 2D-2D model described in the last section. The gas phase equations, however, become uni-dimensional and are coupled to the solid via the heat and mass transfer coefficients. The mole balance for the channel is thus written:

$$\frac{\partial}{\partial z}\left(D_{\mathrm{A}} C_f \frac{\partial Y_{\mathrm{A},f}}{\partial z}\right) - v\frac{\partial Y_{\mathrm{A},f}}{\partial z} - k_m C_f \left(Y_{\mathrm{A},f} - Y_{\mathrm{A},WC}\right)\left(\frac{4}{D_H}\right) = 0 \qquad (3.39)$$

$Y_{A,f}$ is the mole fraction in the fluid phase and $Y_{A,WC}$ is the mole fraction at the surface of the washcoat. The boundary conditions are a specified concentration at the inlet and a zero flux condition at the outlet. Because of the discontinuity at the washcoat surface, it is now necessary to introduce a boundary condition there as:

$$-D_{\mathrm{eff}} \frac{\partial Y_{\mathrm{A},f}}{\partial r} = k_m \left(Y_{\mathrm{A},f} - Y_{\mathrm{A},WC}\right) \qquad (3.40)$$

The energy balance equation for the channel is:

$$\frac{\partial}{\partial z}\left(k_f \frac{\partial T_f}{\partial z}\right) - \rho C_{P,f} v \frac{\partial T_f}{\partial z} - h\left(T_f - T_{WC}\right)\left(\frac{4}{D_H}\right) = 0 \qquad (3.41)$$

where, T_f is the fluid temperature and T_{WC} is the surface temperature of the washcoat. The boundary conditions for the channel are specified temperature at the inlet and zero flux at the outlet. A boundary condition at the washcoat surface is introduced:

$$-k_S \frac{\partial T_f}{\partial r} = h\left(T_f - T_{WC}\right) \qquad (3.42)$$

The same kinetic model was used as given in Equation (3.36). The properties such as thermal conductivity, specific heat, density and viscosity were calculated as described before. Simulations were performed with the same conditions as for reaction in washcoat case. For the 1D – 2D model, Nu and Sh numbers were set equal to 4.

Figure 3.10 shows the comparison of how the conversion varies along the length of reactor for three cases (a) 1D – 2D model (b) 2D – 2D model and (c) 2D – 1D model. From the results, we can see that the 1D – 2D model and the 2D – 2D model give the same conversion (both lines overlap each other). For this simulation, with a 1 m/s inlet velocity, the Reynolds number is about 10. Therefore, the entry region is short (about 0.4 mm) and little reaction occurs there. In the fully developed region, we have seen that the Nu should be between 3.66 and 4.36, and therefore the approximation of 4 gives a good result. Simulations were also performed with varying Nu and Sh number values to determine the effect on the conversion. The results from the simulation are shown in Figure 3.11. It is observed that increasing the Nu and Sh number values does not have a significant effect on the conversion and therefore, it may not be that important on what value of Nu and Sh number we choose to model the monolith channel in the fully developed region for this case. It indicates that the external mass transfer is not important.

However, when we go to higher velocity such that the entry length is about half the length of the reactor, we see a difference in the conversion for the above three cases. Results are shown in Figure 3.12. A better match between 1D – 2D and 2D – 2D models would be obtained if we modeled correctly the Nu in this region.

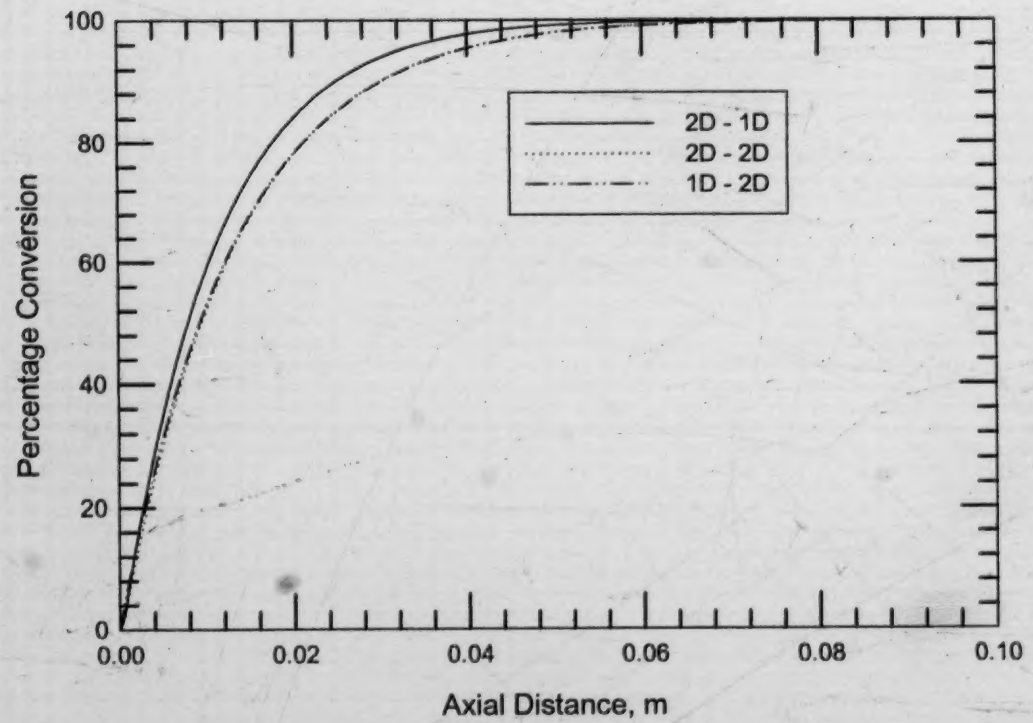

Figure 3.10: Comparison of conversion for the case of 1D – 2D model, reaction in the washcoat and reaction at the wall for an inlet velocity of 1 m/s.

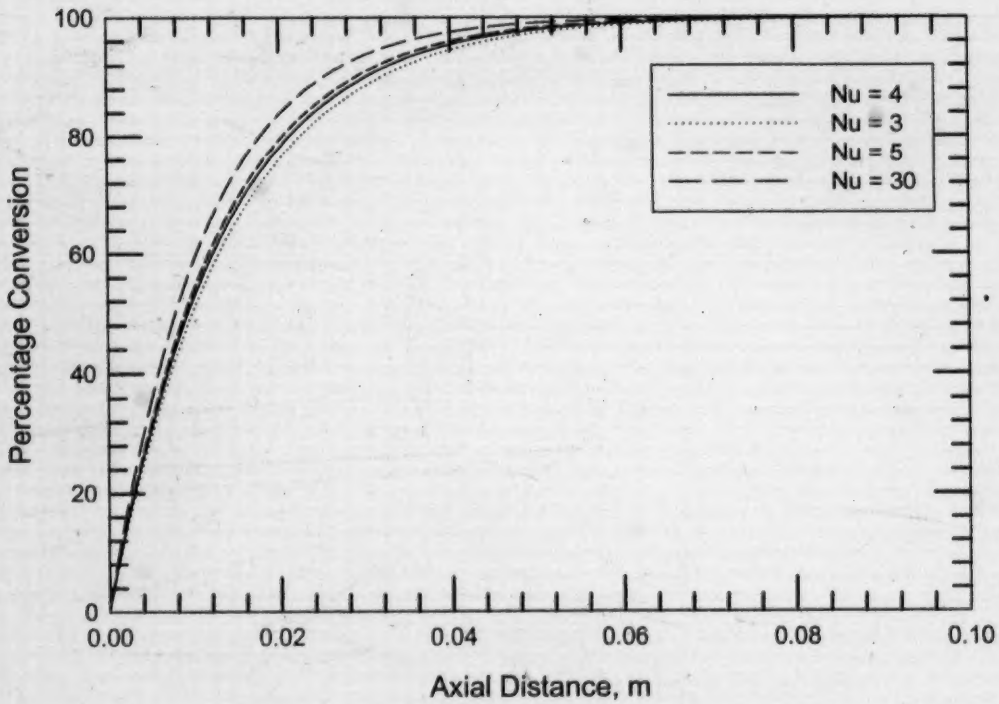

Figure 3.11: Effect of varying the Nusselt number on conversion for a 1D- 2D model at an inlet velocity of 1 m/s.

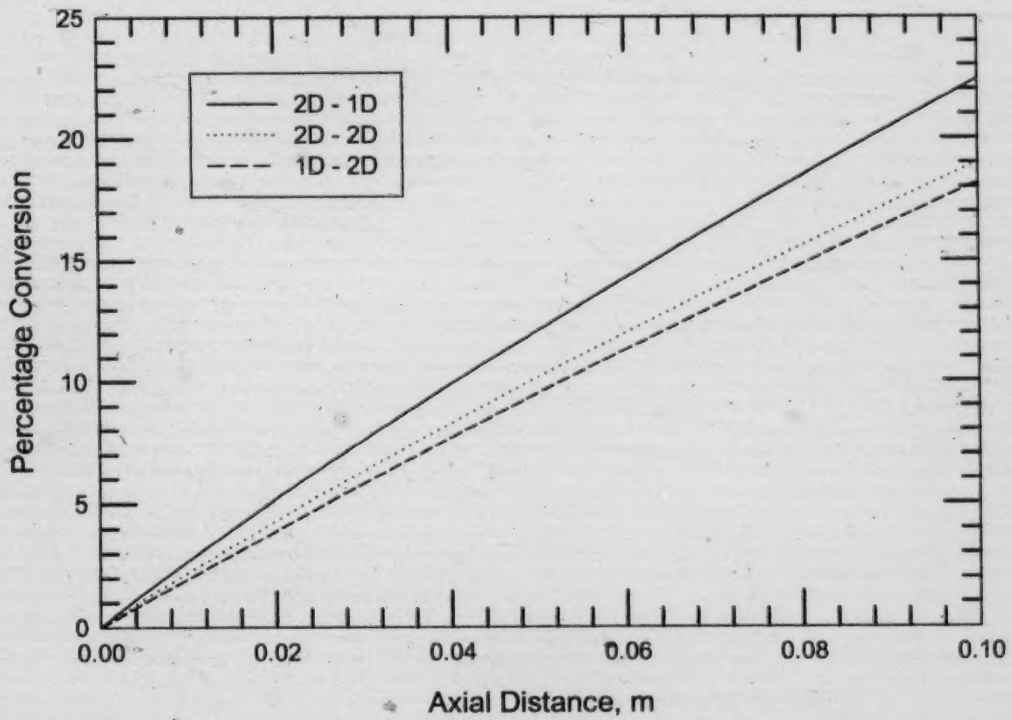

Figure 3.12: Comparison of conversion for the case of 1D – 2D model, reaction in the washcoat and reaction at the wall for an inlet velocity of 36 m/s.

3.5 Concluding remarks

Considering all of the results obtained, we can conclude that the correlation of the entry effects for gas mixtures, especially with surface reaction in this region, is not accurately modelled by any of the existing literature correlations. The entry length Nusselt and Sherwood numbers may vary between the constant wall temperature and constant wall flux cases. However, the constant wall temperature Nu depends on the temperature driving force, and therefore it is not an easy task to determine what the exact value should be.

For many practical applications, the entry length may not be that significant, however for higher Re flows or short reactors, care should be taken when selecting the appropriate mass and heat transfer coefficients.

Overall, based on the results of the simulations conducted here, we can conclude that it is not an easy task to generalize about the Nu and Sh number values, and as a result, the controversy in the literature will likely continue.

For steady state simulations, it may not be that important to model the reactor and the external heat and mass transfer coefficients correctly, but implications for that have to seen for the light-off studies. Some of these effects are considered in the next chapter.

4. Comparison of model performance in predicting light-off

The background on the modelling of catalytic monolith reactors was given in Chapter 2, and is summarized briefly here. The model of a single channel of a monolith reactor can be written in one, two or three space dimensions. For the one dimensional model, the radial concentration and temperature gradients are ignored, and the gas in the channel is coupled to the solid wall using heat and mass transfer coefficients. The correct determination of these values can determine the accuracy of the model, and was discussed in Chapter 3. The channel can also be modelled in two space dimensions by assuming axi-symmetry and using cylindrical coordinates. To account for non-uniform washcoat distribution or non-circular channels a three dimensional model may be used. Catalytic monoliths used in commercial applications have different cross sectional shapes such as circular, square, triangular, sinusoidal and hexagonal (Bhattacharya et al., 2004). These different geometries show different behavior because of there asymmetric nature, which lead to variation in heat and mass transfer coefficients along the circumferential direction. In the study of monolith reactor, it is common to use 1D model with circumferentially averaged heat and mass transfer coefficients. At present, there is no general agreement in the literature on the accuracy of such models compared to more detailed 2D and 3D models. It should be noted that 3D studies are rare in the literature, and fully three dimensional transient models that incorporate washcoat diffusion effects have not been reported.

The purpose of this chapter is to present a comparison of two and three dimensional model performance with various approximations. We are interested in exploring the difference in the computed light-off curves. The light-off curve is a plot of outlet conversion as a function of inlet reactor temperature for a fixed operating condition (concentration, space velocity etc). Normally the inlet temperature is slowly increased and the outlet conversion is measured. The point at which 50 % conversion is reached is called the light-off temperature. The light-off curve is important because it represents the reactor behaviour under cold start conditions, where the majority of emissions are produced. Furthermore, the light-off curve is increasingly being used to develop kinetic

models for the reactions occurring. Since this latter optimization problem requires the use of a reactor simulator, it is important to know how various approximations and simplifications affect the results.

4.1 Two dimensional model of a single monolith channel

The complete two dimensional model of a monolith reactor channel is based on the solution of momentum, mole and energy balance equations. The domain is considered to be an axi-symmetric right circular cylinder. We consider the fluid phase, the solid washcoat and the substrate. The actual washcoat and channel sizes from the real three dimensional shape are mapped onto the cylinder in a manner to preserve the cross sectional areas of channel, washcoat and substrate. In this way, the total thermal mass of the channel is conserved, which is extremely important when comparing light-off curves between two and three dimensional models. This model considers a washcoat of circular perimeter in a circular substrate, and thus for later reference we call this the circle-in-circle model. A diagram of the solution domain is shown in Figure 4.1 below:

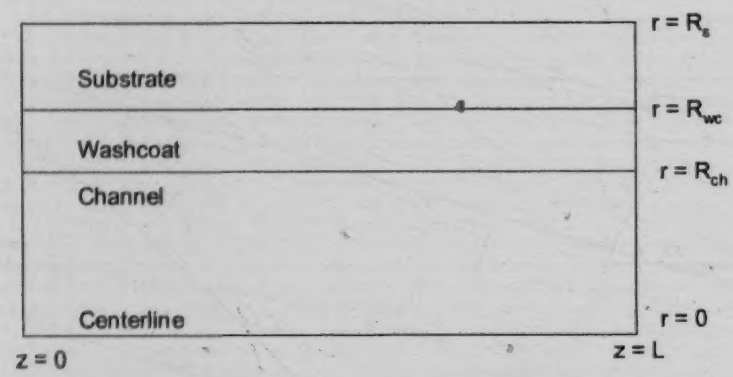

Figure 4.1: Solution domain for a 2D single monolith channel

Most of the equations necessary to model the channel in two dimensions were given in Chapter 3, and are repeated here for convenience. The flow is governed by the Navier Stokes equations, which is written:

$$\rho(v\bullet\nabla)v = \nabla\bullet\left[-pI + \eta\left(\nabla v + (\nabla v)^T\right) - \left(\frac{2\eta}{3} - \kappa\right)(\nabla\bullet v)I\right] \tag{4.1}$$

The equation of continuity is:

$$\nabla\bullet(\rho v) = 0 \tag{4.2}$$

The boundary conditions used were flat or parabolic inlet velocity profile, no slip conditions at the walls, symmetry conditions at the axis and zero normal shear stress at the outlet. The model is transient, and therefore the time dependent terms should be included in the conservation equations. However, the time scales for the gas and solid phases are widely different, and it is usually assumed that the gas phase may be modelled as a pseudo steady state, as well as the species equation for the solid. The only transient term that needs to be preserved is the one for the solid energy balance equations. Pseudo steady state assumption was adopted in this work.

The mole balance for the gas phase written in terms of the concentration is given by:

$$\nabla\cdot(D_A\,\nabla C_A) - \nabla\cdot(vC_A) = 0 \tag{4.3}$$

The boundary conditions used were:

$$C_A = C_{Ao} \text{ at z = 0 and } r \neq R \tag{4.4}$$

$$\frac{\partial C_A}{\partial r} = 0 \text{ at r = 0 for all z} \tag{4.5}$$

$$\frac{\partial C_A}{\partial z} = 0 \text{ at z = L and } r \neq R \tag{4.6}$$

The molecular diffusion coefficient for species A, D_A, was calculated from the Fuller equation (Fuller et al., 1966).

$$D_A = a_A \left(\frac{T^{1.75}}{P} \right) \tag{4.7}$$

The temperature has units of Kelvin and pressure has units of Pa, to give D_A in m^2/s. The value of constant a_A depends on the species.

Note that at the channel wall the rate of diffusion in the gas phase is equal to the rate of diffusion in the washcoat. However, because the solution domain is continuous across the boundary, this becomes an internal boundary condition that is handled naturally by the finite element solution. The energy balance for the gas is given by:

$$\nabla \cdot \left(k_f \nabla T \right) - \left(\rho C_p \right)_f v \cdot \nabla T = 0 \tag{4.8}$$

The boundary conditions are:

$$T = T_o \text{ at z = 0 and } r \neq R \tag{4.9}$$

$$\frac{\partial T}{\partial z} = 0 \text{ at z = L and } r \neq R \tag{4.10}$$

$$\frac{\partial T}{\partial r} = 0 \text{ at r = 0 for all z} \tag{4.11}$$

In this study we used the properties of air in the mole and energy balances. Although the

properties of an engine exhaust gas would be slightly different, this should not affect the general conclusions. The thermal conductivity of the gas is (Incropera and DeWitt, 2002):

$$k_f = 1.679\times10^{-2} + 5.073\times10^{-5}T \tag{4.12}$$

The heat capacity was expressed as fourth order polynomials in temperature and viscosity was expressed as second order polynomial using values from (Hayes and Kolaczkowski, 1997). The density was calculated from the ideal gas law. The steady state mole balance equation for species A in the catalytic washcoat, assuming that the effective diffusion coefficient is not a function of concentration, is given by:

$$(D_{\text{eff}})_A \nabla^2 C_A - (-R_A) = 0 \tag{4.13}$$

$(D_{\text{eff}})_A$ is the effective diffusivity of species A in the washcoat based on the entire cross sectional area of the washcoat, both solid and void space, and includes terms for the washcoat porosity and tortuosity. If Knudsen diffusion dominates, the effective diffusion coefficient can be written as (Hayes and Kolaczkowski, 1997):

$$(D_{\text{eff}})_A = \frac{\varepsilon}{\tau} 97 d_p \left(\frac{T}{M_A}\right)^{0.5} \tag{4.14}$$

Equation (4.14) uses the parallel pore model to represent the porous structure. In this study we used the properties of air in the mole and energy balances. The transient energy balance for the washcoat for a single reaction is:

$$\nabla\bullet\left(k_{\text{eff}}\nabla T\right) + \left(-\Delta H_R\right)(-R_A) = \left(\rho C_p\right)_S \frac{\partial T}{\partial t} \tag{4.15}$$

k_{eff} is the effective thermal conductivity. The density and heat capacity are the bulk values of the porous matrix. The washcoat density was taken as 1300 kg/m^3, washcoat

conductivity was taken as 1.5 W/ (m.K) and specific heat of washcoat was taken as 1005 J/ (kg.K) (Hayes and Kolaczkowski, 1997).

For the substrate, the energy balance is:

$$\nabla\cdot\left(k_{\text{eff}}\nabla T\right) = \left(\rho C_p\right)_S \frac{\partial T}{\partial t} \tag{4.16}$$

The substrate density was taken as 1667 kg/m^3, substrate conductivity was taken as 1.5 W/ (m.K) and specific heat of substrate was taken as 1050 J/ (kg.K) (Hayes and Kolaczkowski, 1997).

The aspect ratio of the channel is very low, that is, the axial length is much greater than the radius. From a modelling perspective, to reduce the number of finite elements, the domain can be scaled. Define a length scale:

$$z' = \frac{z}{L_R} \tag{4.17}$$

L_R is an arbitrary scaling factor. The scaled mole balance equations can then be written in two dimensions in cylindrical coordinates as:

Channel:

$$\frac{1}{r}\frac{\partial}{\partial r}\left(Dr\frac{\partial C_i}{\partial r}\right) + \frac{\partial}{\partial z'}\left(\frac{D}{L_R^2}\frac{\partial C_i}{\partial z'}\right) - \frac{v_z}{L_R}\frac{\partial C_i}{\partial z'} - v_r\frac{\partial C_i}{\partial r} = 0 \tag{4.18}$$

Washcoat:

$$D_{\text{eff},i}\frac{1}{r}\frac{\partial}{\partial r}\left(r\frac{\partial C_i}{\partial r}\right) + \frac{D_{\text{eff},i}}{L_R^2}\frac{\partial^2 C_i}{\partial z'^2} - \left(-R_i\right) = 0 \tag{4.19}$$

Substrate:

$$D_{\text{eff},i}\frac{1}{r}\frac{\partial}{\partial r}\left(r\frac{\partial C_i}{\partial r}\right) + \frac{D_{\text{eff},i}}{L_R^2}\frac{\partial^2 C_i}{\partial z'^2} = 0 \tag{4.20}$$

The scaled energy balance equations are:

Channel:

$$\frac{1}{r}\frac{\partial}{\partial r}\left(k_f\, r\frac{\partial T}{\partial r}\right)+\frac{\partial}{\partial z'}\left(\frac{k_f}{L_R^2}\frac{\partial T}{\partial z'}\right)-\frac{\rho C_{p,f} v_z}{L_R}\frac{\partial T}{\partial z'}-\rho C_{p,f} v_r\frac{\partial T}{\partial r}=0 \qquad (4.21)$$

Washcoat:

$$\frac{1}{r}\frac{\partial}{\partial r}\left(k_{\text{eff}}\, r\frac{\partial T}{\partial r}\right)+\frac{\partial}{\partial z'}\left(\frac{k_{\text{eff}}}{L_R^2}\frac{\partial T}{\partial z'}\right)+\sum_{i=1}^{n}\left(-\Delta H_{R,i}\right)\left(-R_i\right)=\rho_s C_{p,s}\frac{\partial T}{\partial t} \qquad (4.22)$$

Substrate:

$$\frac{1}{r}\frac{\partial}{\partial r}\left(k_{\text{eff}}\, r\frac{\partial T}{\partial r}\right)+\frac{\partial}{\partial z'}\left(\frac{k_{\text{eff}}}{L_R^2}\frac{\partial T}{\partial z'}\right)=\rho_s C_{p,s}\frac{\partial T}{\partial t} \qquad (4.23)$$

In addition to the solution obtained using the Navier Stokes equation to solve for the velocity profile, the problem was also solved using a fully developed velocity profile that was imposed. The flow is assumed parabolic at the entrance, and simply adjusted for the temperature change along the axial direction assuming an ideal gas. The analytical velocity profile used in this case is given below. The radial velocity component was set to zero in this case.

$$v_z = 2v_m\left(1-\frac{r^2}{R^2}\right)\frac{T}{T_o} \qquad (4.24)$$

The solution to the reactor model was obtained using the finite element method package COMSOL multiphysics. Triangular elements were used with a fine mesh near the wall to capture the sharp gradients there. The total number of elements was 25000. The total simulation time for one run was around 20 minutes.

The kinetic model used is based on the LHHW type model proposed by Voltz et al. (1973) for the oxidation of CO over platinum. In an excess of oxygen, the reaction rate

can be written:

$$(-R_{CO}) = \frac{k_{CO} C_{CO}}{(1 + K_{CO} C_{CO})^2} \tag{4.25}$$

We used a modified form of the original Voltz model, with the rate expressed in terms of concentration, whereas the original model is typically expressed in terms of mole fraction. The model with the appropriate kinetic constants, expressed in terms of the washcoat volume, is:

$$(-R_{CO}) = \frac{9.2\times10^{12} \exp\left(\frac{-12028}{T}\right) C_{CO}}{\left(1 + 2.7 \exp\left(\frac{962}{T}\right) C_{CO}\right)^2} \quad \frac{\text{mol}}{\text{m}^3\text{s}} \tag{4.26}$$

The values of the kinetic constants were selected to give light-off in the range normally expected for a typical automotive catalytic converter on a platinum catalyst under lean conditions. The adsorption parameters used are those suggested by Voltz et al. (1973), modified for the change in form of the rate expression from mole fraction to concentration.

For the first case, the solutions were obtained with the imposed fully developed velocity profile at the inlet boundary and then the mass and energy balance were solved simultaneously to obtain the light off curve. Light-off curves (plots of conversion as a function of inlet gas temperature) were generated for different reactor lengths and different inlet temperature ramp rates. Note that for the operating conditions used, a 25 mm long reactor corresponds to a GHSV of 80 000 h^{-1} at an inlet velocity of 1 m/s, a 10 cm reactor 20 000 h^{-1}, etc, referenced at 298 K and 1 atm pressure. Typical laboratory tests use a GHSV of around 50 000 h^{-1}. The first results were obtained for 5000 ppm by volume CO at an inlet temperature ramp rate of 30 K/min. The initial temperature was set at 350 K.

The effect of reactor length on light-off is shown in Figure 4.2. It is evident that in shorter monoliths the light-off occurs at a higher inlet temperature and that there is a limit beyond which increasing the length does not reduce the light-off temperature. This behaviour is caused by the nature of the kinetics. For the non-linear kinetic model used, the reaction rate increases as the concentration decreases, and as the temperature increases. As the reactor increases in temperature, and some small reaction occurs in the front section of the monolith, the reaction rate will start to increase. At some point the rate of reaction begins to increase rapidly. The point at which this occurs depends on local temperature and concentration. For short reactors, this ignition point is located at the reactor exit. However, as the reactor length increases, a point is reached where ignition occurs before the reactor exit, and the conversion rises rapidly. Beyond this length, a longer reactor will have no effect on the light-off temperature.

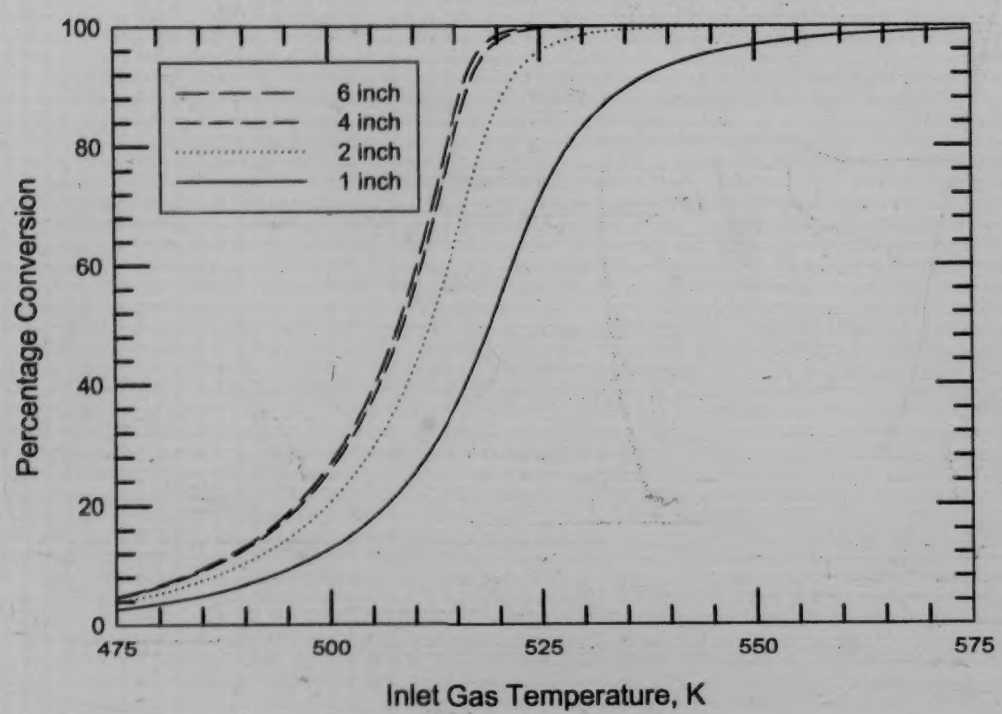

Figure 4.2: Effect of length of reactor on the light-off curve for an inlet temperature ramp rate of 30 K/min at increasing reactor length for 2D model. The CO concentration is 5000 ppm.

Different results were observed when the inlet temperature ramp rate was increased by an order of magnitude to 300 K/min. For the range of GHSV tested (80 000 h^{-1} and lower) there was no significant effect on the light-off curve as a function of length. Figure 4.3 shows the effect of length on light-off curves for higher ramp rate. Again, this result can be explained by the relationship between temperature, concentration and reaction rate. For the high ramp rate, the front end of the monolith heats up very quickly, and the ignition point is reached after a short distance; thus the reactor length is of lesser importance.

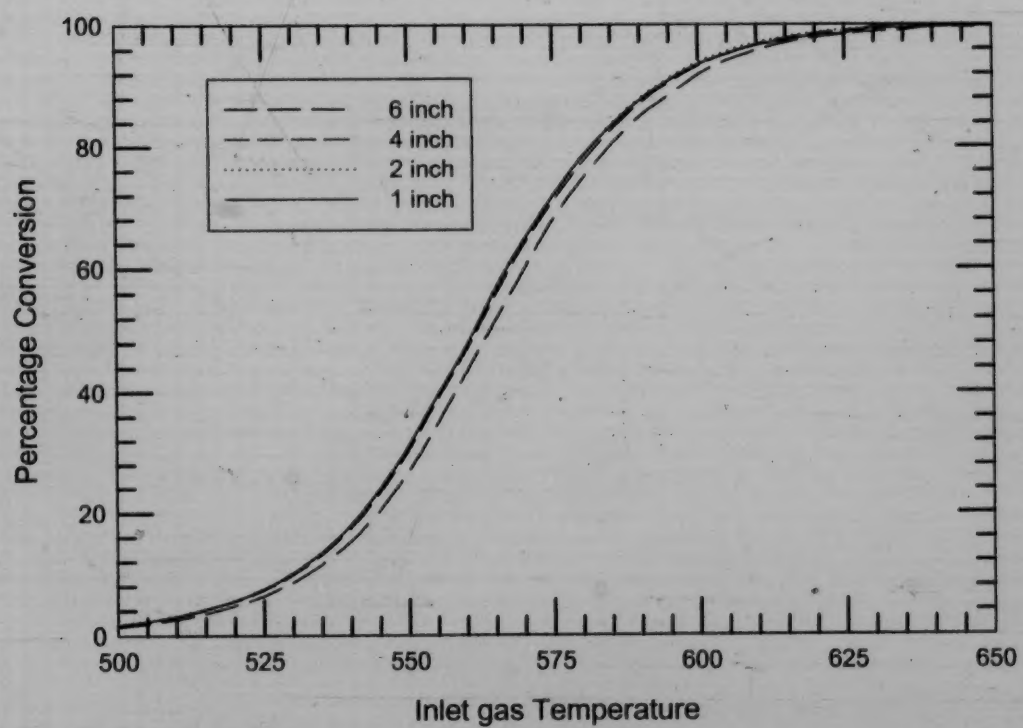

Figure 4.3: Effect of length of reactor on the light-off curve for an inlet temperature ramp rate of 300 K/min for 2D model. The CO concentration is 5000 ppm.

To reduce computational cost, many investigators who use a 2D model neglect the momentum balance equation, and rather impose a fully developed velocity profile. Figures 4.4 and 4.5 shows the result for the 2D geometry when the model is solved with and without momentum balance for a ramp rate of 30 K/min and 300 K/min respectively. The simulation time for one run also increases from 20 minutes to 35 minutes. When we neglect solving the momentum balance equation significant differences can be seen in the tail of the light off curve, although the light off point (50 % conversion) is the same with both the conditions. The difference is more pronounced at the higher temperature ramp rate. One should be careful when solving the model with or without momentum balance equation.

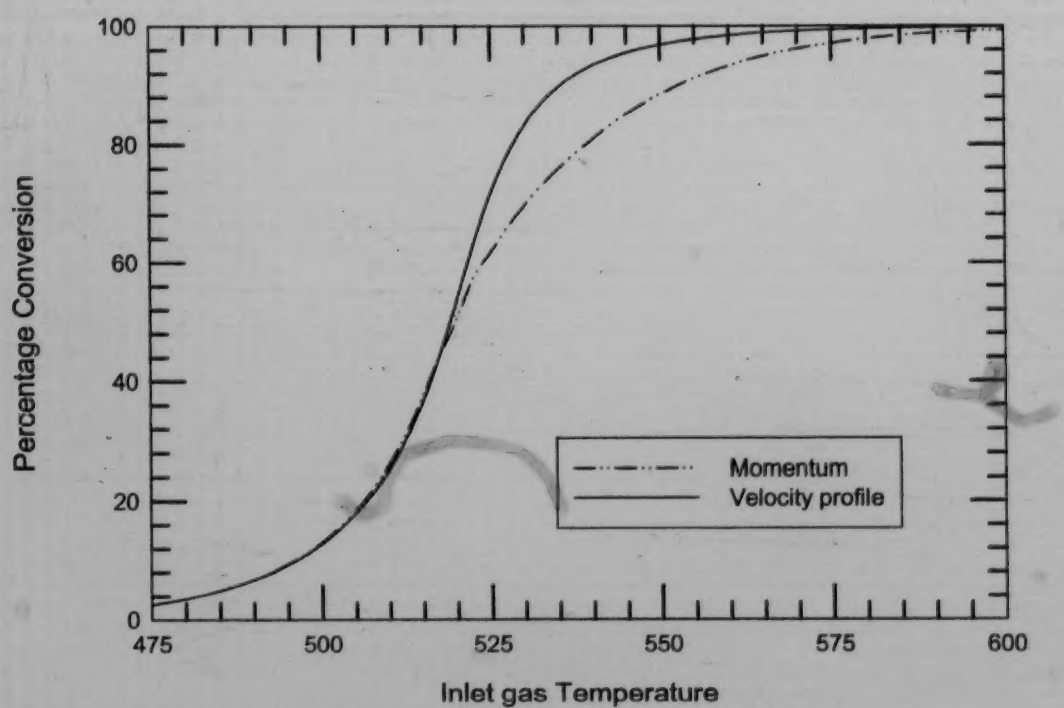

Figure 4.4: Effect of neglecting momentum balance on the light-off curve for an inlet temperature ramp rate of 30 K/min at a GHSV of 80 000 h^{-1} for 2D model. The CO concentration is 5000 ppm.

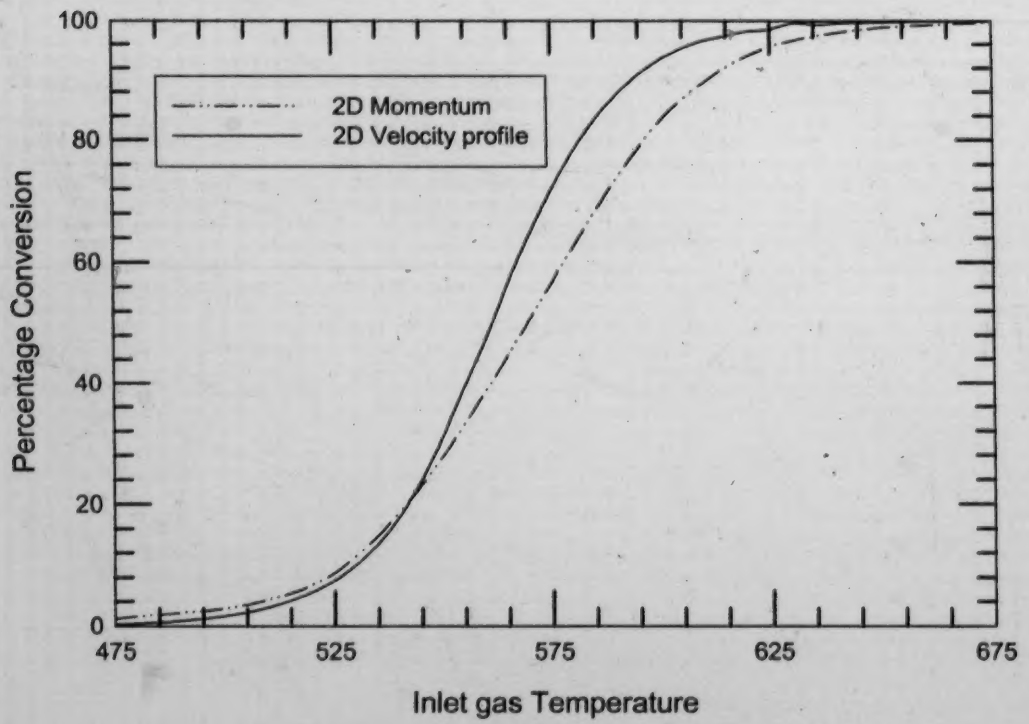

Figure 4.5: Effect of neglecting momentum balance on the light-off curve for an inlet temperature ramp rate of 300 K/min at a GHSV of 80 000 h^{-1} for 2D model. The CO concentration is 5000 ppm.

To illustrate the importance of washcoat diffusion, we performed some simulations on the 2D model in which the effective diffusion coefficient in the washcoat was increased by a factor of 10 000. Using an extremely large effective diffusion coefficient is equivalent to eliminating washcoat diffusion resistance. For steady state simulations (see Chapter 3) this can be achieved by allowing all of the reaction to occur at the wall. However, for transient simulations it is necessary to preserve the washcoat to ensure that the thermal mass is correct. Figure 4.6 shows the results for the 2D model when analytical velocity profile is used at the inlet. It is seen that the light-off occurs in a similar location; however, the shape of the curve is much steeper. This observation is consistent with earlier observations on the effect of diffusion on the shape of the light-off

curve (Hayes et al., 2003). We recall that the effect of diffusion limitation on the reaction rate is not always a priori obvious with non-linear kinetics, where effectiveness factors greater than unity can be obtained. Under the conditions prevailing in real converter cold starts, the CO oxidation reaction invariable lies in the region where the reaction rate increases with decreasing CO concentration.

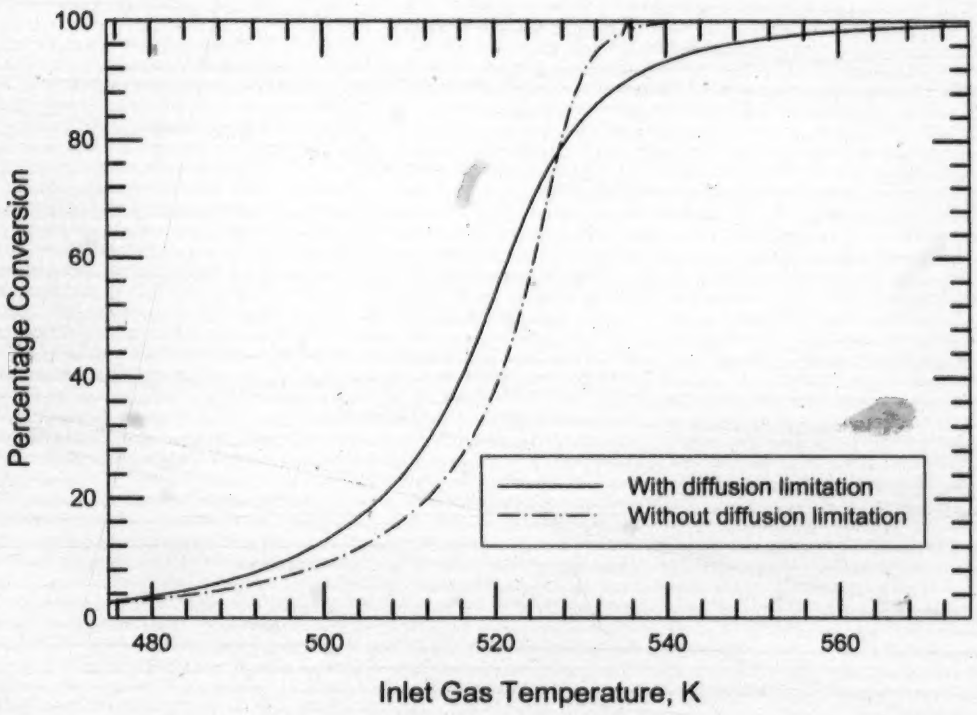

Figure 4.6: Effect of diffusion on the light-off curve for an inlet temperature ramp rate of 30 K/min at a GHSV of 80 000 h^{-1}. The CO concentration is 5000 ppm.

Figure 4.7 shows the effect of neglecting the momentum balance for the case of no diffusion limitation, and no significant effect is seen in the light-off curve. These results indicate that one should be careful when solving the model with or without momentum balance equation.

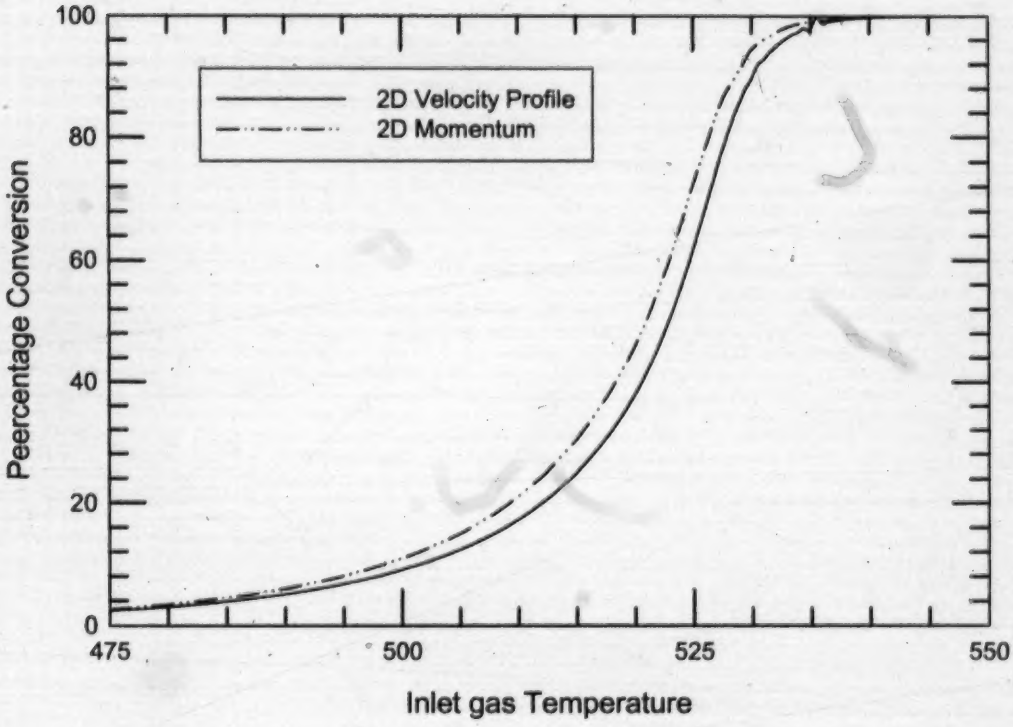

Figure 4.7: Effect of momentum balance without diffusion limitation on the light-off curve for an inlet temperature ramp rate of 30 K/min at a GHSV of 80 000 h^{-1} for 2D geometry. The CO concentration is 5000 ppm.

4.2 Three dimensional model of a single monolith channel

Real channels in catalytic converters do not generally have a uniform washcoat distribution around the channel perimeter. The variation of non-uniformity can be fairly extreme; see for example Hayes et al. (2005). There are a number of implications that result from this fact. The first is that the actual heat and mass transfer coefficients can vary significantly around the channel perimeter. This can in turn affect the accuracy of 1D models, which typically assume a uniform Nu or Sh number. See, for example, the work by Hayes et al. (2004). It has been suggested that non-uniformity of washcoat distribution could affect ignition, which could in turn affect the cold start performance. There are two implications arising from this possibility. The first is the accuracy of 1D or 2D models for modelling cold start, and the second relates to the way washcoats should be designed to achieve optimal light-off performance.

In the 3D model of a single monolith channel, the channel, the washcoat and the substrate were modelled three-dimensionally. For symmetry reasons, only one eighth of the channel was modelled. Two washcoat shapes were used with a square channel, as shown in Figure 4.8. In the first one, the washcoat was assumed to be evenly distributed about the perimeter, and is called the square-in-square (SS) model. The second model shape used the same amount of washcoat, however it was distributed so that the channel free space was circular (circle-in-square model, or CS). These two shapes represent extremes for the washcoat distribution in a square channel. The two geometries were based on a square monolith channel from a ceramic monolith of 400 CPSI (typical monolith from Corning, and the most common cell density in commercial catalytic converters). For each case, the appropriate cross sectional areas are: channel, 0.754; washcoat 0.246; substrate, 0.3456, with units of mm^2.

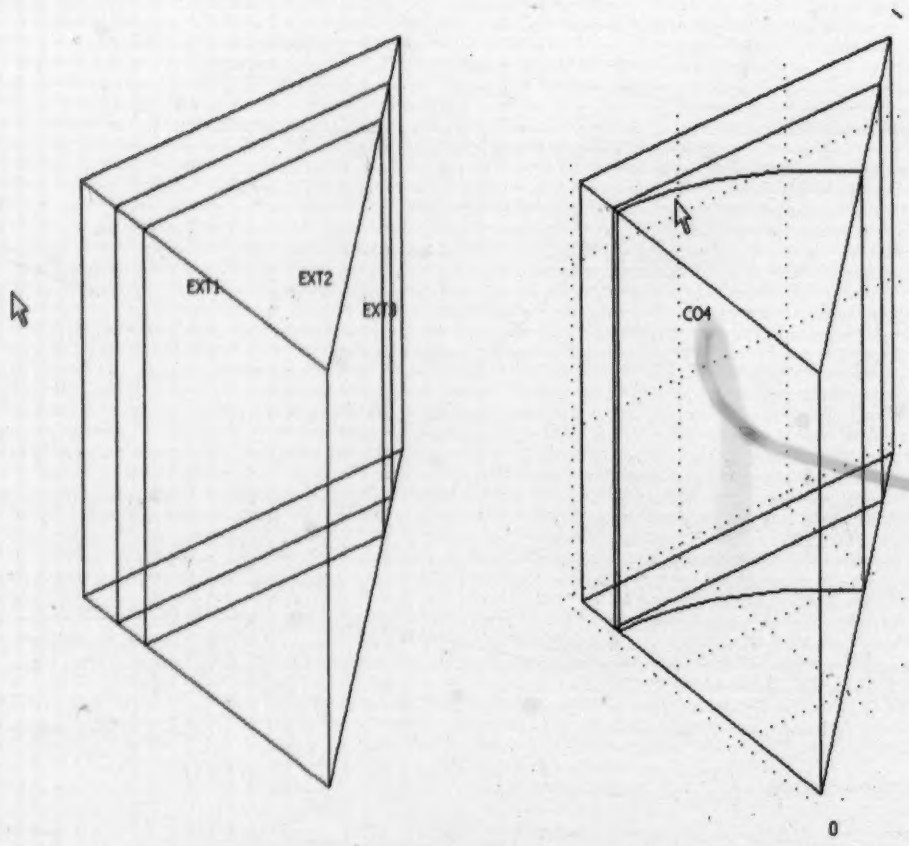

Figure 4.8: Three dimensional model of a single channel monolith

The momentum balance equation for the channel is given by Equations (4.1) and (4.2). The boundary conditions used were flat or parabolic inlet velocity profile, no slip conditions at the walls, symmetry conditions at the axis and zero normal shear stress at the outlet.

The mole balance equation for the channel is given by Equation (4.3). The mole balance equation for the washcoat is given by Equation (4.13). The boundary conditions used were constant inlet concentration, symmetry conditions at the axis and convective flux condition at the outlet.

The energy balance equation for the gas is given by Equation (4.8). The energy balance equation for the washcoat is given by Equation (4.15). The energy balance equation for substrate is given by Equation (4.16). The boundary conditions used were ramping inlet temperature, symmetry conditions at the axis and convective flux condition at the outlet.

The molecular diffusion coefficient D_A was calculated from Equation (4.7). $(D_{\text{eff}})_A$ is the effective diffusivity of species A and is given by Equation (4.14). Because no reaction occurs in the substrate, it is not necessary to solve the mole balance in that domain. The same physical properties as given in the 2D model (refer Chapter 2) were used for the 3D model. The kinetic model used is given in Equation (4.26).

The solution to the reactor model was obtained using the finite element method package COMSOL multiphysics. Tetrahedral elements were used with a fine mesh near the wall to capture the sharp gradients there. The total number of elements was 100,000. The total simulation time for one run was around 30 hours when the model was solved without momentum balance and the run time for one simulation was around 100 hours when the model was solved with momentum balance.

For the first case, simulations were performed with the imposed fully developed velocity profile at the inlet boundary and then the mass and energy balance were solved simultaneously to obtain the light off curve. The analytical velocity profiles used for the two different geometries are as given below. Also we compared the results obtained from 3D model with the 2D axi-symmetric model (called here the circle-in-circle geometry)

For the 3D circle-in-square model the fully developed profile can be approximated by (Shah and London, 1978):

$$v = 2v_m\left(1-\frac{x^2+y^2}{r^2}\right)\frac{T}{T_o} \tag{4.27}$$

For the 3D square-in-square model the fully developed profile can be approximated by (Shah and London, 1978):

$$v_z = 2.09 v_m \left(1-\left(\frac{2|x|}{b}\right)^{2.2}\right)\left(1-\left(\frac{2|y|}{b}\right)^{2.2}\right)\frac{T}{T_o} \qquad (4.28)$$

Light-off curves (plots of conversion as a function of inlet gas temperature) were generated for different reactor lengths and different inlet temperature ramp rates. For the operating conditions used, a one inch reactor corresponds to a GHSV of 80 000 h^{-1} at an inlet velocity of 1 m/s, a four inch reactor 20 000 h^{-1}, etc, referenced at 298 K and 1 atm pressure. The first results were obtained for 5000 ppm by volume CO at an inlet temperature ramp rate of 30 K/min. The initial temperature was set at 350 K.

With the ramp rate, of 30 K/min several observations were made. The first is that the difference between the light-off curves disappears as the length of the reactor increases. For example, Figure 4.9 shows the case for a four inch reactor. It is seen that the light-off curves are essentially the same. The results for the one inch reactor are shown in Figure 4.10, where significant differences can be seen in the tail of the light-off curve. The circle in square geometry achieves complete conversion the quickest, with the square in square geometry the worst performing shape.

The effect of reactor length on light-off is shown in Figure 4.11 and 4.12 for circle-in-square and square-in-square geometry respectively. It is evident that in shorter monoliths the light-off occurs at a higher inlet temperature and that there is a limit beyond which increasing the length does not reduce the light-off temperature. This behaviour is caused by the nature of the kinetics, as discussed previously.

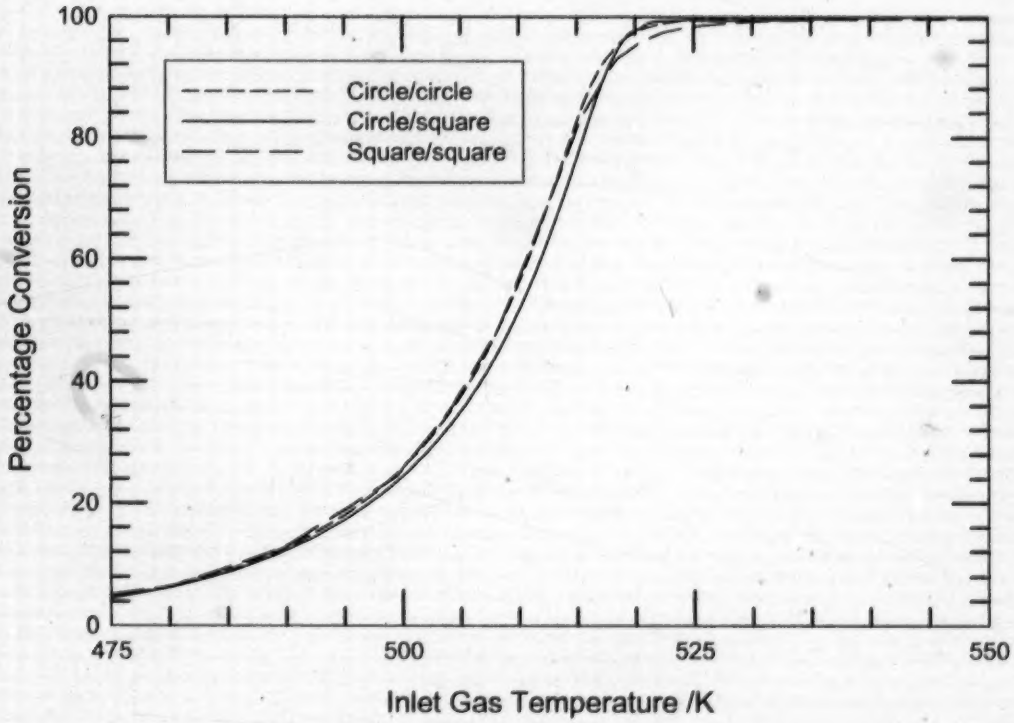

Figure 4.9: Effect of washcoat shape on the light-off curve for an inlet temperature ramp rate of 30 K/min at a GHSV of 20 000 h^{-1}. The CO concentration is 5000 ppm. Four inch long reactor.

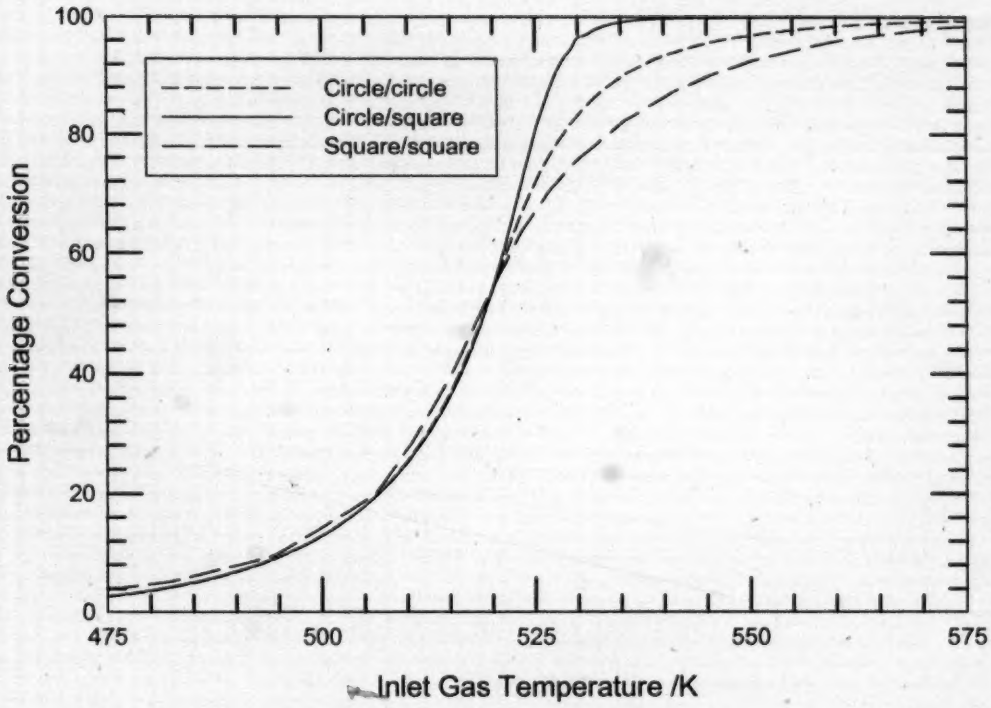

Figure 4.10: Effect of washcoat shape on the light-off curve for an inlet temperature ramp rate of 30 K/min at a GHSV of 80 000 h-1. The CO concentration is 5000 ppm. One inch long reactor.

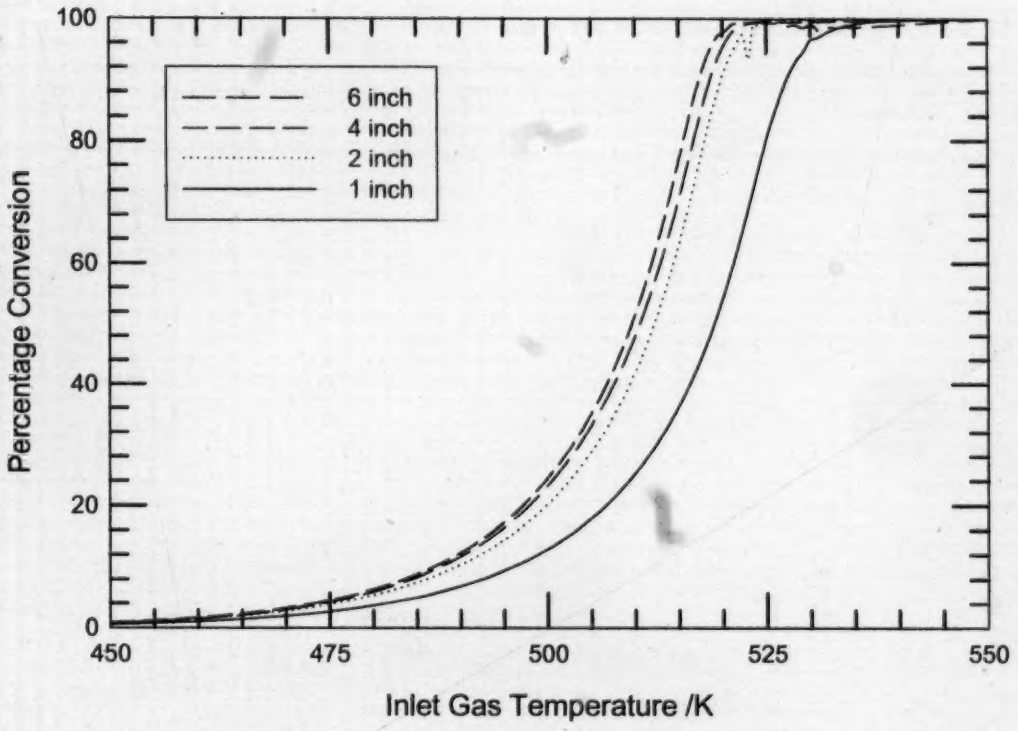

Figure 4.11: Effect of length of reactor on the light-off curve for an inlet temperature ramp rate of 30 K/min at increasing reactor length for circle-in-square geometry. The CO concentration is 5000 ppm.

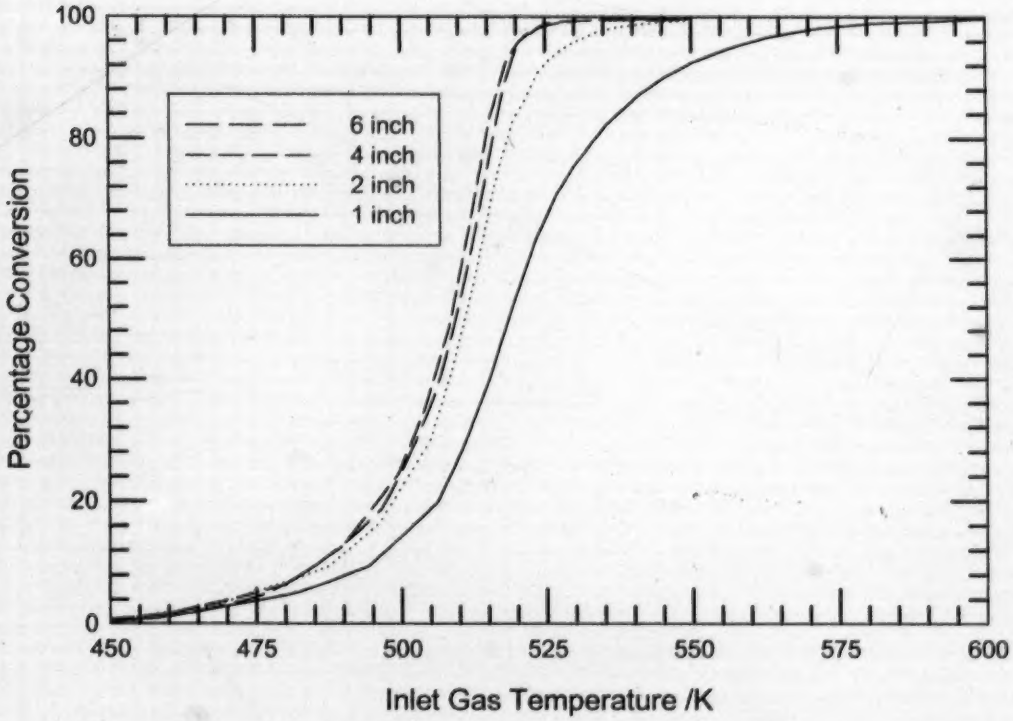

Figure 4.12: Effect of length of reactor on the light-off curve for an inlet temperature ramp rate of 30 K/min at increasing reactor length for square-in-square geometry. The CO concentration is 5000 ppm.

Different results were observed when the inlet temperature ramp rate was increased by an order of magnitude to 300 K/min. For the range of GHSV tested (80 000 h^{-1} and lower) there was no significant effect on the light-off curve as a function of length. The explanation for this is similar to the case with a ramp rate of 30 K/min. However, at high ramp rates, the inlet portion of the monolith heats more quickly, and thus the ignition point was always within one inch of the inlet. At much shorter lengths (much higher GHSV, there is expected to be an effect. Although the effect of length disappears, the washcoat shape had a larger influence on the shape of the light-off curve, and the value of the light-off temperature. Figure 4.13 shows the result obtained for the one inch reactor which explains the influence of washcoat shape on the light-off curve. Figure 4.14 and

4.15 shows that the effects of length on light-off curves for higher ramp rates are essentially the same for circle-in-square and square-in square geometry. Slight deviation in square-in-square is because of numerical errors.

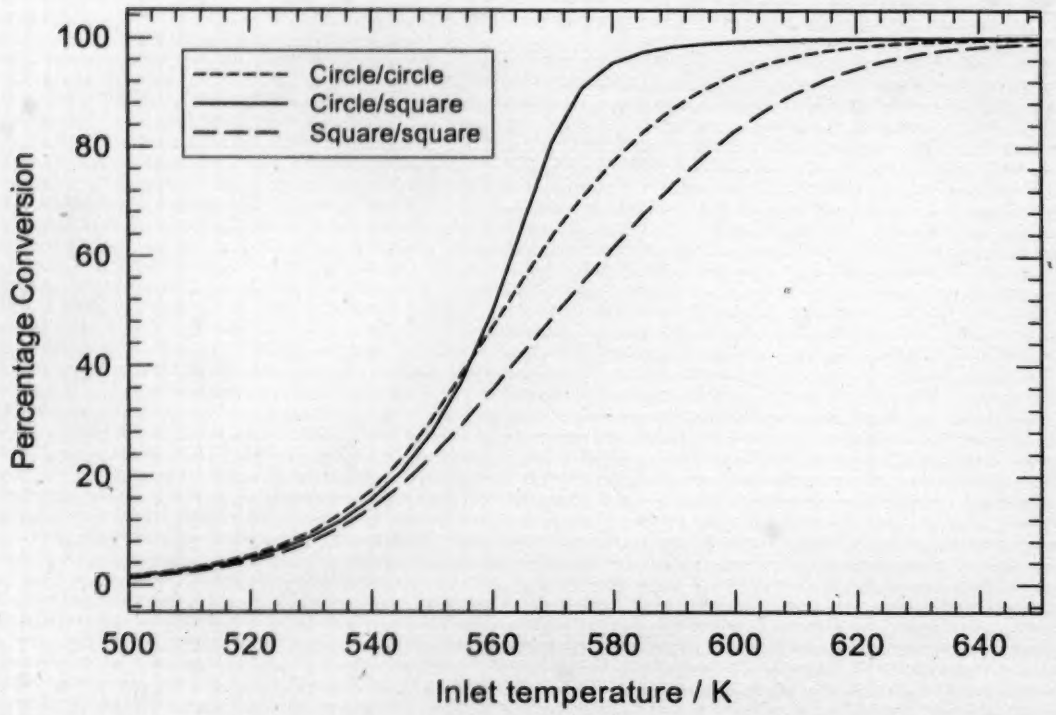

Figure 4.13: Effect of washcoat shape on the light-off curve for an inlet temperature ramp rate of 300 K/min at a GHSV of 80 000 h^{-1}. CO concentration is 5000 ppm. One inch long reactor.

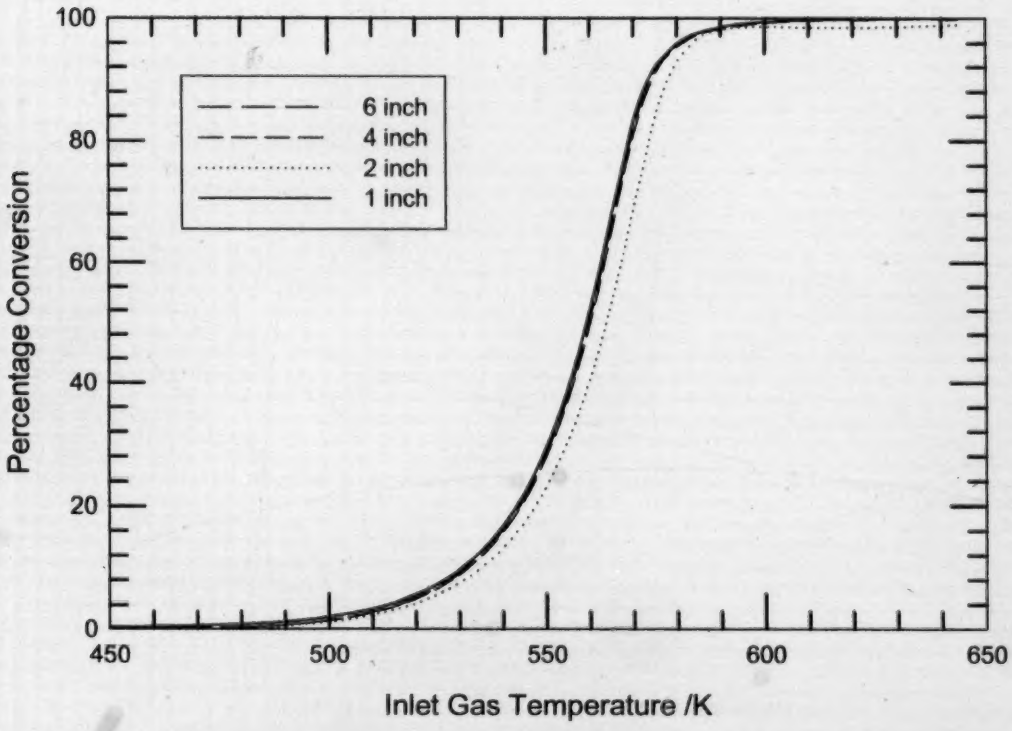

Figure 4.14: Effect of length of reactor on the light-off curve for an inlet temperature ramp rate of 300 K/min for circle-in-square geometry. The CO concentration is 5000 ppm.

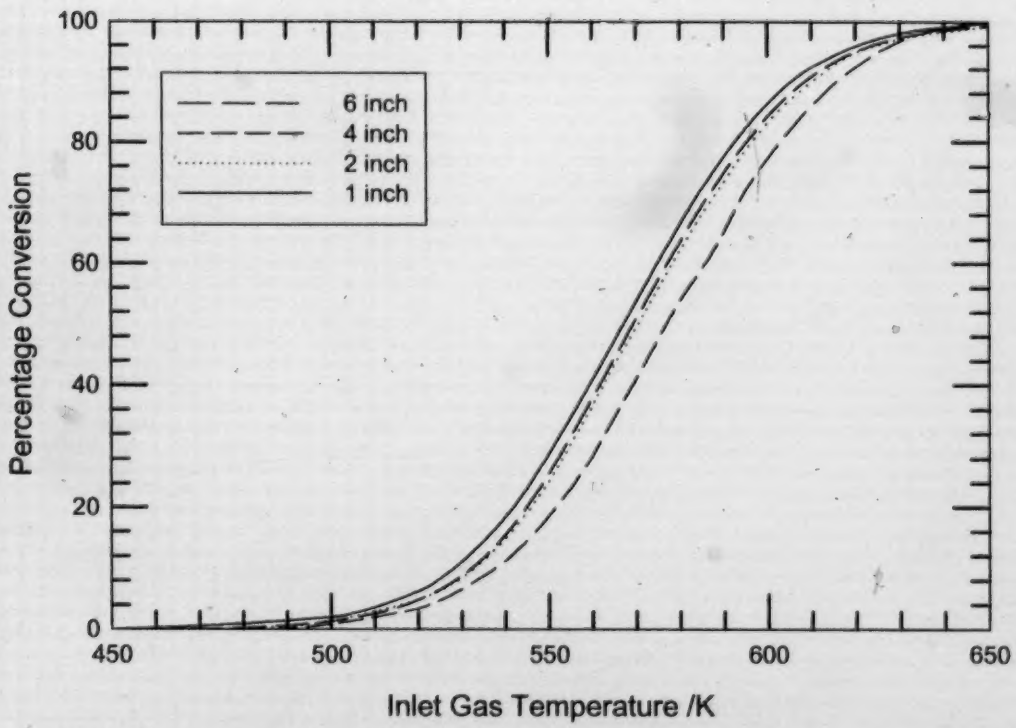

Figure 4.15: Effect of length of reactor on the light-off curve for an inlet temperature ramp rate of 300 K/min for square-in-square geometry. The CO concentration is 5000 ppm.

Simulations were performed when the inlet temperature ramp rate was increased by twice the order of magnitude to 600 K/min. For the range of GHSV tested (80 000 h^{-1} and lower) there was no significant effect on the light-off curve as a function of length. The explanation for this is similar to the case with a ramp rate of 300 K/min. Figure 4.16 shows the result obtained for the one inch reactor which explains the influence of washcoat shape on the light off curve. The circle in square geometry achieves complete conversion the quickest, with the square in square geometry the worst performing shape.

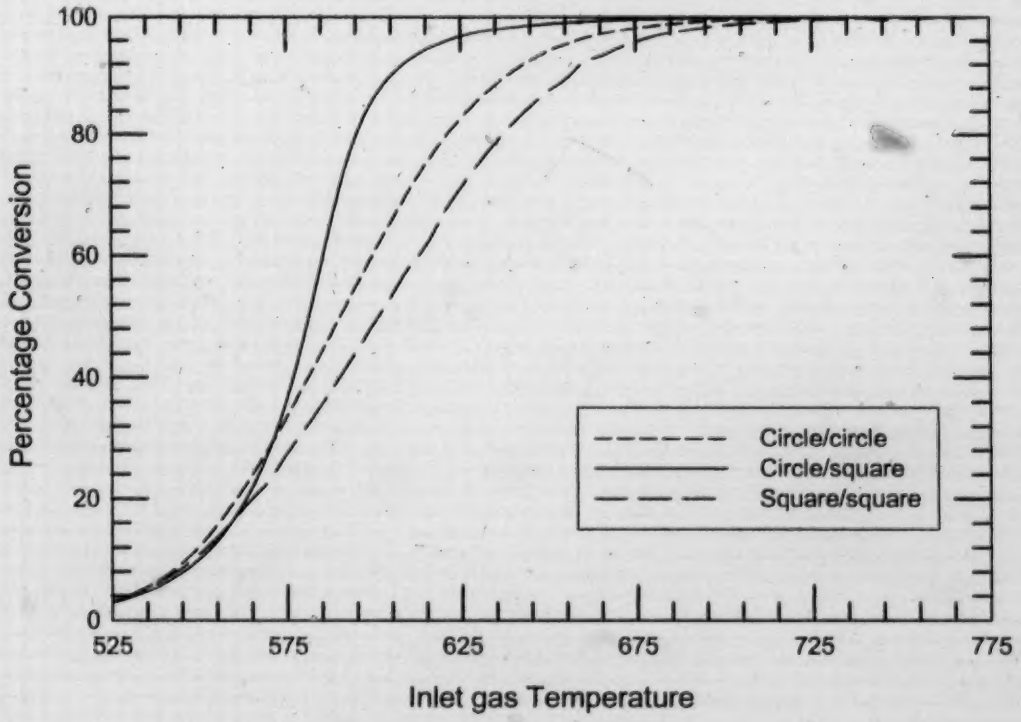

Figure 4.16: Effect of washcoat shape on the light-off curve for an inlet temperature ramp rate of 600 K/min at a GHSV of 80 000 h^{-1}. The CO concentration is 5000 ppm. One inch long reactor.

For the 2nd case, the solutions were obtained by solving the momentum, mass and energy balance simultaneously with an imposed and flat velocity profile at the inlet boundary to obtain the light off curve. Light-off curves (plots of conversion as a function of inlet gas temperature) were generated for a one inch reactor which corresponds to a GHSV of 80 000 h^{-1} referenced at 298 K and 1 atm pressure. The first results were obtained for 5000 ppm by volume CO at an inlet temperature ramp rate of 30 K/min. The initial temperature was set at 350 K.

With the ramp rate, of 30 K/min following observations were made for the one inch reactor when imposed velocity profile is used at the inlet boundary to solve for momentum balance. The result is shown in Figure 4.17, where significant differences can

be seen in the tail of the light-off curve. The circle in square geometry achieves complete conversion the quickest, with the circle in circle geometry the worst performing shape.

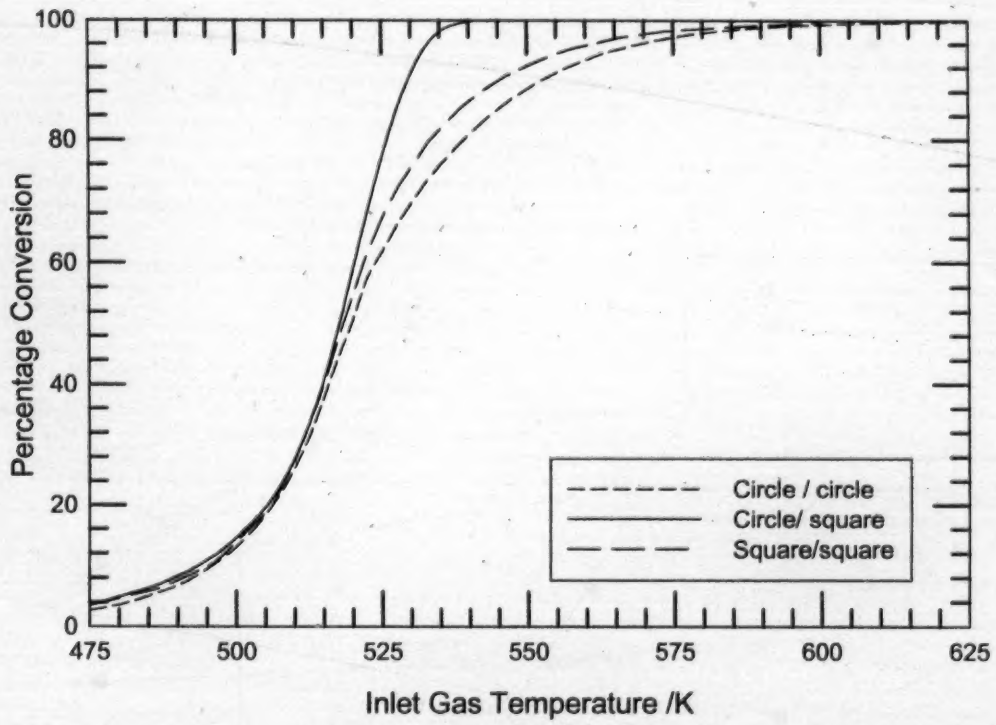

Figure 4.17: Effect of washcoat shape on the light-off curve for an inlet temperature ramp rate of 30 K/min at a GHSV of 80 000 h^{-1} with an fully developed velocity profile at the inlet. The CO concentration is 5000 ppm. One inch long reactor.

With the ramp rate, of 30 K/min following observations were made for the one inch reactor when flat velocity profile is used at the inlet boundary to solve for momentum balance. The result is shown in Figure 4.18, where significant differences can be seen in the tail of the light-off curve. The circle in square geometry achieves complete conversion the quickest, with the square in square geometry the worst performing shape.

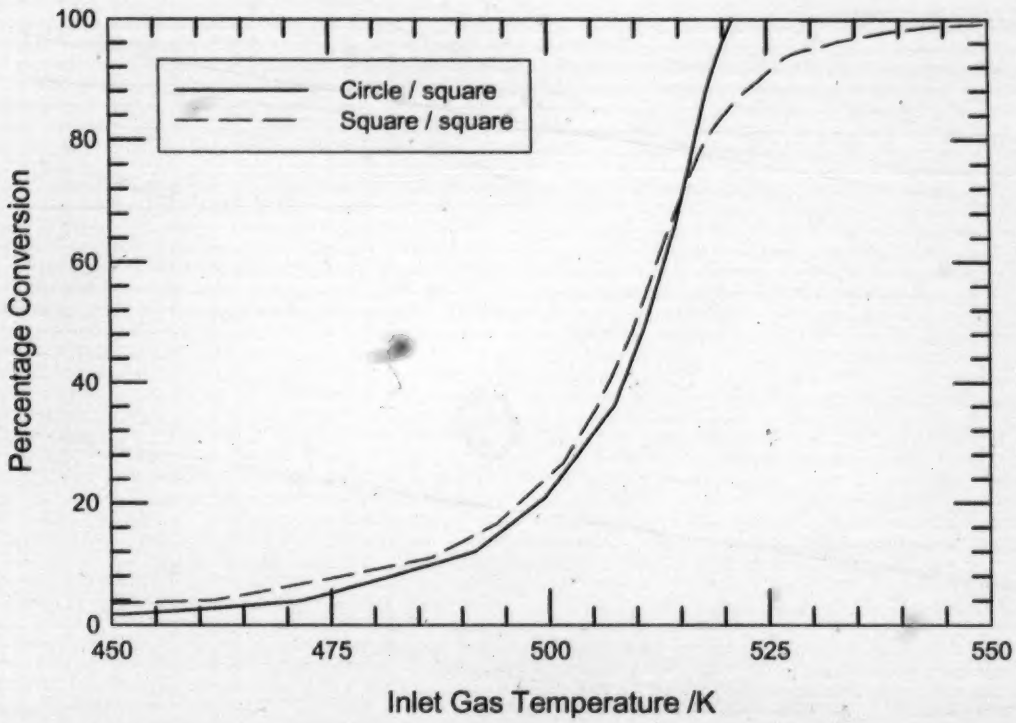

Figure 4.18: Effect of washcoat shape on the light-off curve for an inlet temperature ramp rate of 30 K/min at a GHSV of 80 000 h^{-1} with a flat velocity profile at the inlet. The CO concentration is 5000 ppm. One inch long reactor.

Figure 4.19 and Figure 4.20 shows the concentration profile along the length of reactor for circle-in-square geometry at different time steps for ramp rates of 30 K/min and 300 K/min respectively. From the concentration profile it is clear that the ignition takes place at the back end of the reactor. Similarly, Figure 4.21 and Figure 4.22 shows the temperature profiles along the length of reactor for circle-in-square geometry at different time steps for ramp rates of 30 K/min and 300 K/min respectively.

Figure 4.23 and Figure 4.24 show the concentration profiles along the length of reactor for square-in-square geometry at different time steps for ramp rates of 30 K/min and 300 K/min respectively. Similarly, Figure 4.25 and Figure 4.26 shows the temperature profiles along the length of reactor for square-in-square geometry at different time steps

for ramp rates of 30 K/min and 300 K/min respectively. Significant difference can be seen in the concentration profile for circle-in-square and square-in-square geometry. Complete conversion is achieved quickest for circle-in-square geometry.

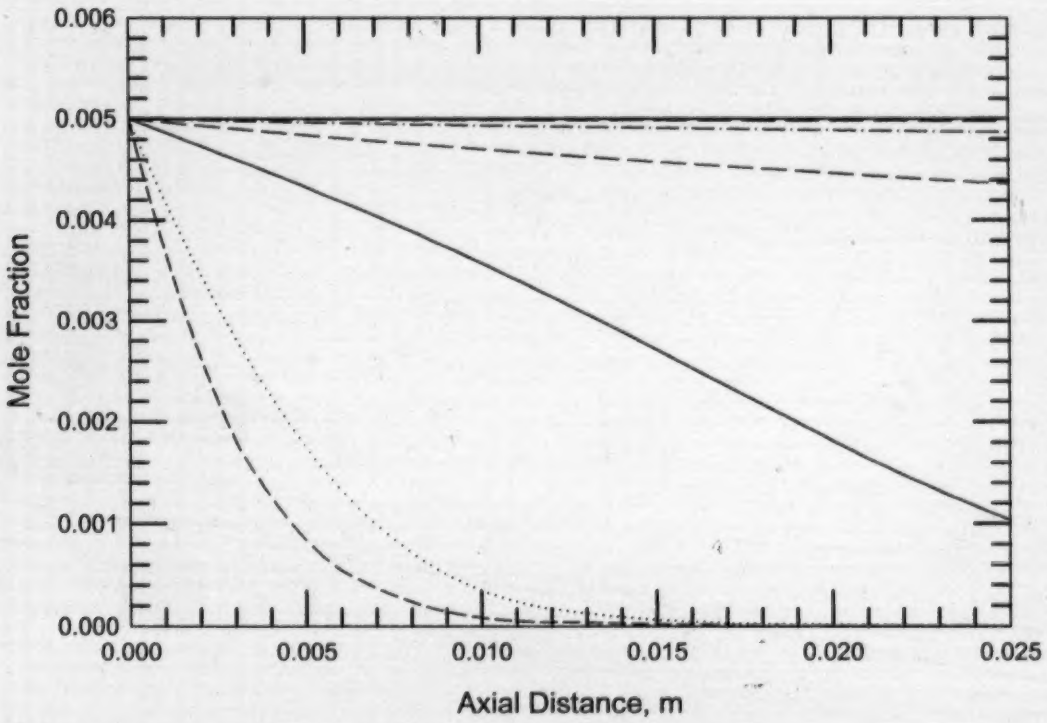

Figure 4.19: Concentration profile for circle-in-square geometry along the length of reactor for an inlet temperature ramp rate of 30 K/min at a GHSV of 80 000 h^{-1} with an imposed velocity profile at the inlet. The CO concentration is 5000 ppm.

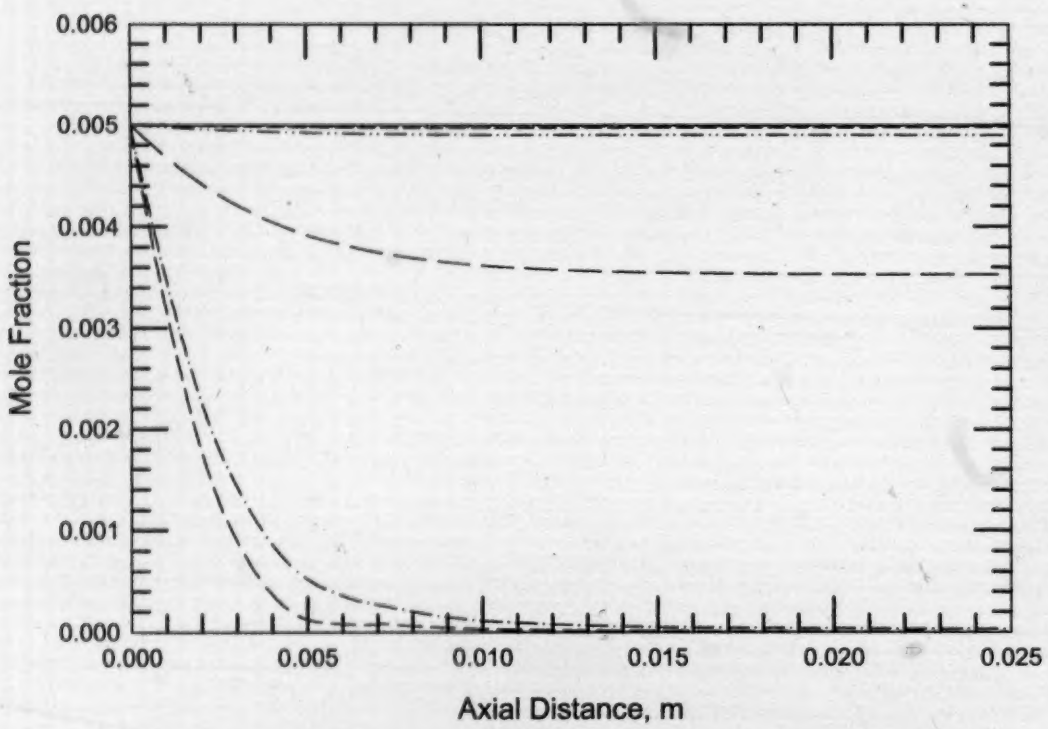

Figure 4.20: Concentration profile for circle-in-square geometry along the length of reactor for an inlet temperature ramp rate of 300 K/min at a GHSV of 80 000 h^{-1} with an imposed velocity profile at the inlet. The CO concentration is 5000 ppm.

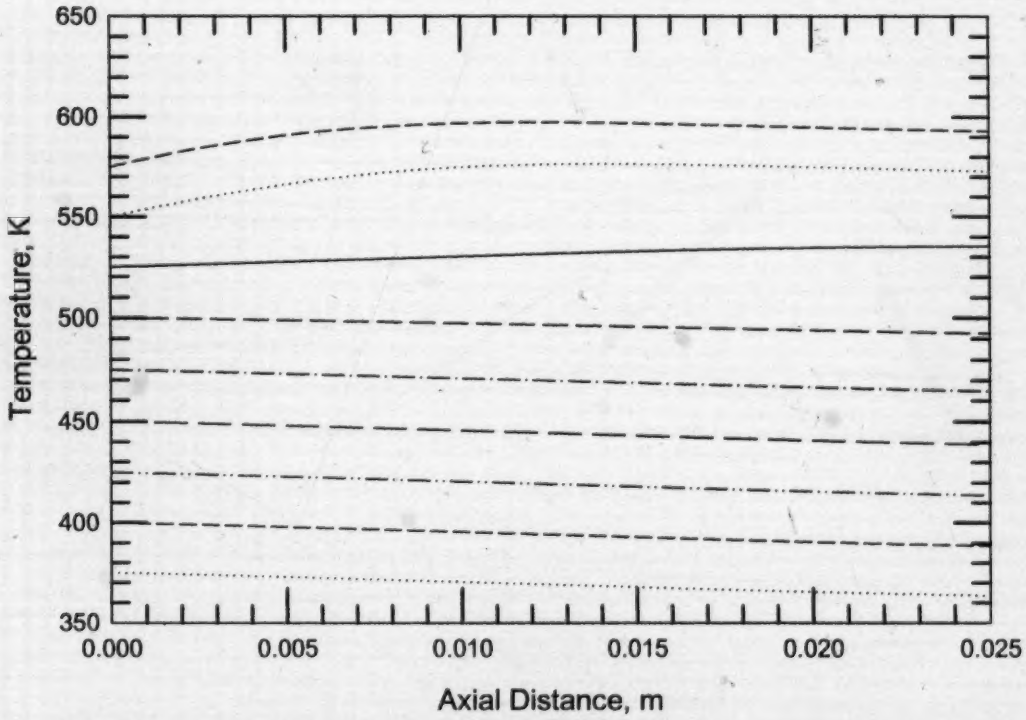

Figure 4.21: Temperature profile for circle-in-square geometry along the length of reactor for an inlet temperature ramp rate of 30 K/min at a GHSV of 80 000 h^{-1} with an imposed velocity profile at the inlet. The CO concentration is 5000 ppm.

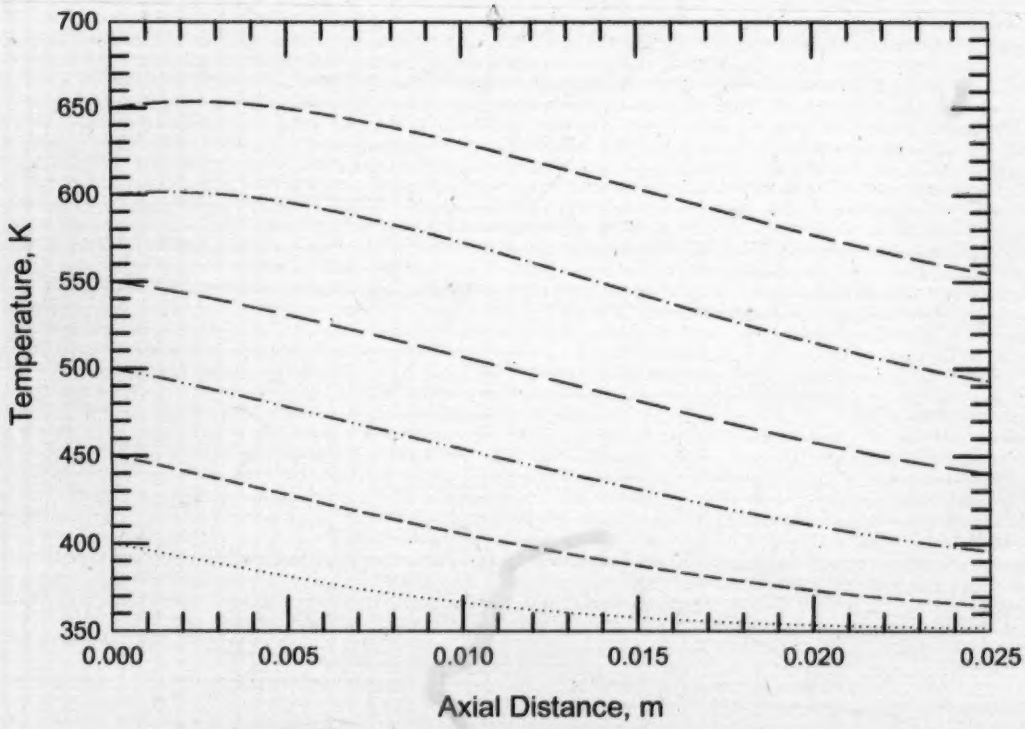

Figure 4.22: Temperature profile for circle-in-square geometry along the length of reactor for an inlet temperature ramp rate of 300 K/min at a GHSV of 80 000 h^{-1} with an imposed velocity profile at the inlet. The CO concentration is 5000 ppm.

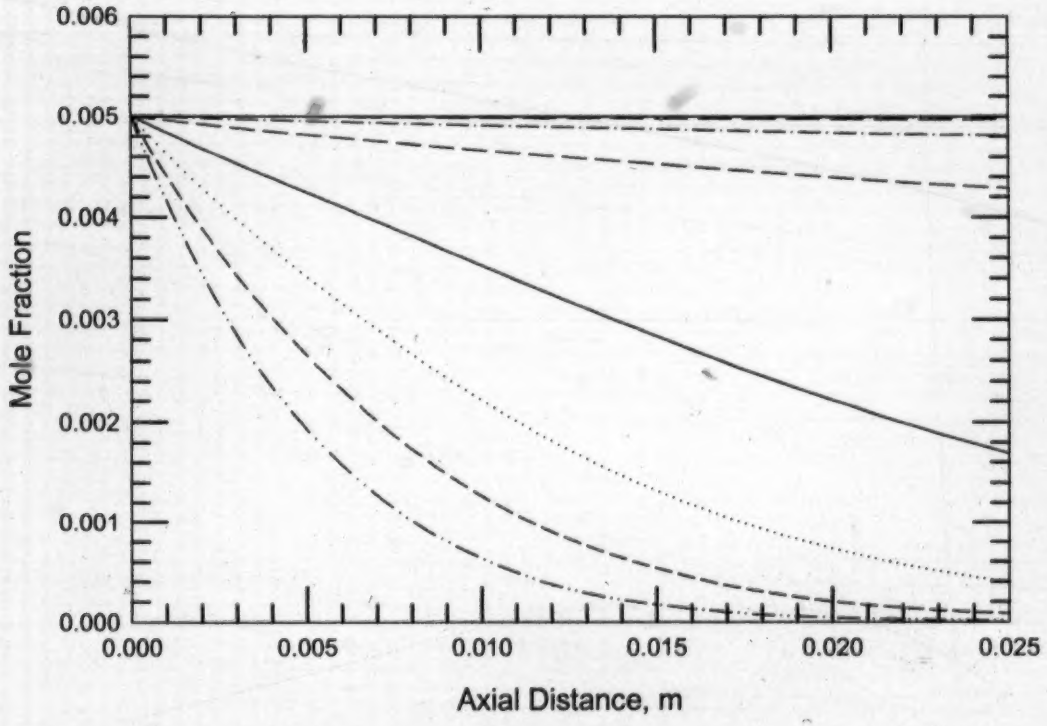

Figure 4.23: Concentration profile for square-in-square geometry along the length of reactor for an inlet temperature ramp rate of 30 K/min at a GHSV of 80 000 h^{-1} with an imposed velocity profile at the inlet. The CO concentration is 5000 ppm.

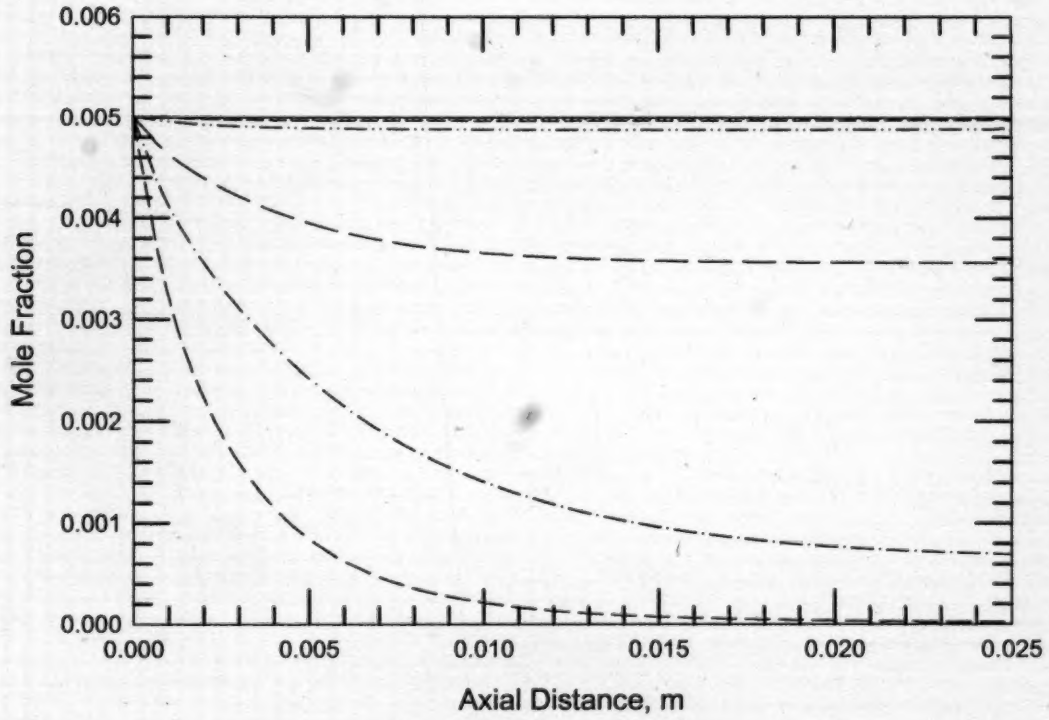

Figure 4.24: Concentration profile for square-in-square geometry along the length of reactor for an inlet temperature ramp rate of 300 K/min at a GHSV of 80 000 h^{-1} with an imposed velocity profile at the inlet. The CO concentration is 5000 ppm.

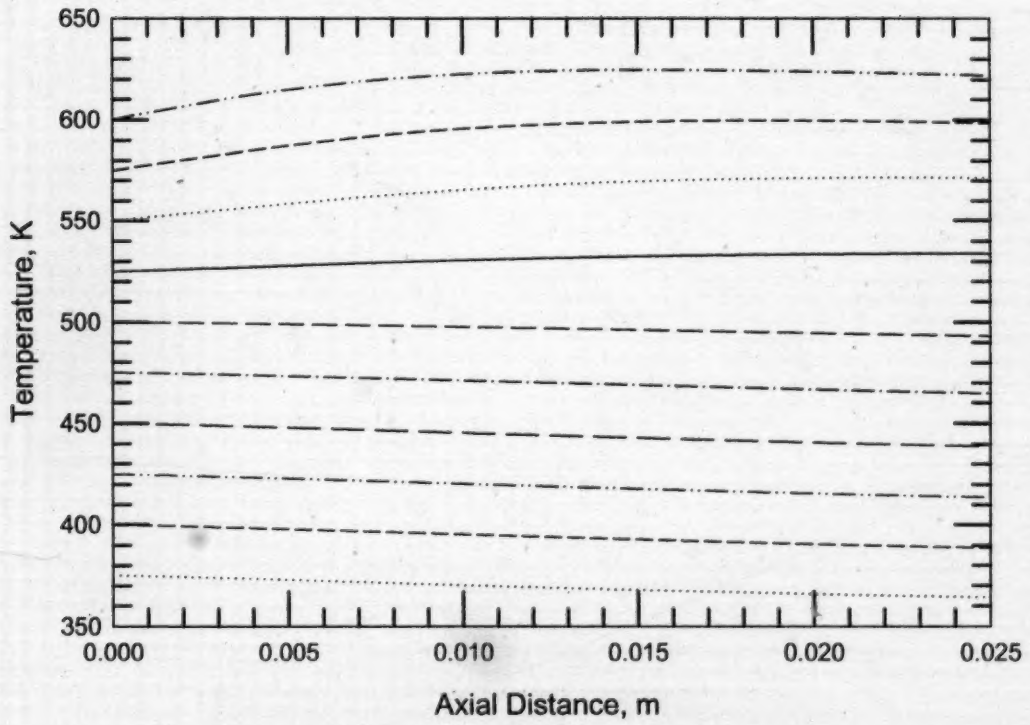

Figure 4.25: Temperature profile for square-in-square geometry along the length of reactor for an inlet temperature ramp rate of 30 K/min at a GHSV of 80 000 h^{-1} with an imposed velocity profile at the inlet. The CO concentration is 5000 ppm.

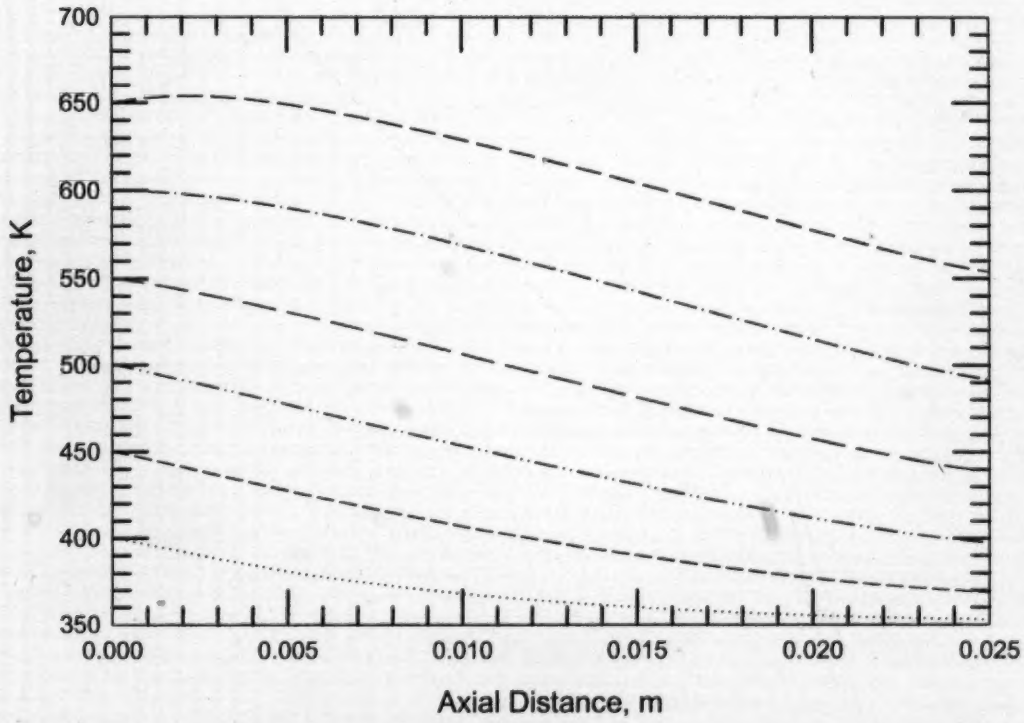

Figure 4.26: Temperature profile for square-in-square geometry along the length of reactor for an inlet temperature ramp rate of 300 K/min at a GHSV of 80 000 h^{-1} with an imposed velocity profile at the inlet. The CO concentration is 5000 ppm.

4.3 Concluding remarks

It is clear that there are conditions where the washcoat shape has a significant influence on the simulated light-off. The comparisons of temperature ramp rates are significant, because the standard testing procedures and driving cycle simulations typically use a slow ramp rate, whereas under real operating conditions the ramp rates tend to be much higher. Therefore, under real operating conditions, the washcoat design is expected to play a significant role in the observed light-off. Indeed, the best performance was observed for the circle in square geometry, which mimics to an extent the fillet shape observed in practice. Another ramification relates to the use of light-off curves to back calculate kinetic parameters using parameter optimisation methods (Hayes et al., 2003). For computational reasons it is common to use a 2D model for the reactor (when diffusion is considered). We have shown that there are potential dangers in this approximation, and the range of conditions used should be chosen with care. Because the low temperature ramp rates gave the least discrepancy, it is suggested that this mode of operation be used when kinetic optimisation is the goal.

5. Heat and Mass Transfer in Turbulent Flow

In recent years a variety of factors, including toxic emissions limits, fuel economy, greenhouse gas emissions, cost and overall efficiency; have coincided to bolster the use of turbocharged Diesel engines in the automotive sector. Compared with gasoline engines, Diesel engines have some emission control problems, including lean operation, soot formation and low exhaust gas temperature. Different types of catalytic converters have been proposed, including close coupled catalysts in addition to standard under floor converters.

With their low exhaust temperature, modern Diesel engine exhaust may be below the light-off temperature of a diesel oxidation catalyst for large parts of the test cycle. One proposed solution (Carberry et al., 2005; Reizig et. al, 2001; Saroglia et al., 2002) to this problem is to place a small catalyst before the turbocharger, where the exhaust temperature is generally about 100 °C higher than in the post-turbo position. Owing to higher temperature and increased mass and heat transfer by turbulent flow, conversion efficiency during cold start is highly increased. Also, owing to space and back pressure considerations, these pre-turbo catalysts must be very small and operate at very short residence times. It is expected that these small pre-turbo catalysts will operate in the transition or turbulent flow regimes and further that most of the reactor will be in the entry region.

As we may deduce from the review in Chapter 2, there is not a large amount of work reported on the Sherwood and Nusselt numbers in this region. The purpose of this aspect of the work was to estimate a probable range of conversions that could be obtained in a pre-turbo catalyst with a standard activity automotive oxidation catalyst by exploring the effect of the Nu and Sh numbers over their realistically expected ranges. In this work, we present results obtained from the modelling of a single monolith channel under lean oxidation conditions. A non-linear kinetics model was used.

5.1 The 1D-2D single channel model

A single channel model of the monolith converter was used to simulate the performance of the pre-turbo catalyst. As usual, the single channel model assumes that it is representative of all of the channels, and that all channels are the same. As noted in the introduction, we wish to do an examination of realistically possible Nu and Sh numbers, without involving the complexity of modelling exactly the flow. We therefore adopted a one dimensional model for the gas phase, where it is easy to adjust Nu and Sh in any desired manner. Further, because we expect that diffusion in the washcoat would also be important, a two dimensional model for the washcoat was adopted. Thus the channels were modelled as axi-symmetric right circular cylinders. A representation of a 1D – 2D model of a single monolith channel is shown in Figure 5.1.

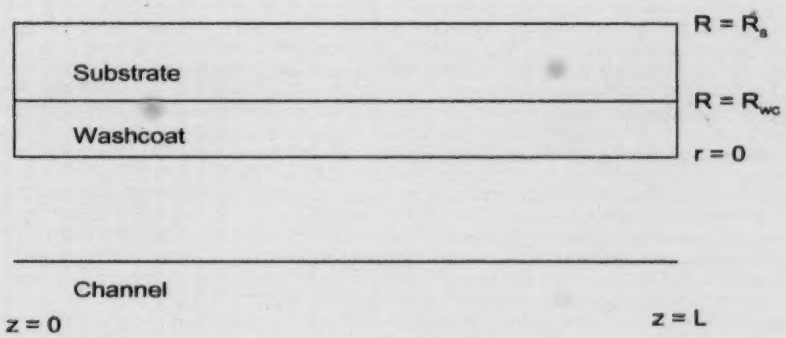

Figure 5.1: Schematic representation of a 1D – 2D model

The model equations for the 1D-2D model were given in Chapter 3, and are repeated here for ease of reference. Note that all of the simulations reported in this Chapter are at steady state. The mole balance equation in terms of the mole fraction for the channel is:

$$\frac{\partial}{\partial z}\left(D_{AB} C_f \frac{\partial Y_{A,f}}{\partial z}\right) - v \frac{\partial Y_{A,f}}{\partial z} - k_m C_f \left(Y_{A,f} - Y_{A,WC}\right)\left(\frac{4}{D_H}\right) = 0 \qquad (5.1)$$

The boundary conditions are a specified concentration at the inlet and a zero flux condition at the outlet. The mole balance in terms of mole fractions for the washcoat is:

$$(D_{\text{eff}})_A \nabla(C \nabla Y_A) - (-R_A) = 0 \tag{5.2}$$

Because of the discontinuity at the washcoat surface, we introduce a boundary condition at the washcoat surface as:

$$-D_{\text{eff}} \frac{\partial Y_{A,f}}{\partial r} = k_m \left(Y_{A,f} - Y_{A,WC}\right) \tag{5.3}$$

The end surfaces of the washcoat are modelled as zero flux boundaries. It is not necessary to model the mole balance in the substrate, however the equation is:

$$(D_{\text{eff}})_A \nabla(C \nabla Y_A) = 0 \tag{5.4}$$

The outside surfaces of the substrate were modelled as zero flux boundaries. The energy balance equation for the channel is:

$$\frac{\partial}{\partial z}\left(k_f \frac{\partial T_f}{\partial z}\right) - \rho C_{P,f} v \bullet \frac{\partial T_f}{\partial z} - h\left(T_f - T_{WC}\right)\left(\frac{4}{D_H}\right) = 0 \tag{5.5}$$

The boundary conditions for the channel are specified temperature at the inlet and zero flux at the outlet. The energy balance equation for the washcoat is:

$$\nabla \bullet (k_{\text{eff}} \nabla T) + (-\Delta H_R)(-R_A) = 0 \tag{5.6}$$

The boundary condition at the washcoat surface is:

$$-k_S \frac{\partial T_f}{\partial r} = h\left(T_f - T_{WC}\right) \tag{5.7}$$

A zero flux condition was specified at the ends of the monolith. The energy balance equation for the substrate is:

$$\nabla\bullet\left(k_{\text{eff}}\nabla T\right) = 0 \tag{5.8}$$

The boundary conditions are zero flux at the outside surfaces.

The model reaction was the oxidation of carbon monoxide in an excess of oxygen. The rate expression used was based on the Voltz model (Voltz et al., 1973), and is given by:

$$\left(-R_{\text{CO}}\right) = \frac{k_{\text{CO}}\, Y_{\text{CO}}\, Y_{\text{O2}}}{T\left(1 + K_{\text{CO}}\, Y_{\text{CO}}\right)^2} \tag{5.9}$$

The values of the kinetic constants were selected to give light-off in the range normally expected for a typical automotive catalytic converter on a platinum catalyst under lean conditions. Thus the pre-exponential factor was adjusted until light-off (50 % conversion) was achieved at 450 K with a GHSV of 50 000 h^{-1}, 1000 ppm CO, 6 % O_2 and a temperature ramp rate of 20 K/min. The final model with the kinetic constants, expressed in terms of the washcoat volume, is:

$$\left(-R_{\text{CO}}\right) = \frac{9.25\times10^{19}\exp\left(\dfrac{-105\,000}{R_g T}\right) Y_{\text{CO}}\, Y_{\text{O}_2}}{T\left(1 + 65.5\exp\left(\dfrac{7990}{R_g T}\right) Y_{\text{CO}}\right)^2} \quad \frac{\text{mol}}{\text{m}^3\text{s}} \tag{5.10}$$

The washcoat thickness was 42.6 microns. All physical properties of the monolith structure used were standard values for ceramic supported monolith systems (refer Chapter 3).

The coupled system of partial differential equations was solved by using the finite element method with the software package COMSOL Multi-physics version 3.2. For the 1D geometry the software divides the sub-domain into smaller intervals and triangular elements were used for the 2D geometry. The execution time for one run was about 20 minutes.

5.2 Effect of gas velocity on conversion

The first step was to study the variation of conversion with space velocity at various temperatures, and to determine the effect of the Nusselt and Sherwood numbers, which respectively govern heat and mass transfer. Following the usual heat and mass transfer analogy, reinforced by literature results (Hayes and Kolaczkowski, 1997), the Nu and Sh were set to be equal. Although standard catalytic converters operate within the laminar region, pre-turbo catalysts could operate in the transition or turbulent regions because the converter is necessarily of small diameter. It is to be expected that the maximum conversion that can be achieved in such pre-turbo catalysts will be limited by transport effects in both the channel and in the porous washcoat.

Mass and heat transfer effects in catalytic monoliths have been widely investigated in the laminar flow region, for a wide variety of channel shapes and operating conditions. We review briefly the main concepts required to conduct an order of magnitude analysis for the efficacy of a pre-turbo catalyst. Attention is paid to the developing region, because for the short pre-turbo catalyst it is expected that most of the flow will occur in this region. For external heat transfer, the Nusselt number decreases logarithmically from a high value at the entrance to an asymptotic value in the fully developed region.

Consider, for illustration purposes, a pre-turbo catalyst based on a standard 400 CPSI ceramic monolith substrate. This reactor has 1 mm diameter channels and is 50 mm in length. At the limit of laminar flow (Re=2100), the thermal entry length in a circular channel is about 80 mm. The combined entry length Nusselt number has a value of about 18 at a distance of 1.6 mm from the inlet, which falls to about Nu = 5 at the end of the

reactor (Equation (2.49)). The exact values depend on the reaction rate, and are affected by the internal diffusion resistance.

At the onset of fully developed turbulence (Re = 10 000), the Dittus-Boelter correlation predicts a value for Nu of about 32 (Incropera and DeWitt, 2002). The thermal entry length is expected to be of the order of 15 mm, and the maximum Nu enhancement factor in this region should be around 2.5 (Millis, 1963). Transition flow, that is, for Re $\in$ [2100, 10 000] is more complicated than either laminar or turbulent flow. For example, at Re = 4000 the correlation of Gnielinski (see chapter 2) predicts a fully developed Nu of 14. Although this discussion is a generalization, and there are many complexities in the computation of accurate heat and mass transfer coefficients in monolith reactors, it is likely safe to assume that the range of Nu and Sh over the expected range of operation of a pre-turbo catalyst is 4 to 100.

Therefore, in the first instance a monolith based on a standard 400 CPSI substrate 50 mm in length was considered. The conversion of CO obtained for a 1000 ppm feed with 6 % oxygen over a wide velocity range was studied. Note that a velocity of 1 m/s (referenced to 298 K) corresponds to a GHSV of 50000 h^{-1} and a velocity of 100 m/s gives a GHSV of 5000000 h^{-1}. At 600 K for a 1 mm diameter channel, the corresponding range of Reynolds number is about 40 to 4000. We note that ceramic 100 CPSI monolith with 2 mm channels would increase the Reynolds number by a factor of 2, still below the value for fully developed turbulent flow.

Figure 5.2 shows the conversion as a function of velocity (referenced at 298 K) at inlet temperatures of 550 K and 600 K (expected in the converter at steady state), for three Nusselt numbers. As noted, these values span the range of the expected Nu number. If we assumed that at 100 m/s the average Nu and Sh were between 10 and 100, then we would expect a conversion of CO in the range of 24 to 36 % at 600 K and 10 to 16 % at 550 K. It is noticeable that the conversion has less dependence on Nu and Sh at low temperatures.

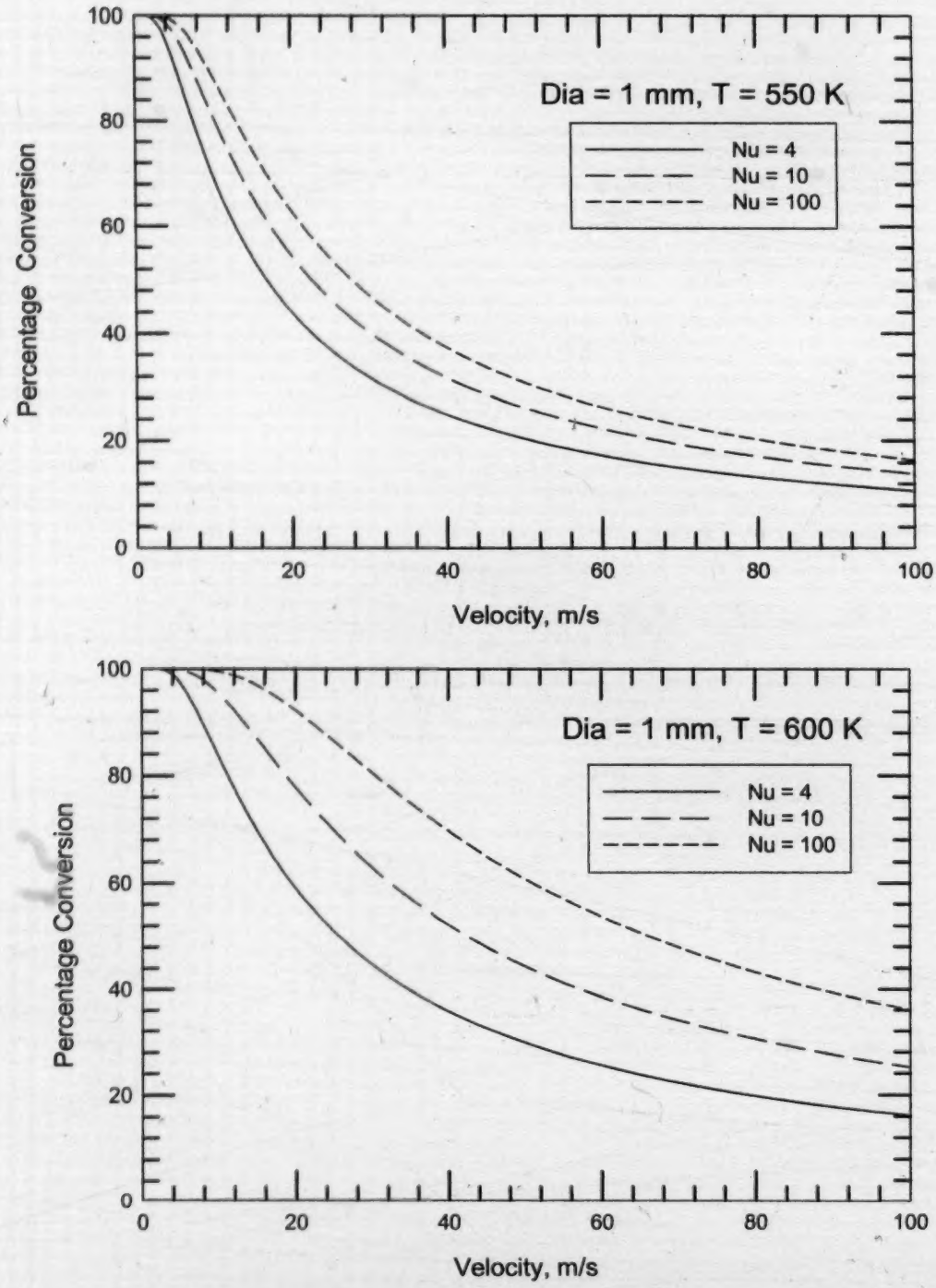

Figure 5.2: Variation of the fractional conversion with inlet channel velocity for three different Nusselt and Sherwood number values for inlet temperatures of 500 and 600 K.

5.3 Effect of channel diameter

If reduced back pressure is desired, then one option may be to increase the channel diameter, although one must consider the flow regime. For fully developed laminar flow, the pressure decreases linearly with Re, then jumps when the flow regime moves into the transition region, where after it falls as the fourth root of Re (Bird et al., 2002). The effect on the heat and mass transfer is less obvious. For fully developed flow in the laminar region, Nu and Sh are independent of Re, whereas in transition and turbulent flow they increase roughly with $Re^{0.8}$. However, the quantities of interest are the actual heat and mass transfer coefficients, which will always decrease with increasing channel diameter. Furthermore, because the channel surface area to volume ratio decreases with increasing diameter, the overall driving force decreases further. Therefore, within a given fully developed flow regime, an increase in channel diameter should lead to a lower conversion, so the main benefit of increasing diameter would come if it results in a change in flow regime from laminar to transition or turbulent. For a pre-turbo catalyst the situation is less obvious, because much of the flow is in the developing region. The entry length will increase directly with the diameter, although this increase should not be huge. For example, for laminar flow with a combined entry length, the average Nu increases with $D^{0.67}$. Finally, it should be noted that there are also two circumstances where reduced heat and mass transfer coefficients can increase reaction rate; (1) the increase in wall temperature accelerates the reaction rate more than the decrease in wall concentration decelerates it, or (2) the reactant inhibits the reaction, so a reduction in concentration leads to an increase in rate (such as in CO oxidation).

The 1 mm channel diameter experiments were repeated at channel diameters of 1.5 and 2 mm. The results are shown in Figure 5.3 for 600 K. For a given average Nu, the conversion drops as the channel diameter increases. As noted, for a given flow regime, the main effect of the increased diameter is to lengthen the entry region. While it is uncertain what Nu enhancement ratio will be thus obtained, it is probably a safe assumption that it is less than two, and thus there is not an advantage in moving to higher diameters, provided that the pre-turbo catalyst operates in the transition or turbulent region.

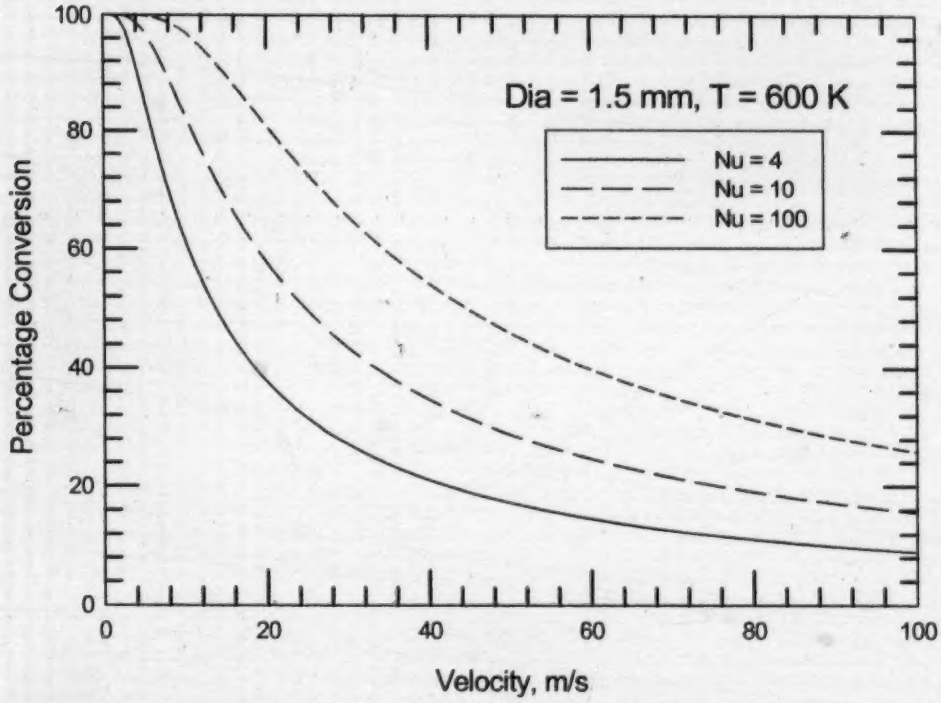

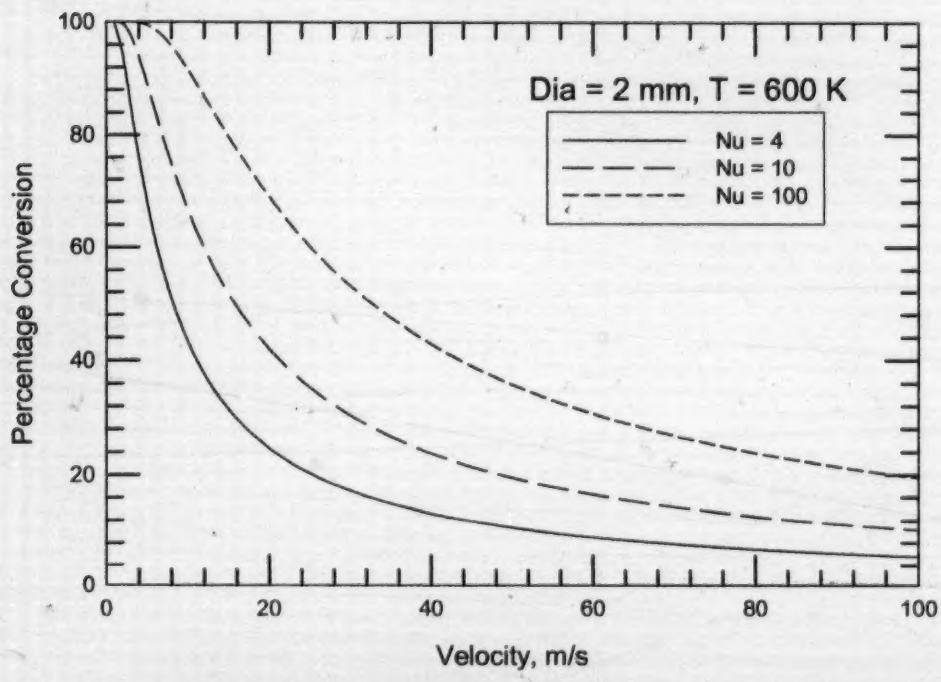

Figure 5.3: Variation of the fractional conversion with inlet channel velocity for three different Nusselt and Sherwood number values for inlet temperature 600 K with channel diameter of 1.5 and 2 mm.

5.4 Effect of internal diffusion

As a final result we examine the effect of internal diffusion. We expect that at temperatures of 550 to 600 K the oxidation of CO will be influenced by diffusion in the washcoat. We present therefore a curve showing the effect of reducing the washcoat thickness by one half. Figure 5.4 shows the result for 600 K and Nu = Sh =100. Three curves are shown; the base case, the result obtained when the washcoat thickness is one half the original, and the third obtained when the washcoat is one half the original thickness but the catalyst activity is increased by a factor of two. The last case corresponds to a situation where the same amount of active catalyst is added to a thinner washcoat. We see that reducing the washcoat thickness for constant catalyst activity results in no reduction in conversion, indicating the existence of strong internal mass transfer resistance. Increasing the catalyst activity, on the other hand increases the conversion.

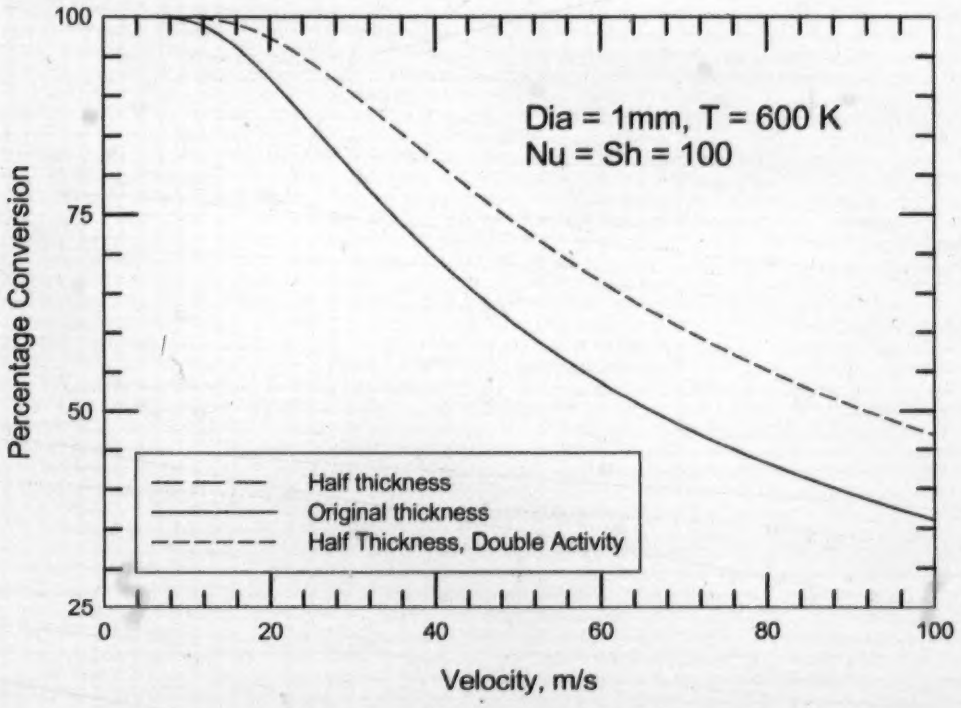

Figure 5.4: Variation of the fractional conversion with inlet channel velocity for fixed Nu and Sh with modified washcoat thickness and activity. The two curves for half thickness and original thickness coincide.

5.5 Prediction of Nu/Sh number for flow at high velocities

As discussed earlier pre-turbo catalyst operates at very high GHSV with the velocity of the order of 100 m/s; therefore the flow regime will be either transitional or turbulent. It is expected that the reaction will be significantly influenced by the external heat and mass transfer, about which little is known, especially for the entrance region and for reacting case.

For laminar flow, the Navier-Stokes equations can be solved numerically to give the velocity and pressure. However, for turbulent or transitional flow, the situation is more complicated. Turbulent flow is characterized by its chaotic, stochastic, transient and three-dimensional behaviour. There are wide ranges of eddy sizes, ranging from the size of the flow domain down to micro scale eddy. Energy is passed on from the larger eddies down to smaller and smaller ones, until energy is dissipated into heat.

As discussed in Chapter 2 and during the discussion on pre-turbo catalysts, it was seen that not much of work has been done on the study of heat and mass transfer effects when the flow is in the transition or turbulent region especially in the entry region. So to predict the values of Nusselt and Sherwood number in the transitional or turbulent region, simulations were performed with a 2D axi-symmetry model and to model the flow at high velocities, standard k-ε model was used in the reactor coupled with mass and energy balance equation.

The k-ε model is one of the most used turbulence models for many industrial applications (Wilcox, 1994). In this model, two extra transport equations are solved for two introduced variables; the turbulence kinetic energy, k, and the dissipation rate of turbulence energy, ε. Turbulent transport of momentum is then quantified using a gradient flux. This gives closure to the system and results in the following equations for the conservation of momentum and continuity:

$$\rho\frac{\partial v}{\partial t} - \nabla\cdot\left[\nu_T\left(\nabla v + (\nabla v)^T\right)\right] + \rho v\cdot\nabla v + \nabla p = F \qquad (5.11)$$

and

$$\nabla . v = 0 \tag{5.12}$$

ν_T is the turbulent viscosity and is given by:

$$\nu_T = C_\mu \frac{k^2}{\varepsilon} \tag{5.13}$$

Here, k is the turbulent energy and ε the dissipation rate of turbulence energy. The equation for k can be derived by taking the trace of the equations for the Reynolds stresses and is given by:

$$\rho \frac{\partial k}{\partial t} - \nabla . \left[\left(\eta + \rho \frac{C_\mu}{\sigma_k} \frac{k^2}{\varepsilon} \right) \nabla k \right] + \rho v . \nabla k = \rho C_\mu \frac{k^2}{2\varepsilon} \left(\nabla v + (\nabla v)^T \right)^2 - \rho \varepsilon \tag{5.14}$$

The equation for ε can be derived in a similar manner and is given by:

$$\rho \frac{\partial \varepsilon}{\partial t} - \nabla . \left[\left(\eta + \rho \frac{C_\mu}{\sigma_\varepsilon} \frac{k^2}{\varepsilon} \right) \nabla \varepsilon \right] + \rho v . \nabla \varepsilon = \rho C_{\varepsilon 1} \frac{k}{2} \left(\nabla v + (\nabla v)^T \right)^2 - \rho C_{\varepsilon 2} \frac{\varepsilon^2}{k} \tag{5.15}$$

The model constants used in the k-ε model are determined from experimental data. Different values are suggested in literature. The ones used are given below:

C_μ	$C_{\varepsilon 1}$	$C_{\varepsilon 2}$	σ_k	σ_ε
0.09	0.1256	1.92	1.0	1.3

Boundary condition at the inlet boundary is inflow/outflow with a flat velocity profile and neutral boundary condition at the outlet. Axial symmetry condition is used on the symmetry wall and logarithmic wall condition at the channel wall where turbulence

quantities k and ε are obtained from a standard wall function approach, which gives the following boundary condition for k and ε :

$$k = \frac{u_\tau^2}{\sqrt{C_\mu}} \qquad \text{and} \qquad \varepsilon = \frac{u_\tau^3}{\kappa y} \tag{5.16}$$

The mole and energy balance equations and the boundary conditions for the washcoat and substrate are given earlier, with modified coefficients for diffusion and conduction.. The Nusselt and Sherwood number values are calculated from equations described in Chapter 3. The same physical properties of the gas were used as described before in Chapter 3, except that the gas viscosity was assumed to be constant.

The solution to the reactor model was obtained using the finite element method package COMSOL multiphysics. Triangular elements were used with a finer mesh near the wall to capture the sharp gradients. The total number of elements was about 130,000. The total simulation time for one run was around 40 hours. The long simulation time is because of the difficulty in modelling the flow in this range of Reynolds number. Different solvers and solutions techniques were tried to get a converged solution.

The operating conditions used were a 1.44 mm diameter channel 50 mm in length. The inlet velocity was 100 m/s which corresponds to a Reynolds number of around 7000, referenced at T = 350 K and P = 1 atm. The inlet temperature was set to 550 K.

Figure 5.5 shows the variation of Sh (= Nu) number as a function of Graetz number. As discussed before, at the onset of fully developed turbulence the Dittus-Boelter correlation predicts a Nu value of 32. From the results obtained by simulation, we get a Nu/Sh value of around 10 (and the flow is not yet indicating fully developed regime). The reason for this may be that the constant values used in the k-ε model in COMSOL multiphysics differ from the constant values used in the standard k- ε model. Also, since the channel diameter is very small, we do not know whether the turbulent correlations work at this scale or not. Apart from that for flow in transition region, the wall function may not be

correct. Different researchers have suggested different wall functions if we need to use the k- ε model at low Reynolds number. Moreover, the k- ε model works effectively for highly turbulent flow.

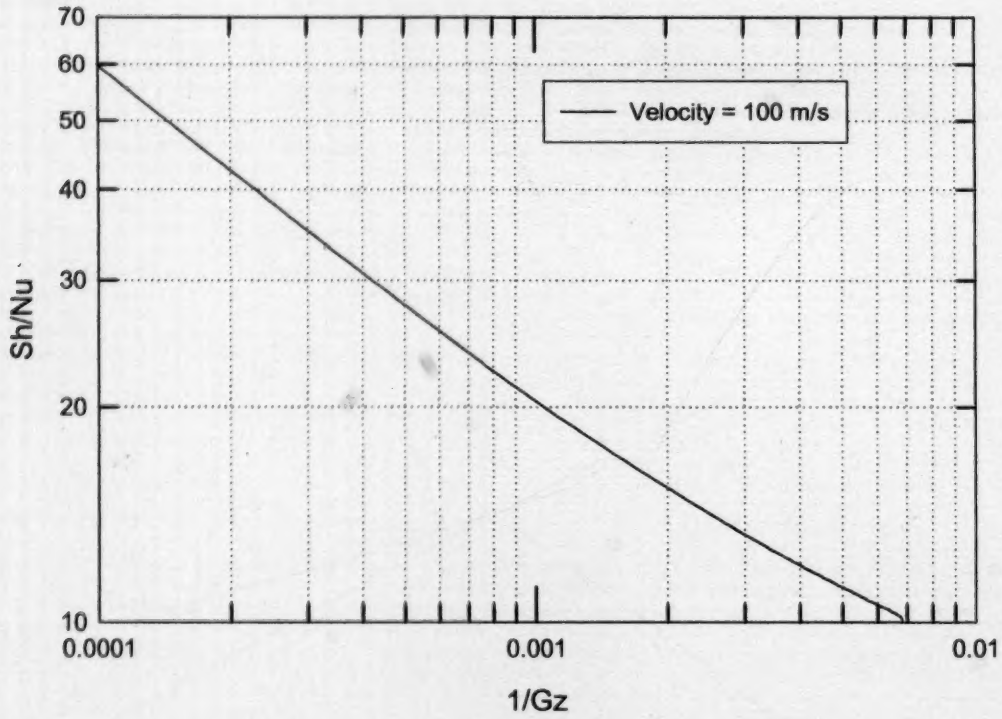

Figure 5.5: Local Sherwood number obtained from entry length solutions for turbulent flow in a channel with reaction at the surface of the catalyst.

Figure 5.6 shows the percentage conversion as a function of length of reactor. From the result obtained, it is seen that we get conversion of the order of 18 % (Sh = 10) at 100 m/s. Comparing the result obtained with the 1D-2D model at 100 m/s, for a 1.5 mm channel, we get a conversion of the order of 24 % (Sh = 100), 16 % (Sh = 10) and 8 % (Sh = 4) respectively at 600 K.

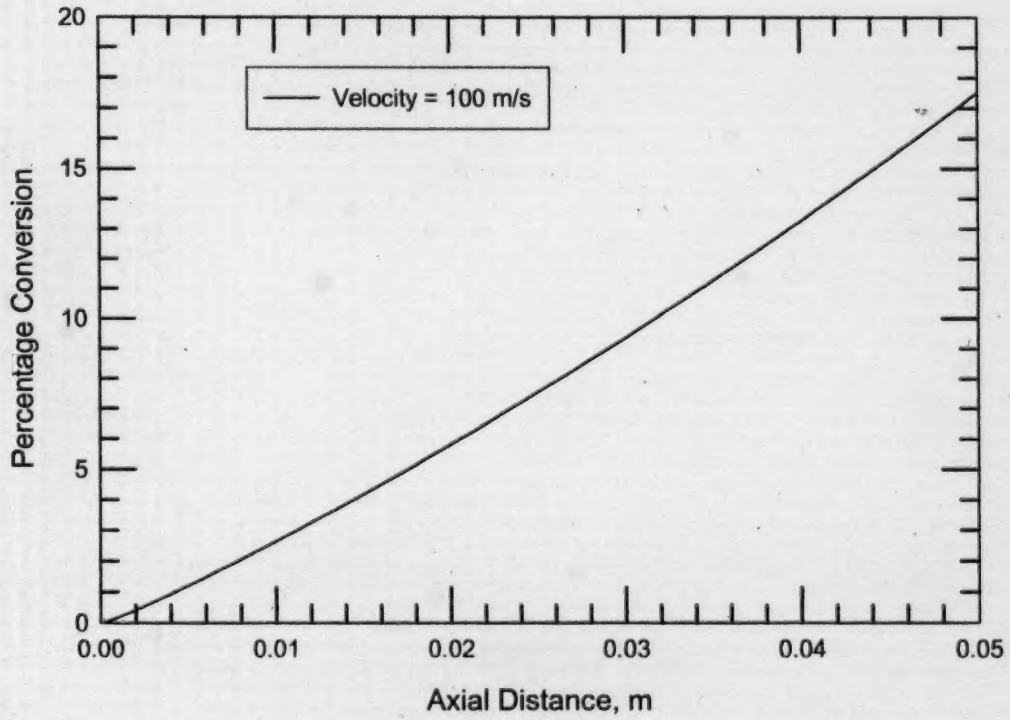

Figure 5.6: Conversion obtained for turbulent flow in a channel with reaction at the surface of the catalyst.

5.6 Concluding Remarks

In conclusion, it can be seen from these results that a pre-turbo catalyst should be beneficial in reducing overall emissions. For a typical size and flow-rate, it would not be unreasonable to expect a CO conversion of the order of 20 %. It is evident that the actual conversion will depend on the values of Nu and Sh, which in turn will lie primarily in the entrance region. We do not as yet have a very good understanding of the exact values for the developing region, especially in transition and turbulent flow. However, attempt was made to predict the exact values of Nu and Sh number using the k-epsilon model but the accuracy of model has to be investigated by doing more simulations for the fully developed flow and comparing those results with the standard correlations given in the literature. Once we have sufficient confidence in these values, we can study the effects of operating conditions on pre turbo catalysts with more detailed 2D and 3D modelling.

6. Conclusions and Future Work

In this work a series of numerical experiments were performed to study various aspects of the heat and mass transfer phenomena occurring in monolith catalytic converters. Based on the results, a number of conclusions and recommendations can be made.

With regard to the hydrodynamic entry length for laminar flow in circular channels, it was seen that the classical linear relationship between entry length and Reynolds number is not valid. Rather, it was observed that hydrodynamic length for laminar flow varies between two asymptotic solutions; with a constant entry length at low Reynolds number. This observation has practical ramifications for the thermally developing flow as well. However, for practical applications in catalytic converters, it is not likely to affect the performance significantly because at these low Re values the entry length will likely be an insignificant fraction of the total reactor length. However, from an academic perspective it may be interesting to explore these effects further, as they might have some application in very short reactors.

It was found in the investigation of the entry length Nu and Sh numbers for laminar flow that the entry length Nu (and by analogy the Sh) depends strongly on the physical properties of the fluid. Primarily, the expansion of a gas with heating generates a different solution from the well known and classical example obtained with constant physical properties. This effect was especially significant with the constant wall temperature boundary condition, and to a lesser extent with the constant wall flux condition. Furthermore, the heating rate in the inlet affects the Nu value as well. Although these results may have been known, or even obvious, they have not been reported to the best of my knowledge. When it comes to considering the Nu and Sh values that result when there is a reaction at the wall, it is not immediately evident how to compute this. The interpolation formula based on the two solutions for constant wall temperature and constant wall flux is less than ideal, since it is now shown that these cases are not obvious for the flow of a gas. Therefore, it is likely not possible to make a general conclusion about the best way to calculate entry length Nu and Sh in the developing flow region.

When most of the flow is in the fully developed region, and for steady state conditions, a one dimensional model can give similar results to the two dimensional model when a constant value of Nu and Sh is imposed. The value that is imposed may or may not be too important, depending on the degree of external mass transfer control.

The effect of various operating parameters and model assumptions was studied for the two dimensional model. It was seen that there is a potentially significant difference in light-off curve obtained when the momentum balance equation is included in the calculation, as opposed to using an imposed fully developed velocity profile. Although the light-off point is the same, the shape of the curve is different. This difference has implications for parameter estimation programs, where the flow model is used to optimize kinetic parameters by matching experimental to predicted light-off curves.

A series of numerical experiments were performed to test the influence of washcoat shape on the light-off curve. It has been shown that the shape can have a significant influence on the simulated light-off curve and under some operating conditions it is important to model the monolith correctly. The extent of the effect of shape of washcoat varies with operating condition. The most extreme effects are observed with higher temperature ramp rates. Also, difference between the light-off curves disappears for higher ramp rate as the length of the reactor increases. The results of this study also have significance for the simulation of experimental results, especially when experimental light-off curves are used to calculate kinetic parameters. There are also potential design implications.

We have investigated numerically the expected performance of a pre-turbocharger catalyst at the expected flow rates. For an oxidation catalyst with activity comparable to a standard Diesel oxidation catalyst, conversions of CO of the order of 20 % or more can be obtained depending on the operating conditions. It is evident that the actual conversion will depend on the values of Nu and Sh, which in turn will lie primarily in the entrance region. We do not as yet have a very good understanding of the exact values for the

developing region, especially in transition and turbulent flow. However, based on the results shown, the concept of a pre-turbo catalyst is worth exploring further.

Attempts were made to predict the Nu and Sh numbers at higher velocities using the k-epsilon turbulence model, but the results are inconclusive. This is also an area worth exploring further.

Further work could be done to quantify more accurately the heat and mass transfer coefficients prevailing in the catalyst, and also to consider as well the effects of hydrocarbons and hydrogen. In the study of light-off characteristics using 3D model, it might be worthwhile to study the variations of the heat and mass transfer coefficient as quantified by Nusselt and Sherwood number around the channel perimeter. Also the results should be tested for more realistic shapes of washcoat such as fillets and with wider range of operating conditions using three dimensional models.

For the case of turbulent flow model, more simulations need to be done with varying operating conditions and the accuracy of the tools need to be tested. Future work should focus on improving the correlations in this region, as well as studying the sensitivity of the conversion to Nu and Sh at high velocity. Once sufficient confidence in these values is obtained, it will be possible to couple the pre-turbo catalyst to reactor models of the under floor catalysts to study total emissions reduction under driving cycle conditions.

REFERENCES

Alexander, J.T., and Umehara, K., "Ceramic Honeycomb for Air Pollution Control", NKG Insulator Ltd., Nagoya, Japan, Reference JH-952121, July (1995)

Al-Ali, H.H., and Selim, M.S., "Analysis of Laminar Flow Forced Convection Heat Transfer with Uniform Heating in the Entrance Region of a Circular Tube" Can. J. Chem. Eng., Vol. 78, No. 6, 1101-1107 (1992).

Benedetto, A.D., Donsi, F., Marra, F.S., and Russo, G., "Heat and Mass Fluxes in Presence of Fast Exothermic Superficial Reaction", Combustion Theory and Modelling, Vol. 9, No. 3, 463-477 (2005)

Bhattacharya, M., Harold, M.P., and Balakoatiah, V., "Mass-Transfer Coefficients in Washcoated Monoliths", AIChE , Vol. 50, No. 11, 2939-2955 (2004).

Bird, R.B., Stewart, W.E., Lightfoot, E.N., "Transport Phenomena", John Wiley, New York, 2002.

Boersma, M.A., Tielen, W.H.M., and Van Der Bann, H.S., "Experimental and Theoretical Study of Simultaneous Development of the Velocity and Concentration Profiles in the Entrance Region of a Monolithic Converter", ACS Symposium Series, 65, 72-82 (1978).

Brauer, H.W., and Fetting, F., "Stofftransport bei Wandreaktion im Einlaufgebeit eines Strömungsrohres", Chem. Ing. Technol., 38, 30-35 (1966)

Carberry, B., Grasi, G., Guerin, S., Jayat, F., and Konieczny, R., "Pre-Turbocharger Catalyst – Fast Catalyst Light-off Evaluation", SAE, 2005-01-2142 (2005).

Churchill, S.W., "Comprehensive Correlating Equations for Heat, Mass and Momentum Transfer in Fully Developed Flow in Smooth Tubes", Ind. Eng. Chem. Fundam., Vol. 16, No. 1, 109-116, 1977.

Cybulski, A., and Moulijn, J. A., "Monoliths in Heterogeneous Catalysis", Catalysis Reviews – Science and Engineering, 36 (2), 179-270 (1994).

Dalla Betta, R.A., Tsurumi, K., Ezawa, N., Ribeiro, F.H., and Garten, R.L., "Palladium Partial Combustion Catalysts and a Process for using them. Patent Application Number : PTC/US91/08919, Publication Number : WO 92/09848 (1992).

Donsi, F., Pirone, R., and Russo, G., "Oxidative DeHydrogenation of Ethane over a Perovskite-Based Monolithic Reactor", J. Catal., Vol. 209, No. 1, 51-61 (2002).

Donsi, F., Benedetto, A.D., Marra, F.S., and Russo, G., "CFD simulation of Heat Transfer in a Circular Channel: Effect of Pe Number", Int. Journal of Chem. Reactor Engg., Vol. 3, A36 (2005).

Durst, F., Ray, S., Ünsal, B., and Bayoumi, O.A., "The Development Lengths of Laminar Pipe and Channel Flows", Journal of Fluids Engineering, Vol. 127, 1154-1160 (2005).

Eigenberger, G., "On the Dynamic Behavior of the Catalytic Fixed-Bed Reactor in the Region of Multiple Steady States – I. The Influence of Heat Conduction in Two Phase Models, Chem. Engg. Sci., 27, 1909-1915 (1972).

Fuller, E.N., Schettler, P.D., and Giddings, J.C., "New Method for Prediction of Binary Gas-phase Diffusion Coefficients" Ind. Eng. Chem., Vol. 58, 19 (1966).

Gnielinski, V., "New equations for heat and mass transfer in turbulent pipe and channel flow" Int. Chem. Eng., Vol. 16, 359 (1976).

Grigull, V., and Tratz, H., "Thermercher Einlauf in Ausgebildetu Laminarer Rohrstromung", Int. J. of Heat and Mass Transfer, 8, 669 (1965).

Groppi, G., Bellolo, A., Tronoconi, E., and Forzatti, P., "A Comparison of Lumped and Distributed Models of Monolithic Catalytic Combustors", Chem. Engg. Sci., Vol.50, No. 17, 2705-2715 (1995).

Groppi, G., and Tronoconi, E., "Theoretical Analysis of Mass and Heat Transfer in Monolith Catalysts with Triangular Channels", Chem. Engg. Sci., 52, No. 20 , 3521-3526 (1997).

Gupta, N., and Balakotaiah, V., "Heat and Mass Transfer Coefficients in Catalytic Monoliths", Chem. Engg. Sci., 56 , 4771-4786 (2001).

Hawthorn, R.D., "Afterburner Catalysts – Effect of Heat and Mass Transfer between Gas and Catalyst Surface", A.I.Ch.E Symp. Ser. 70, 428-438 (1974).

Hayes, R.E., Bertrand, F.H., Audet, C., and Kolaczkowski, S.T., "Catalytic Combustion Kinetics: Using a Direct Search Algorithm to Evaluate Kinetic Parameters from Light-off Curves", Can. J. Chem. Eng., Vol. 81, 1192-1199 (2003).

Hayes, R.E., and Kolaczkowski, S.T., "Mass and Heat Transfer Effects in Catalytic Monolith Reactors", Chem. Eng. Sci., Vol. 49, 3587-3599 (1994).

Hayes, R.E., and Kolaczkowski, S.T., "Introduction to Catalytic Combustion", Gordon and Breach, Reading, 1997.

Hayes, R.E., and Kolaczkowski, S.T., "A Study of Nusselt and Sherwood Numbers in a Monolith Reactor", Catalysis Today, Vol. 47, 295-303 (1999).

Hayes, R.E., Kolaczkowski, S.T., Li, P.K., and Awdry, S., "The palladium catalysed oxidation of methane: reaction kinetics and the effect of diffusion barriers", Chem. Eng. Sci., Vol. 56, 4815 (2001).

Hayes, R.E., Liu, B., Moxom, B., R., and Votsmeier, M., "The Effect of Washcoat Geometry on Mass Transfer in Monolith Reactors", Chem. Eng. Sci., Vol. 59, 3169-3181 (2004).

Hayes, R.E., Kolaczkowski, S.T., Thomas, W.J., and Titiloye, J., "Transient Experiments and Modelling of the Catalytic Combustion of Methane in a Monolith Reactor", Industrial Engineering Chemistry Research, 35, 406-414 (1996).

Hayes, R.E., Liu, B., and Votsmeier, M., "Calculating effectiveness factors in non-uniform washcoat shapes", Chem. Eng. Sci., Vol. 60, 2037 (2005).

Hayes, R.E., Mukadi, L.S., Votsmeier, M., and Gieshoff, J., "Three-Way Catalytic Converter Modelling with Detailed Kinetics and Washcoat Diffusion", Topics in Catalysis 30/31, 411 (2004).

Heck, R.H., Wei, J., and Katzer, J.R., "Mathematical Modelling of Monolithic Catalysts", AIChE Journal, 22, 477-484 (1976).

Hegedus, L.L., "Temperature excursions in catalytic monoliths", AIChE J. , Vol. 21, 849 (1975).

Hegedus, L.L., Oh, S.H., and Baron, K., "Multiple Steady State in an Isothermal Integral Reactor: The Catalytic Oxidation of Carbon Monoxide over Platinum-alumina", AIChE Journal, 23, 632-642 (1977).

Holmgren, A., and Andersson, B., "Mass Transfer in Monolith Catalysts – CO Oxidation Experiments and Simulation", Chem. Engg. Sci., Vol.53, No. 13, 2285-2298 (1998).

Incropera, F.P., and DeWitt, D.P., "Introduction to Heat Transfer", John Wiley, New York, 2002.

Kakac, S., Shah, R.K., and Aung, W., "Handbook of Single-Phase Convective Heat Transfer", John Wiley & Sons, New York, 1987.

Kays, W.M., and London, A.L., "Compact Heat Exchangers", 2nd Ed., McGraw-Hill, Newyork (1964)

Keith, J.M., Chang, H. –C., and Leighton, D.T., "Designing of Fast-igniting Catalytic Converter System", AIChE Journal, Vol. 47, No. 3, 650-663 (2001)

Lee, A., and Aris, R., "On the Effects of Radiative Heat Transfer in Monoliths", Chem. Engg. Sci., 32, 827 (1977).

Leighton, D.T., and Chang, H. –C., "A Theory for Fast-igniting Catalytic Converters", AIChE Journal, Vol. 41, No. 8, 1898-1914 (1995).

Leung, D., Hayes, R.E., and Kolaczkowski, S.T., "Diffusion limitation effects in the washcoat of a catalytic monolith reactor", Can. J. Chem. Eng., Vol. 74, 94 (1996).

Michelsen, M.L., and Villadsen, J., "The Graetz Problem with Axial Heat Conduction", Int. J. Heat Mass Transfer, Vol. 17, 1391-1402 (1974)

Mills, A.F., J. Mech. Eng. Sci., Vol. 4, 63 (1963).

Mukadi, L.S., and Hayes, R.E., "Modelling the three-way catalytic converter with mechanistic kinetics using the Newton–Krylov method on a parallel computer", Comp. & Chem. Eng., Vol. 26, 439 (2002).

Oh, S.H., Baron, K., Cavendish, J.C., and Hegedus, L.L., "Carbon Monoxide Oxidation in an Integral Reactor: Transient Response to Concentration Pulses in the Regime of Isothermal Multiplicites", ACS Symposium Series, 65, 461-474 (1978).

Oh, S.H., and Cavendish, J.C, "Transients of Monolithic Catalytic Converters: Responses to Step Change in Feed Stream Temperature as Related to Controlling Automobile Emissions", Industrial and Engineering Chemistry, Product Research and Development, 21, 29-37 (1982).

Otto, N.C., and LeGray, W.J., "Mathematical model for catalytic converter performance", SAE paper No. 800841 (1980)

Pagliarini, G., "Steady Laminar Heat Transfer in the Entry Region of Circular Tubes with Axial Diffusion of Heat and Momentum", Int. J. Heat Mass Transfer, Vol. 32, No. 6, 1037-1052 (1989).

Pagliarini, G., "Conjugate Heat Transfer for Simultaneous Developing Laminar Flow in a Circular Tube", J. Heat Trans-T. ASME, Vol. 113, No. 3, 763-766 (1991).

Papadias, D., Edsberg, L., and Björnbom, P., "Simplified method for effectiveness factor calculations in irregular geometries of washcoats", Chem. Eng. Sci., Vol. 55, 1447 (2000).

Papadias, D., Edsberg, L., and Björnbom, P., "Simplified method of effectiveness factor calculations for irregular geometries of washcoats - A general case in a 3D concentration field", Catal. Today, Vol. 60, 11 (2000).

Pfefferle, L.D., and Pferrerle, W.C., "Catalysis in combustion", Catal. Rev. Sci. Eng., Vol. 29, 219 (1987).

Please, C.P., Hagan, P.S., and Schwendeman, D.W., "Light-off Behavior of Catalytic Converters", SIAM Journal of Applied Maths, 54 (1), 72-92 (1994).

Papoutsakis, E., and Ramkrishna, D., "The Extended Graetz Problem with Prescribed Wall Flux", AIChE J., Vol. 26, No. 5., 779-787 (1980).

Prasad, R., Kennedy, L.A., and Ruckenstein, E., "Catalytic combustion", Catal. Rev. Sci. Eng., Vol. 26, 1 (1984).

Ramanathan, K., Balakotaiah, V., and West, D.H., "Geometry effects on ignition in catalytic monoliths", AIChE J., Vol. 50, 1493 (2004).

Ramanathan, K., Balakotaiah, V., and West, D.H., "Light-off Criterion and Transient Analysis of Catalytic Monoliths", Chem. Engg. Sci., Vol. 58, 1381-1405 (2003).

Ramanathan, K., Balakotaiah, V., and West, D.H., "Ignition Criterion for General Kinetics in a Catalytic Monolith", AIChE J., Vol. 52, No. 4, 1623-1629 (2006).

Reizig, M., Bruck, R., Konieczny, R., and Treiber, P., "New Approaches to Catalyst Substrate Application for Diesel Engines", SAE, 2001-01-0189 (2001).

Saroglia, G., Basso, G., Presti, M., Reizig, M., and Stock, H., "Application of New Diesel Aftertreatment Strategies on a Production 1.9 L Common-Rail Turbocharged Engine, SAE, 2002-01-1313 (2002).

Shah, R.K., "Thermal entry length solutions for the circular tube and parallel plates" Proc. 3rd National Heat Mass Transfer Conference, Indian Institute of Technology Bombay, Vol. I, Paper HMT-11-75 (1975).

Shah, R.K., and London, A.L., "Laminar Flow Forced Convection in Ducts", John Wiley, New York, 1978.

Shome, B., and Jensen, M.K., "Correlations for Simultaneous Developing Laminar Flow and Heat Transfer in a Circular Tube", Int. J. of Heat and Mass Transfer, Vol. 36, No. 6, 2710-2713 (1993).

Silvia Telles, A., Queiroz, E.M., and Elmor Filho, G., "Solutions of the Extended Graetz Problem", Int. J. of Heat and Mass Transfer, Vol. 44, No. 2, 471-483 (2001).

Sinha, N., Bruno, C., and Bracco, F.V., Physicochemical Hydrodynamics, Vol. 6, 373 (1985).

Spiga, M., and Morini. G.L., "Nusselt Numbers in Laminar Flow for H2 Boundary Conditions", Int. J. of Heat and Mass Transfer, Vol. 39, No. 6, 1165-1174 (1996).

Tao, L.N., "On Some Laminar Forced Convection Problems", J. Heat Transfer, Vol. 83, 466-472 (1961).

Tronoconi, E., and Forzatti, P., "Adequacy of Lumped Parameter Models for SCR Reactors with Monolith Structure", AIChE Journal, 38, 201-210 (1992).

Tunc, G., and Bayazitoglu, Y., "Heat Transfer in Rectangular Microchannels", Int. J. of Heat and Mass Transfer, Vol. 45, No. 4, 765-773 (2002).

Tyagi, V.P., "Laminar Forced Convection of a Dissipative Fluid in a Channel", J. Heat Transfer, Vol. 88, 161-169 (1966).

Uberoi, M., and Pereira, C.J., "Mass Transfer Coefficients for Monolith Catalysts", Ind. Engng. Chem. Res., 35, 113-116 (1996).

Ullah, U., Waldrum, S.P., Bennett, C.J., and Turex, T., "Monolithic Reactors: Mass Transfer Measurements Under Reacting Conditions", Chem. Engg. Sci., 47, 2413-2418 (1992).

Van Male, P., de Croon, M.H.J.M., Tiggelaar, R.M., van den Berg, A., and Schouten, J.C., "Heat and Mass Transfer in a Square Microchannel with Asymmetric Heating:, Int. J. Heat Mass Transfer, Vol. 47, No. 1, 87-99 (2004).

Voltz, S.E., Morgan, C.R., Leiderman, D., and Jacob, S.M., "Kinetic Study of Carbon Monoxide and Propylene Oxidation on Platinum Catalysts", Ind. Eng. Chem. Prod. Res. Dev., Vol. 12, 294 (1973).

Votruba, J., Sinkule, J., Hlavacek, V., and Skrivanek, J., "Heat and Mass Transfer in Honeycomb Catalysts I, Chem. Eng. Sci., 30, 117-123 (1975).

Votruba, J., Mikus, O., Khue Nguen, Hlavacek, V., and Skrivanek, J., "Heat and Mass Transfer in Honeycomb Catalysts II, Chem. Eng. Sci. , 30, 201-206 ((1975).

Wanker, R., Raupenstauch, H., and Staudinger,G., "A Fully Distributed Model for the Simulation of a Catalytic Combustor", Chem. Engg. Sci., 55, 4709-4718 (2000)

Wei, J., "The Catalytic Muffler", Am. Chem. Soc., 148, 1-25 (1975).

Wendland, D. W., "The Segmented Oxidizing Monolith Catalytic-Converter – Theory and Performance", Journal of Heat Transfer – Transaction of the ASME 102 (2), 194-198 (1980).

Wilcox, D. C., "Turbulence Modeling for CFD", DCW Industries Inc., La Canada, 1994.
Young, L.C., and Finlayson, B.A., "Mathematical Models of Monolith Catalytic Converters", AIChE Journal, 22, 331-353 (1976).

Zygourakis, K., "Design of Monolithic Catalysts for Improved Transient Performance, In E. R. Becker, and C. J. Pereira (Eds.), Computer Aided Design of Catalysts, 297 – 334, Marcel Dekker Inc., NewYork, 1993